

https://dspace.org/

Geophysical study of acid rock drainage in the City Deep area, Johannesburg, Gauteng

Audouin, Jeanne-Claire

2016
http://hdl.handle.net/10539/21331

Downloaded from a DSpace repository. https://dspace.org/

1. INTRODUCTION

The world-wide pursuit for economic growth and development in the twentieth century has lead to uncontrolled exploitation of valuable natural resources and the subsequent deterioration of the environment. The ensuing threat to human health and environmental integrity have placed these issues near the top of the political agenda throughout the world today. It is not merely political fashion but a genuine concern for the way in which humanity is increasingly living outside the carrying capacity of the earth, thereby reducing its ability to support human life. Sitarz (1993) states in a summary of Agenda 21 that:

> *"Humanity is at a cross-roads of enormous consequence. Never before has civilisation faced an array of problems as critical as the ones now faced. As forbidding and portentous as it may sound, what is at stake is nothing less than the global survival of humankind."*

These mounting public concerns are also evident in the newly-found democratic South Africa. If economic and social development are to progress in the country, it must be recognised, as stated in the ANC mandated environmental mission report, that:

> *"...the environment, as provider of natural resources and ultimate absorber of all waste, underwrites the ability of economic growth and social distribution."*
>
> *(Sole, Sunday Tribune, 25/09/94, p19)*

One of the most critically threatened of these resources, is that of potable water. During the past century the great impetus and drive to the development of South Africa has been provided by the rapid emergence and advancement of the mining industry. Water has always been integral to mining operations and thus mining-related problems such as mine flooding, pressure containment and general safety have dictated the evolution of sophisticated water control techniques by most mines in South Africa. In contrast, however, developments aimed at counteracting the adverse environmental effects of mining operations have been somewhat neglected.

List of Tables

Table 1.1	*South African gold mining waste streams*	2
Table 2.1	*Mean chemical composition of water at selected sites*	10
Table 5.1	*Exploration depths for EM34-3 at various frequencies and intercoil spacings*	38
Table 6.1	*Velocity and depth ranges for refraction seismic profile 1*	63
Table 6.2	*Results of vertical electrical soundings, Ves 1-3*	67
Table 8.1	*Optimal sites for dewatering monitoring boreholes and dewatering trenches*	79
Table D1	*Results of the refraction seismic time-depth conversion*	107

Figure 5.9 *Depth determination of electromagnetic conductors* 42

Figure 5.10 *Snesll's Law relations for incident P-waves* 44

Figure 5.11 *Delay-Time methods used int he interpretation of seismic depths*.....47

Figure 5.12 *Layout of conductivity and seismic traverses* 49

Figure 6.1 *Electromagnetic Traverse 1 - HLEM* 51

Figure 6.2 *Electromagnetic Traverse 1 - VLEM* 52

Figure 6.3 *Electromagnetic Traverse 2 - HLEM* 54

Figure 6.4 *Electromagnetic Traverse 2 - VLEM* 55

Figure 6.5 *Electromagnetic Traverse 3 - HLEM* 57

Figure 6.6 *Electromagnetic Traverse 3 - VLEM* 58

Figure 6.7 *Electromagnetic Traverse 4 - HLEM* 61

Figure 6.8 *Electromagnetic Traverse 4 - VLEM* 62

Figure 6.9 *Seismic Refraction Traverse*.....64

Figure 6.10 *Vertical Electrical Sounding 1 (VES 1)*.....68

Figure 6.11 *Vertical Electrical Sounding 2(VES 2)*..... 69

Figure 6.12 *Vertical Electrical Sounding 3 (VES 3)*..... 70

Figure 7.1 *Conceptual geohydrological model of the City Deep study area* 76

Figure 7.2 *Comparison of average total dissolved salts composition for sites S11 and S12* 77

List of Figures

Figure 1.1 *Location of selected deposits, guaging weirs, surface and ground water sampling sites* 6

Figure 1.2 *Tailings Dam 4L3 showing well-vegetated sides and little evidence of erosion* 7

Figure 1.3 *Pollution in the Rosherville stream bordering Tailings Dam 4L4* 7

Figure 1.4 *Evidence of erosion in the form of gullies on Tailings Dam 4L4* 8

Figures 1.5 and 1.6
Evidence of oxisised iron at the base of Tailings Dam 4L4 8

Figure 2.1 *Total Count Radiometric Image of the West Rand Gold Mine* 15

Figure 2.2 *Radiometric Coverage of the Springs Area (2628AD)* 15

Figure 3.1 *Schematic showing concept of acid generation and ARD migration* 18

Figure 4.1 *Geological map of the City Deep Study Area* 23

Figure 5.1 *Relationship between resistivity and concentration for various salt solutions at a temperature of 18 degrees Celcius* 27

Figure 5.2 *Resistivity of solutions of sodium chloride as a function of concentration and temperature* 28

Figure 5.3 *The resistivity of a rock formation as a function of porosity* 30

Figure 5.4 *Schematic diagram illustrating the Schlumberger electrode configuration* 32

Figure 5.5 *Four basic types of three-layered resistivity curves* 34

Figure 5.6 *A typical four layer Shclumberger sounding curve* 35

Figure 5.7 *Horizontal loop electromagnetic response for a vertical thin sheet conductor of poor and good conductivity* 40

Figure 5.8 *Response diagram used in the interpretation of EM 34-3 anomalies showing effect of varying dip on profile shape* 42

Appendix C:

Calculation of seismic depths 96

Appendix D:

Seismic refraction results 100

Appendix E

Results of field work and resistivity modelling 108

Appendix F

Classification of rock hardness, texture and seismic velocity 111

5.3.2 Field procedure 38
5.3.3 Interpretation 40
5.4 The Seismic Refraction Method 43
5.4.1 Instrumentation 45
5.4.3 Data processing and interpretation 45
5.5 Geophysical Survey Layout 48

6. Results and Analysis 50
6.1 Electromagnetic Traverse 1 50
6.2 Electromagnetic Traverse 2 53
6.3 Electromagnetic Traverse 3 56
6.4 Electromagnetic Traverse 4 56
6.5 Seismic Refraction Profile 1 63
6.6 Resistivity Profiles 67
6.6.1 Electrical layer 1 - colluvial material 67
6.6.2 Electrical layer 2 - resistive tailings material 72
6.6.3 Electrical layer 3 - perched aquifer 73
6.6.4 Electrical layer 4 - resistive basement 73

7. Conceptual Geohydrological Model 74

8. Conclusions and Recommendations 78

9. References 82

Appendix A:
Theory of operation at low induction numbers 88

Appendix B:
Seismic refraction survey. field procedure and ES-1225
Seismograph settings 91

Table Of Contents

1. Introduction

1.1 Nature of the problem 2

1.2 Site location 5

1.3 Broad objectives 5

2. Review of Previous Studies

2.1 Study of the impact of Witwatersrand gold mine residues on water pollution 8

2.2 Detection and monitoring pollution from tailings dams using the airboren radiomeric method 11

3. The Acid Generation Process 14

3.2 The metal leaching and migration process 17

3.2.1 Physical controls 17

3.2.2 Chemical controls 19

3.2.3 Biological controls 20

4. Geology of the City Deep Study Area 20

5. Geophysical Methods 24

5.1 The electrical properties of earth materials 25

5.1.1 Resistivity and porosity 28

5.1.2 Effects of rock texture and geological processes 29

5.2 The resistivity method 30

5.2.1 Instrumentation 31

5.2.2 Electrode layout and field procedure 32

5.2.3 Interpretation 33

5.3 The Electromagnetic Method 36

5.3.1 Instrumentation 37

Abstract

During the past century, gold has been mined from the Witwatersrand conglomerates. Throughout this period, little attention has been paid to the environmental impacts of the ore-extraction process. Generally, uncontrolled waste discharges have, in many cases, led to large-scale degradation and contamination of the water, air and soils of the Witwatersrand.

This study focuses on the environmental impact of two mine residues in the City Deep Area, due South of Johannesburg. Research involved the application of geophysical techniques, namely; terrain conductivity and seismic refraction methods, as tools in the geohydrological "mapping" of the area. Electromagnetic measurements were successful in delineating relatively shallow fractures of faults in the subsurface lithology which serve as conduits for the flow of contaminated water from the mine residues towards the Rosherville Stream. Direct electric current (resistivity) results provided information about the subsurface "layering" of the tailings dam. The depth of the "perched water table" was thus deduced. The seismic refraction method yielded structural information by "mapping" the basement topography down-gradient of the mine residues. Basement lows or depressions provide pathways for the flow of contaminated water. These results, all assisted in the recommendation of optimal monitoring and dewatering borehole sites.

It was concluded that in order to provide more insight into the environmental problems related to the Witwatersrand Basin, it is necessary to initially conduct regional studies on a drainage-basin scale (as opposed to present-day studies which are conducted on the individual mine-scale) and then focus rigorous studies on localised problematic areas. The use of an integrated "Master Database" incorporating all fields of research would provide a far more accurate picute of drainage and contamination patterns, thereby allowing for the prioritisation of remedial measures.

Acknowledgments

I wish to thank Stephen Trickett, my family, Lindsay Andersen, Paul Knottenbelt and Joseph for their time and assistance in carrying out the field work,. My thanks also go to my supervisor, Professor Geoff Blight for his guidance and helpful suggestions throughout the course of the project.

Declaration

I declare that this project report is my own, unaided work. It is being submitted for the Degree of Master of Science (Engineering) at the University of the Witwatersrand, Johannesburg. It has not been submitted previously for any degree or examination at any other university.

.....

10th day of June 1997

Geophysical Study of Acid Rock Drainage in the City Deep Area, Johannesburg, Gauteng.

Jeanne-Claire Audouin.

A project submitted to the Faculty of Civil Engineering, University of the Witwatersrand, Johannesburg in partial fulfillment of the Masters degree of Science in Engineering.

June 199

GEOPHYSICAL STUDY OF ACID ROCK DRAINAGE IN THE CITY DEEP AREA, JOHANNESBURG, GAUTENG

JEANNE-CLAIRE AUDOUIN

2.2 *Detection and Monitoring Pollution From Tailings Dams Using The Airborne Radiometric Method*

A high resolution airborne radiometric survey was undertaken by the Council of Geoscience over parts of the Witwatersrand Goldfield. The results of the survey, which commenced in 1991, have provided valuable insight into the nature and extent of pollution originating from mine residues.

The airborne radiometric method is based on the radioactivity or radio-element concentrations of the target and as such, involve the detection of gamma rays from the three primary radioactive elements found in nature, namely, Potassium, Uranium and Thorium. The intensity of gamma radiation, which forms part of the electromagnetic spectrum, is indicative of the concentrations of the individual radio-elements within the source. Complete attenuation of the radiation typically occurs within the first 400cm of its passage through the earth's uppermost layer. Radiometric surveys, therefore, provide information about the distribution of radioactivity (and hence contamination) of surface sediments.

Figures 2.1 and 2.2 illustrate the significantly high total radio-element counts which occur over tailings dams and sand dumps in the West and the East Rand, respectively. These illustrations are just two examples of pollution patterns which were found to occur throughout the Witwatersrand Basin (Coetzee, 1996). Many of the anomalies relating to the tailings dams have distinctive "tails" which tend to follow the courses of local rivers. In general these "tails" extend for only a few kilometres downstream of the mine residues, with the implication that the residues are the source of radioactive contamination of the surface sediments. The limited extent of the radioactive plumes may indicate the settling out of suspended sediment load of rivers or the precipitation of dissolved pollutants induced by a higher pH in the fluvial environment relative to the tailings dams. Furthermore, results showed that the eU : eTh ratio of Witwatersrand ores and their residues is generally in excess of 1.0, significantly higher than the range of values associated with naturally occurring rocks, viz. 0.1 - 0.3 (Coetzee, 1996).

In order to achieve a better insight into the processes governing the transportation of salt loads from mine deposits to the stream network within the study area, Jones et. al (1988) highlighted the need for further investigation into the following:

- the movement of water through and out of mine residues.
- the direction and rate of movement of ground water affected by seepage from mine residue deposits,
- the changes in salt loads in the baseflow of surface streams in the vicinity of mine residue deposits and
- the mechanisms and rates of recovery in the quality of streamflow during its downstream passage towards the Vaal Barrage

Analysis of the aforementioned geochemical results and calculations of the annual export of TDS and sulphate from the study area , together with studies of ground water movement and contamination all led to a number of notable findings, namely;

i) The streams in the study area are perennial and are partly fed by ground water.

ii) The chemical quality of water upstream from the monitored deposits (Sites S1 to S4 and S7) is of moderate quality but a marked deterioration occurs in the vicinity of the sand dump 3A17 (S8). This deterioration persists into the eastern section of the study area (S10 and S11) where, however, no further deterioration was observed. The water quality measured in the vicinity of the Rosherville Stream (S12 and S13) is better than that at sites S10 and S11, but is nevertheless acidic and high in TDS and sulphate.

iii) Estimates based on data gathered during this study and on information supplied by the Chamber of Mines of South Africa reveal that about 50 000 tons/annum of salts originating from the mine deposits in the catchment of the Vaal Barrage are discharged into the near surface environment, as yet, it remains uncertain as to what proportion of this load is eventually transported by surface streams or ground water to the Barrage.

iv) The study was based on the premise that runoff from the dumps was the primary source of the salt loads contributed by the mine residue deposits, however, water chemistry analyses during storm events established that direct runoff serves to dilute the salt concentration in the streamflow and as such is not considered to be a major contributor of salts to the stream network since the high concentration levels exist in the base flow.

It was subsequently concluded that in the study area, the major contributor was response to a near surface ground water system which recharges the stream.

The positions of the aforementioned sites are depicted in Figure 1.1. Table 2.1 summarises the mean values for pH, conductivity, total dissolved solids (TDS) and sulphate for the surface sampling points. Also indicated in Table 2.1, are the sites at which the General Effluent Standards originally proposed by Kempster and Smith (1984) are exceeded.

CONSTITUENT	SAMPLING SITES						
	S1	S4	S6	S9	S14	S11	S12
Ca	32.5	34.5	*485.0	47.4	*640.0	66.8	83.8
Mg	7.3	9.7	132.1	103.9	*202.0	35.4	33.5
Na	26.6	25.0	*150.0	11.2	14.3	31.4	62.7
K	5	5	41.3	14.3	4.6	6.6	9.6
NH4	0.07	0.17	3.84	7.36	0.66	0.53	3.96
Fe	0.42	0.16	*24.2	*1043.0	5999.0	*112.51	*15.10
Mn	0.05	0.08	*2.74	**133.3	**42.3	**3.62	**0.91
Ni	0.02	0.12	*1.22	*104.2	*64.7	*1.47	0.82
Al	0.28	0.24	*20.95	1.96	*911.3	*22.90	0.66
Zn	0.11	0.13	0.96	*12.0	**59.6	**1.41	0.87
Total Alk	61	70.94	7.6	1.64	6	8.64	42.3
SO4	62.4	63.6	*2019.0	*4168.0	*1780.0	*57.8	417
Cl	26	23.3	66.3	30.6	49.1	34.9	63.6
NO3	3.9	2.2	0.2		0.5	1.3	0.03
TDS	269	266	3080	56887	28223	973	767
pH	6.5	6.8	*2.8	**2.3	**3.8	*4.5	**2.3

Table 2.1 Mean chemical composition of water at selected sites. (mg/l) (Jones et. al. (1988))

* *Exceeds crivs drinking water limit (after Kempster & Smith, 1984)*

** *Exceeds General Effluent Standard*

2. REVIEW OF PREVIOUS STUDIES

Concern about the production of acid drainage water in mine deposits and the associated pollution of the water supply from the Vaal Barrage has led to numerous and extensive research programmes. The following discussion is a summary of those studies exclusively pertaining to the study area.

2.1 Study Of The Impact Of Witwatersrand Gold Mine Residues On Water Pollution

A regional study of the impact of the Witwatersrand mine residues on water pollution was initiated by the Water Research Commission (WRC) in 1974. The primary objectives of the project were to establish the degree to which runoff and drainage from mine waste deposits contribute to the total dissolved solids load in the Vaal Barrage and to identify those deposits which require control methods and remediation to prevent further pollution. In order to conduct the investigation, a tripartite contract was entered into by the WRC, the Department of Water Affairs (DWA) and Steffen, Robertson and Kirsten (SRK) in August 1983.

Research entailed detailed monitoring of run-off as well as surface and ground-water quality of three selected mine deposits as a basis for estimating the pollution potential from all mine deposits in the catchment of the Vaal Barrage. The three deposits selected in the City Deep Area included a sand dump (SAND), a well-maintained tailings dam (WELL) and a poorly-maintained tailings dam (POOR) (Figure 1.1).

Four weirs were constructed by the DWA in the study area to record daily flow rates, water temperature and conductivity. Fourteen surface water sampling points were sited so as to obtain a comparison between upstream and downstream water quality in relation to the river's course past the selected mine residues.
Furthermore, twelve percussion boreholes were drilled towards the end of 1983 to monitor both "shallow" and "deep" ground water movement and water quality.



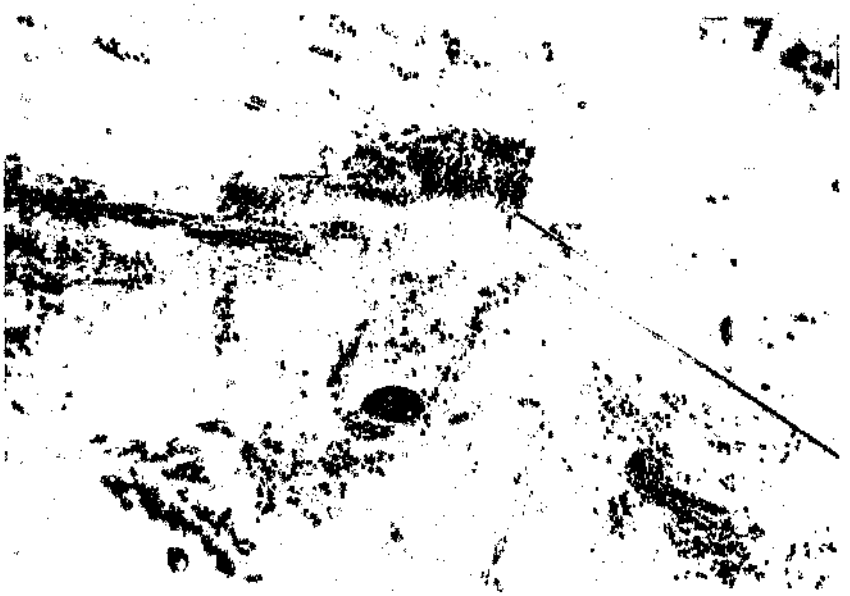

Figure 1.5 and 1.6 Evidence of oxidised iron at the base of Tailings Dam 41.4

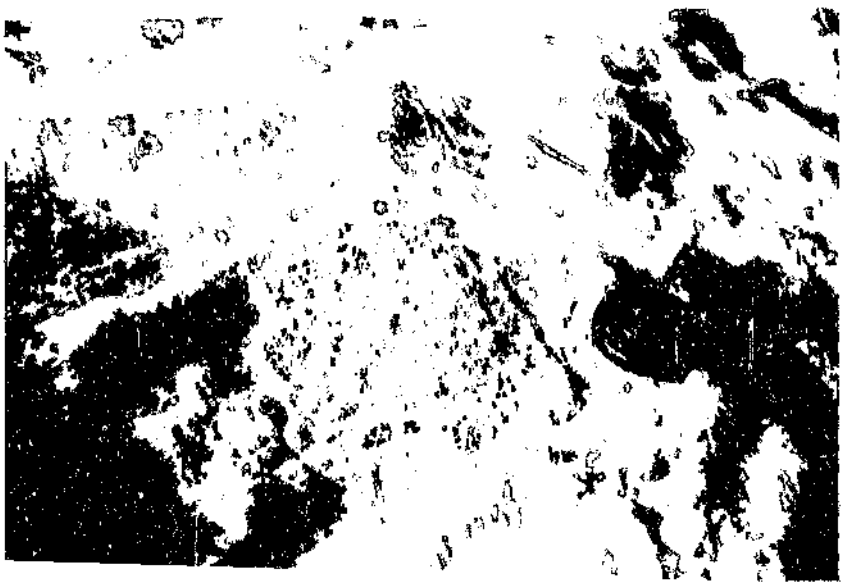



Figure 1.2 Tailings Dam #1 showing well vegetated sides and little evidence of erosion



Figure 1.3 Pollution in the Rockerville stream bordering Tailings Dam #1

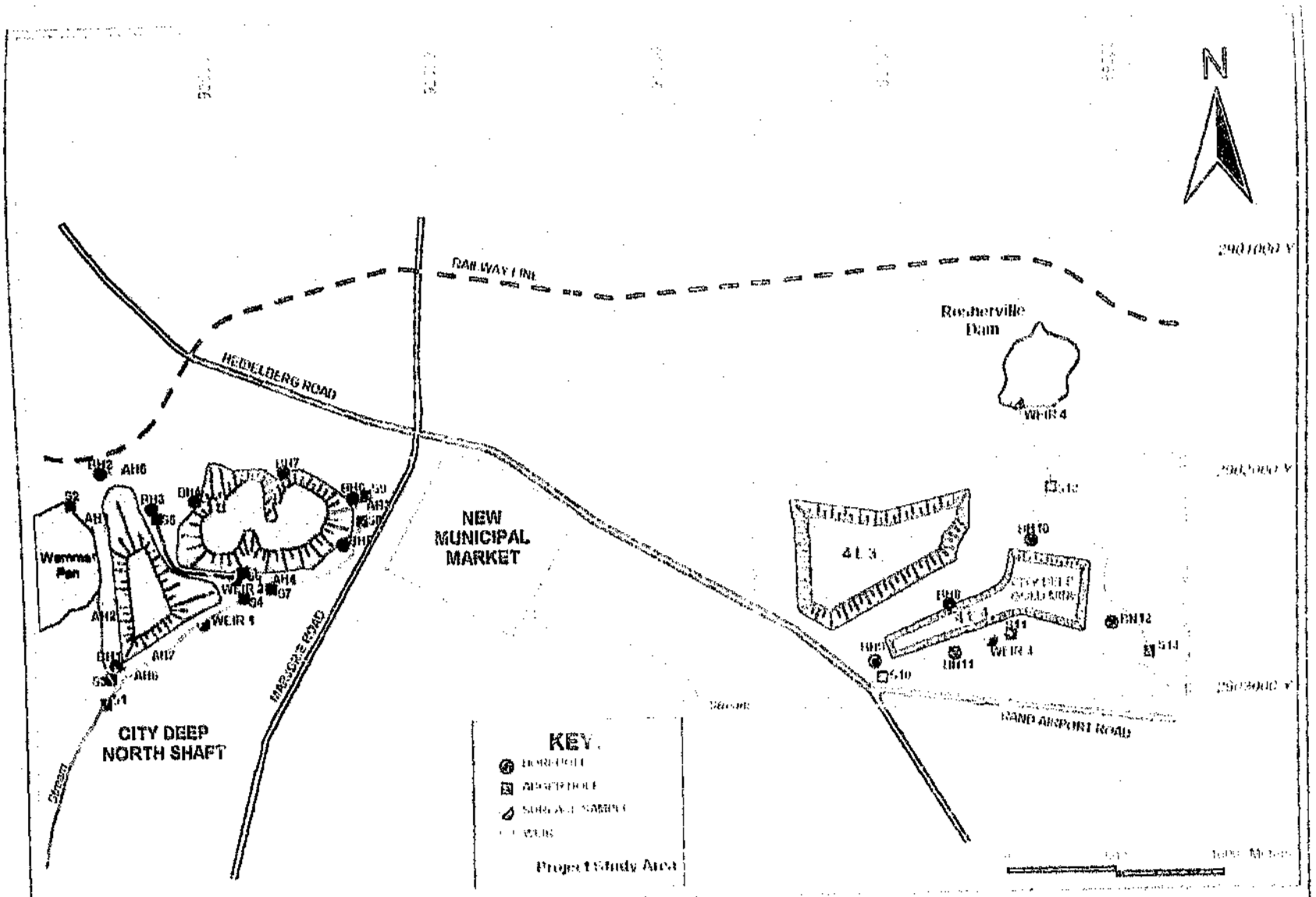

Figure 1.1: Location of selected deposits, gauging weirs, surface and ground water sampling sites. (Jones et al, 1988)

1.2 Site Location

The study area is situated in the highly industrialised City Deep Area and comprises a strip of land spanning an area of approximately 1 8km² which is elongated in an east-west direction (Figure 1 1) The mine residues comprise a moderately maintained and a poorly-maintained tailings dam, 4E3 and 4E4 , respectively The area is drained by perennial streams (Figure 1 3), the confluence of which forms the Natalspruit River The sides of tailings dam 4E3 are fairly well vegetated with little evidence of erosion (Figure 1 2) Tailings dam 4E4, on the other hand, shows extensive evidence of erosion in the form of gullies (Figure 1 4)

One of the most visible elements of environmental pollution in the area is that of oxidised iron shown in Figures 1 5 and 1 6

1.3 Broad Objectives

Investigations of ground water contamination within the City Deep Study Area encompassed the following objectives, namely,

- a detailed review of both the theory behind Acid Rock Drainage and related studies which have been reported in the research area over the past decade
- determination of the structural and hydrogeological characteristics at the site including the detection of the presence of pollutants in the vadose and ground water zones
- recommendations for the judicious siting of monitoring and dewatering boreholes

The numbers refer to the system used by the Chamber of Mines in their classification of mine deposits

This study involves the application of geophysical techniques, in particular, terrain conductivity and seismic refraction methods as tools in the detailed hydrogeological mapping of a gold mine waste disposal site in the City Deep Area. (The reader is referred to Figure 1.1 which shows the site location.) While precautions may have been taken to engineer an adequate disposal site, continuous monitoring of groundwater seepage is required.

Knowledge of local geohydrological conditions is essential to ensure adequate containment. The depth to the water table and the direction of ground water travel are especially important, as most mine-related acid drainage occurs in a band between 3 and 10m depth and can be traced for hundreds or even thousands of metres (GEONEX Aerodat Inc., 1993).

As groundwater contamination is usually associated with an increase in the salt concentration and consequently with a corresponding increase in the electrical conductivity of the water, electrical techniques are ideally suited to the detection and monitoring of water pollution and as such, have been successfully employed in mapping potential leachate problems in the past (Goldstein et. al, 1990). The particular electrical methods most frequently employed are some form of resistivity profiling (Schlumberger, in this case) and electromagnetic profiling. These methods cannot replace ground samples for measuring concentrations but they do have numerous advantages, namely; the determination of subsurface layer thicknesses and resistivities, the delineation of structural features with which ground water is often associated and the approximation of geohydrological parameters such as hydraulic conductivity, porosity, transmissivity and specific capacity. Furthermore, the coverage of data surpasses that obtained by drilling methods; each electromagnetic reading tends to average data over a larger area and so is less susceptible to random errors or short-term fluctuations brought on by changes in precipitation.

its importance to the Pretoria-Witwatersrand-Vereeniging (Gauteng) area for water supply. It is well, therefore, to examine the nature of the constituents of concern, in particular, those added to the surface water directly via runoff, or indirectly, via seepage from the mine deposits within the study area (Table 1.1)

Gold Mining Waste Streams	*Hazard Group*[1]	*Tons/annum*	*Constituents of concern*
Tailings	5	190 181 477	CN^-, SO_4^{2-}, HSO_4
Effluent	2	1 013 363	CN^-, SO_4^{2-}, HSO_4
Inorganic uranium waste	4	825 000	Organics, HSO_4, salt
Organic uranium waste	4	4 070	Organics
Catalyst for sulphuric acid manufacture	4	60	V.O.
Smelting waste	4	2 100	Heavy metals

Table 1.1: South African gold mining waste stream (t/a excluding water)
(C.S.I.R., 1992. 'Hazardous Waste in South Africa').

Environmental scientists involved with the remediation of such hazardous wastes are frequently faced with the problem of locating subsurface contamination and delineating features that influence its development over time, without the expense and disruption caused by drilling. Geophysics offers an array of techniques to assist with mapping and quantifying the extent of these pollution plumes

[1] *Group 1: High hazard waste, Group 2: Moderately hazardous waste, Group 3: Low hazard waste, Group 4: Potentially hazardous waste, and Group 5: Non-hazardous waste*

Prior to the introduction of the Water Act in 1956 (Act 54 of 1956), very little was known about the detrimental environmental impacts of polluted mine drainage and at closure of operations, mine residues were abandoned without the implementation of adequate pollution control measures. As a result, many of South Africa's water resources are contaminated by various polluting constituents which seep into ground water supplies, thereby degrading water quality and limiting its usefulness.

Generally, uncontrolled municipal and industrial discharges and a failure to place water quality issues concurrently with water supply priorities on the development agenda, has led to a situation of water pollution that requires immediate and extensive attention (Department of Environmental Affairs, 1992).

1.1 Nature Of The Problem

For the past century, gold has been mined from the Witwatersrand conglomerates and subsequently extracted from the ore in a process which produces large quantities of waste, rich in sulphides. Oxidation of these sulphides produces sulphuric acid, which in turn, leaches and transports polluting metals into the environment. Furthermore, in many cases, significant concentrations of uranium occur in-situ with the gold ore. On extraction of the gold, the uranium remains and forms part of the waste stream. These waste products pose a threat to communities in the vicinity of the mines, both through airborne and waterborne transport of toxic components.

In their study of Witwatersrand mine deposits, Jones et al (1988) calculated that seepage of acid water from these residues released 50 000t of salts into the catchment of the Vaal Barrage. These waters exhibited typical characteristics of acid drainage emanating from mine residues elsewhere in the world. Water samples extracted from many of the local rivers have yielded very low pH values, ranging between 2.75 and 3.21 (Jones et al, 1988). Moreover, sulphate comprised a large proportion of the tonnage of salts in the drainage and the brown colour of the seepage water in and around the seepage ponds indicated the presence of oxidised iron. This rapidly increasing concentration of salts in the Vaal Barrage is of considerable concern due to

"Mapping refers to the task of appraising the location and extent of ground water contamination near a site at a particular time. Typically such a survey is requested only after contaminant leakage is suspected. Monitoring, on the other hand, refers to the examination of changes in the conductivity patterns with time around a site. Because changes in the anomaly patterns are observed during the monitoring phase, when compared to the initial mapping of the extent of contamination, monitoring has the potential to detect more subtle contamination related conductivity anomalies."

The usefulness of geophysical measurements and their relative reliability and low cost, has led to research by for example, Meyer et al (1994) to define their effectiveness and hydrogeological information content in relation to potential or existing ground water pollution. The instrumental, methodological and interpretational basis for these methods continue to improve rapidly.

5.1 The Electrical Properties Of Earth Materials

Rocks are natural aggregates of one or more minerals which comprise the solid matrix. These minerals are interconnected by a certain percentage of pore space which may range from less than 1% of total rock volume in igneous rocks to more than 10% in unconsolidated sands and gravels. The solid matrices are generally very poor electrical conductors, therefore, for most subsurface materials, conduction is electrolytic, the conducting medium being an aqueous solution of common salts distributed throughout the pore structure of the rock.

Solid conduction mechanisms can be expected to be important in comparison to electrolytic conduction through pore water in three exceptional cases, viz:

i) in a rock containing a high percentage of conducting minerals, for example, metallic sulphides;

ii) in a completely frozen rock and

5. GEOPHYSICAL METHODS

Geophysical surveys are designed to map variations in the physical properties of the subsurface, i.e. magnetic susceptibility, electrical conductivity, density and radioelement concentrations. This translates into a broad range of applications - from detecting ore bodies through mapping contaminated groundwater to locating buried steel objects. The unique advantage of geophysical methods is their ability to sense objects and features below the surface and hidden from direct observation. Short of invasive and expensive detection methods such as drilling or excavation, geophysics is often the only technique capable of defining the subsurface.

At present, seismic and electrical techniques are routinely utilised to investigate the nature and variability of geological and geotechnical parameters that influence the choice of a waste disposal site, tailings dams, etc. In recent years, however, the attention of hydrogeologists and geophysicists has turned to problems revolving the detection of ground water pollution and protection of aquifers from pollution. Success in determining the geometry of aquifer systems was followed by attempts, some of which have proven successful, to determine hydrogeological parameters such as permeability and effective porosity (Mazac et al., 1990; Kelly, 1987; Meyer and Coetzee, 1991).

According to Greenhouse and Mozier-Williams (1988) the application of geophysical techniques to groundwater contamination studies may fall under two broad categories termed *monitoring* and *mapping*, both of which identify contaminated ground water due to the enhanced electrical conductivity associated with abnormally high concentrations of dissolved salts.

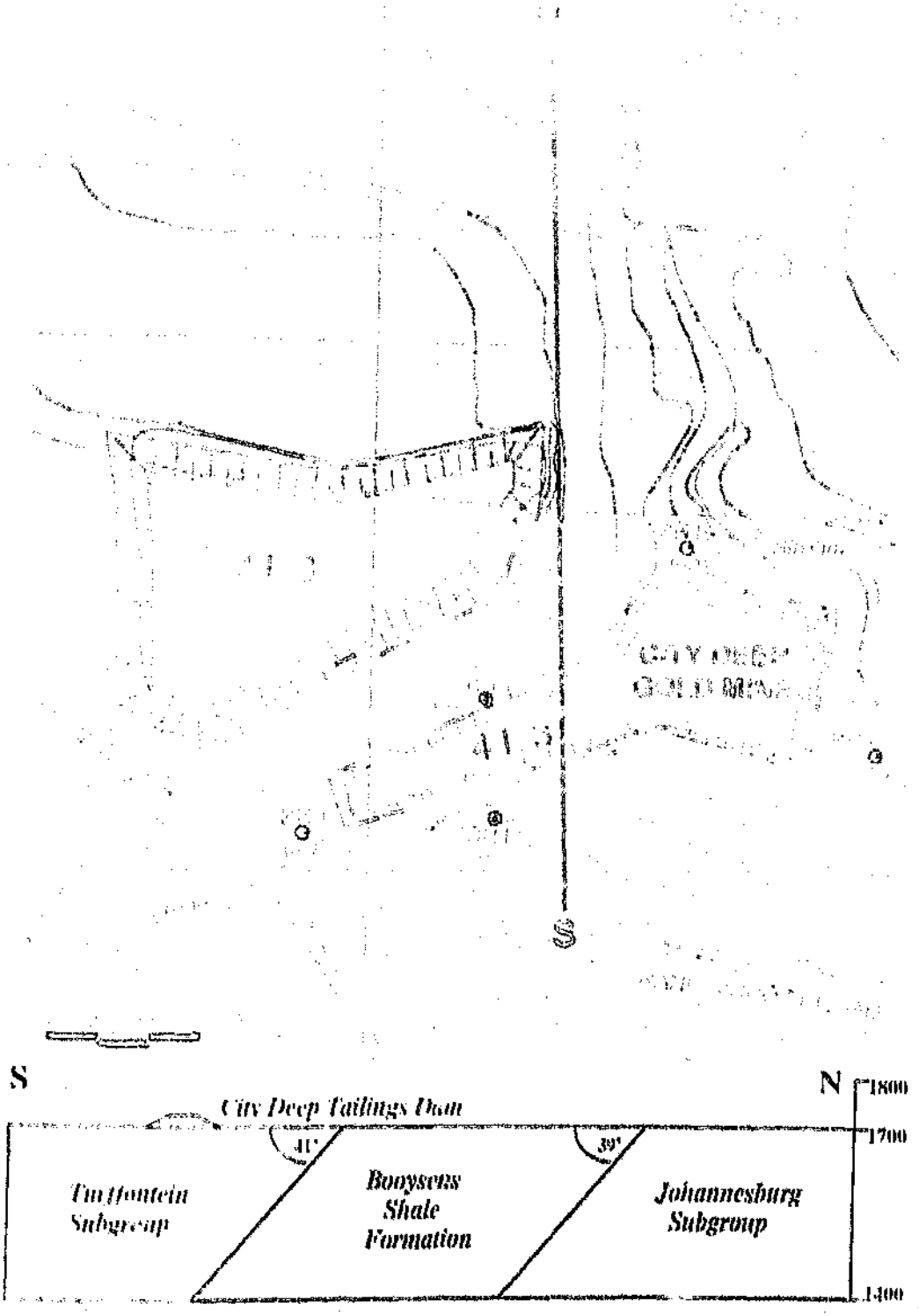

Figure 4.1 Geological map of the City Deep Study Area

4. GEOLOGY OF THE CITY DEEP STUDY AREA

The geology of the study area, shown in a composite geological map (Figure [illegible]), comprises rocks from the Central Rand Group, a subdivision of the Witwatersrand Supergroup. With the exception of a single bed of shale, this group is composed entirely of arenaceous and rudaceous rocks. Two subgroups may be distinguished, namely, the Johannesburg and the Turffontein Subgroups.

A characteristic of the quartzite beds of the Turffontein Subgroup is their yellowish appearance and argillaceous nature, in contrast with the clean, white quartzites encountered in the Johannesburg Subgroup.

The composite geological map was compiled by SRK from the following sources:
- the 1:250 000 scale Geological Survey Sheet No. 2628 of the East Rand.
- the 1:60 000 scale Geological Map of the Witwatersrand Goldfields by F. I. Mellor (1912).
- the Geological Map of Johannesburg by Findlay and Van Nieuwpoort (1976) and a plan of the City Deep Underground Workings on a scale of 1:15 000 supplied by Rand Mines Ltd.

Studies of the *distribution* of the bacteria indicated the presence of significant populations which were confined to two regions, namely, at the base of the sand dump where acid drainage water was seeping through the sand and emerging at the surface or in the interior grey coloured sand exposed on excavated faces where the pyrite had not yet been oxidised to sulphate and yellow or orange oxidised forms of iron. In contrast the outer orange coloured layer of sand dumps away from seepage contained almost no iron-oxidizing bacteria nor sulphur, both observations ing that the pyrite substrate on which the bacteria grow had been lost from this part of the dumps during more than half a century of oxidation. As this process had proceeded to depths of c. 10m in the sand dumps at the time of investigation, the iron-oxidizing bacteria must've been catalysing pyrite oxidation at or beyond this depth. The absence of iron-oxidizing bacteria from most winter samples from the exposed face of the excavated dump, in contrast to their abundance in similar (but moister) grey-coloured samples in summer, suggests that pyrite oxidation is seasonal (Jones et al. 1988).

- Temperature – The process of air penetration is believed to be caused by diurnal and seasonal temperature changes which result in the alternating expansion and contraction of pore-air (Mrost, 1973).
- Availability of oxygen in the gaseous phase.
- Availability of oxygen in the water phase.
- Chemical activity of Fe^{3+} (refer to reaction 4).
- Surface area of exposed metal sulphide and
- Chemical activation energy required to initiate acid generation

3.2.3 Biological controls

Certain bacteria may catalyse or decelerate the rate at which some of the aforementioned reactions proceed. Reactions 2 and 4 may be accelerated by the presence of chemolithotrophic iron-oxidising bacteria, while reaction 1 may be catalysed by bacteria through the enhancement of the rate of reduced-sulphur oxidation (Lundgren and Silver, 1980).

That bacterially catalysed iron oxidation was occurring in the leachate of the City Deep mine residues was indicated by the presence of populations of chemolithotrophic iron-oxidising bacteria of ca 10^{3} to 10^{5} ml in drainage water and ca 10^{5} to 10^{7} g in the brown-coloured soil of the seepage area (Jones et al, 1988). The authors believe that a large proportion, if not all, the bacteria were *Thiobacillus ferrooxidans*. This acidophilic species of bacteria have been found in a variety of dumps throughout the world and appears to be the most common bacterium actively causing the pollution. Thiobacillus ferrooxidans converts the ferrous iron (Fe^{2+}) of pyrite (FeS_2) to its ferric form (Fe^{3+}) in an energy yielding system, either during direct oxidation of the pyrite or following Fe^{3+} production in an indirect oxidation cycle where ferric ions oxidise the pyrite (Kleinmann et al, 1981; Walsh, 1978).

3.2 Metal Leaching And Migration Process

The process of acid generation renders the pore-water capable of mobilising heavy metals and other soluble constituents contained in the waste. The major environmental impact of ARD is not realised until this poor quality water migrates away from the site of generation and enters the receiving environment. It is the high metal loadings in the water emerging from the waste which is most harmful to the environment.

Metal solubility and contaminant migration are controlled by a number of naturally occurring physical, chemical and biological properties of mine waste facilities. The mobilisation of metals is principally controlled by chemical factors while the processes that occur along the migration route are governed by both physical and chemical factors.

3.2.1 Physical Controls

The influence of physical properties are most important in controlling the *rate* of movement of contaminant fronts, the amount of dilution and the degree of mixing that occurs between the contamination source and the receiving environment. Important factors in this regard include climatic conditions, waste permeability and porosity, availability of pore water, pore water pressure and the processes or mechanisms of movement, whether by stream flow or diffusion (S R K, 1989). Generally, the physical properties of the underlying subsurface strata tend to contrast quite significantly with the overlying waste material, resulting in a number of contaminant fronts which all migrate at different rates.

3.2.2 Chemical controls

The primary chemical factors which determine the rate of acid generation may be summarised as follows:

- pH - Primary control on the solubility of metals.

On the other hand, the overall reaction for stable ferric iron that is used to oxidise more pyrite is a combination of reactions 1, 2 and 4 (D W A and S R K., 1990).

$$FeS_2 + \frac{15}{8}O_2 + \frac{13}{2}Fe^{3+} + \frac{17}{4}H_2O \rightarrow \frac{15}{2}Fe^{2+} + 2SO_4^{2-} + \frac{17}{2}H^+$$

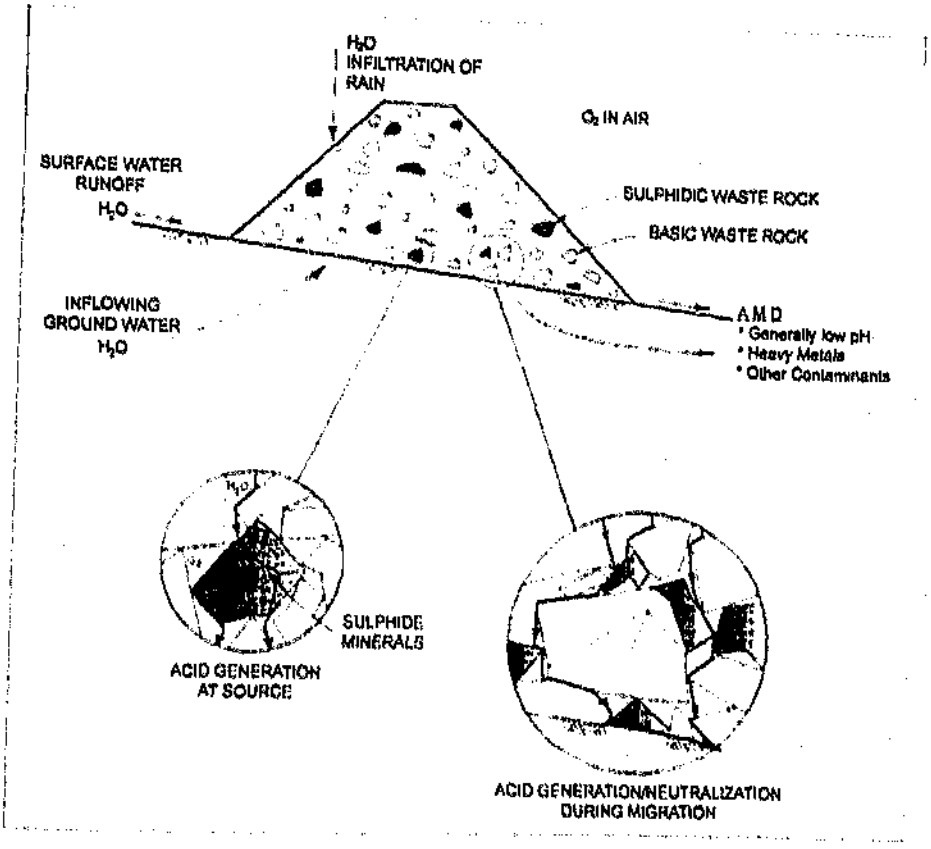

Figure 3.1: Schematic showing concept of acid generation and ARD migration (D.W.A. and S.R.K., 1990).

The initial reaction which involves the oxidation of fine-grained pyrite may be formulated (Lundgren and Silver, 1980) as follows

$$FeS_2 + H_2O + \frac{7}{2}O_2 \rightarrow Fe^{2+} + 2SO_4^{2-} + 2H^+$$

(Solid + water + gas) - (ferrous iron, sulphate and H^+)

Caruccio (1968, cited by Kleinmann et.al, 1981) has shown that the most reactive pyrite is the framboidal form due to the presence of pyrite granules less than 0.5µm in diameter.

The dissolved Fe^{2+}, SO_4^{2-} and H^+ represent an increase in the total dissolved solids and acidity of the water and unless neutralised, the increased acidity is generally associated with a decrease in pH. Providing the surrounding environment is of an oxidising nature, most of the ferrous iron will be oxidised to ferric iron as follows

$$4Fe^{2+} + O_2 + 4H^+ \leftrightarrow 4Fe^{3+} + 2H_2O$$

For pH values exceeding 2.3-3.5, the ferric iron will precipitate as $Fe(OH)_3$, leaving little Fe^{3+} in solution while simultaneously lowering the pH

$$Fe^{3+} + 3H_2O \leftrightarrow Fe(OH)_{3(s)} + 3H^+$$

Any Fe^{3+} from reaction 2 that does not precipitate from solution through reaction 3, may be absorbed in the oxidation of additional pyrite

$$FeS_2 + 14Fe^{3+} + 8H_2O \rightarrow 15Fe^{2+} + 2H_2SO_4^{2-} + 16H^+$$

Based on these simplified basic reactions, the process of acid generation that produces iron which ultimately precipitates as $Fe(OH)_3$ may be represented by the combination of reactions 1, 2 and 3 (D.W.A. and S.R.K., 1990)

$$FeS_2 + \frac{15}{4}O_2 + \frac{7}{2}H_2O \rightarrow Fe(OH)_3 + 2SO_4^{2-} + 4H^+$$

3. Acid Rock Drainage

Acid rock drainage (ARD) is the term used to define drainage that occurs as a result of natural oxidation of sulphide minerals contained in rock which is exposed to air and water (DWA and S.R.K., 1990). This phenomenon is often referred to as acid mine drainage (AMD), however, this term may be misleading as acid drainage is not necessarily confined to mining activities, but can occur wherever sulphide-bearing rock is exposed to the atmosphere and to moisture. For practical purposes, the principal ingredients in the ARD process comprise reactive sulphide minerals, an oxidant, particularly oxygen from the atmosphere or from chemical sources and water or a humid atmosphere. The oxidation reactions are often catalysed by biological activity. The chemical and biological reactions yield acidic water which has the potential to mobilise any heavy metals that may be contained in the waste rock or elsewhere, thereby causing a potentially detrimental impact on water quality in the receiving environment.

3.1 The Acid Generation Process

The process of mining generally results in the exposure of mine wastes and tailings which contain sulphide minerals, most commonly, pyrite (FeS_2), to air and water, resulting in the production of acidity and elevated concentrations of sulphate and metals. This is a consequence of the oxidation of sulphur in the mineral to a higher oxidation state and if aqueous iron is present and unstable, the precipitation of ferric iron with hydroxide (DWA and SRK, 1990). In the cases where the sulphide minerals are non-reactive or the rock contains sufficient alkaline material to neutralise the acid, the acid generation process is prevented.

A waste rock pile is illustrated schematically in Figure 3.1 as an example illustrating the general process of acid generation and migration. The figure shows a mixture of sulphidic and basic rock in the pile, the potential sources of oxygen and water and acid generation or neutralisation occurring where these ingredients are in contact.

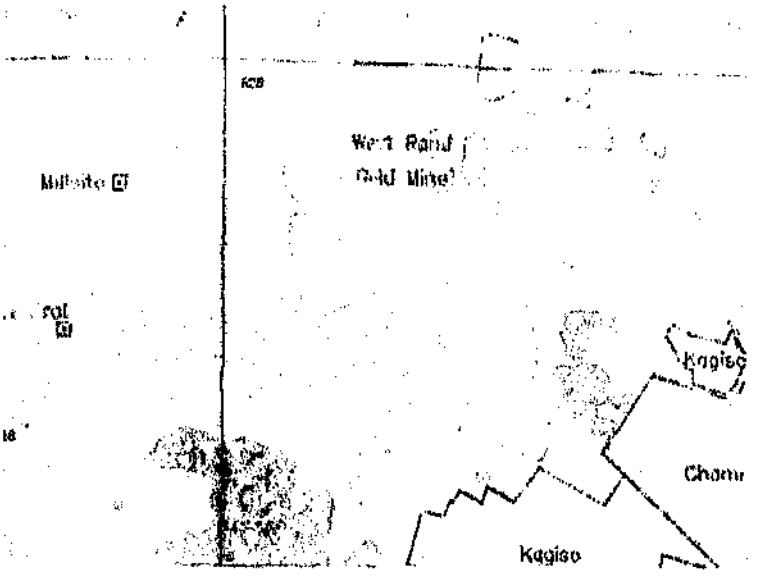

Figure 2.1 Total Count Radiometric Image of the West Rand Gold Mine, showing elevated radioactivity levels over the tailings dams and surrounding wetlands. (Tailings dams and waste rock dumps outlined in dark blue, wetlands indicated in light blue. The Radiometric data are expressed in colour, with blue indicating lower levels and red higher levels) (After Coetzee, 1996)

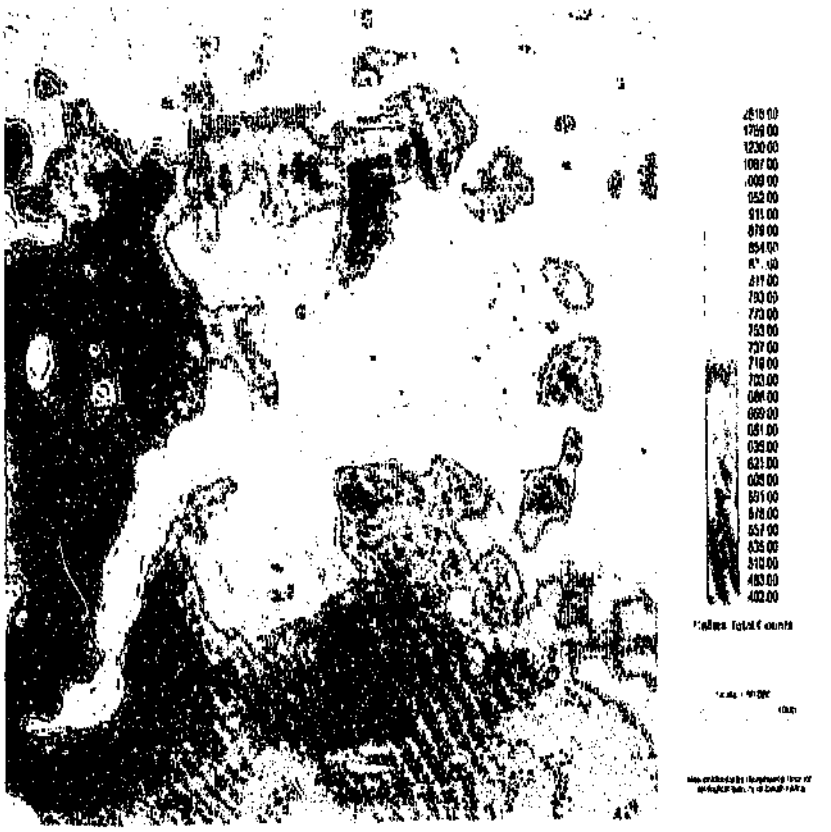

An additional source of environmental pollution arising from mining activities is that of air pollution in the form of dust and radon gas. (a radioactive gas produced by the decay of radium). This gas is odourless and colourless and being denser than air, tends to collect in buildings built on or out of radioactive material. The stable atmospheric conditions typical of the Highveld winter exacerbate the problem by leading to the build-up of atmospheric radon, to levels as high as 200 Bq/m^3 the 'normal' radon content for such soils ranges between 25 and 50 Bq/m^3. The presence of the radon gas thus poses a potential threat to operations which have and still intend to make use of mine tailings for cement manufacture and fill on building sites.

One of the primary concerns regarding such pollution is the bio-accumulation of toxic materials in plant and animal tissue and their consequent concentrations further up the food chain. Although there are numerous reports from local mining communities in the Witwatersrand area pertaining to water-related illnesses, there is very little detailed data available which documents the exact nature and extent of mine-related pollution

In light of this shortage of rigorous research, Coetzee (1996) concludes his report by advocating the application of Geographical Information System (GIS)-based risk assessment methods to the Witwatersrand Basin as a whole. Such assessments would allow one to determine the magnitude and extent of pollution problems and thereby, assist in the prioritisation of remedial actions and the forecasting of potential future problems

$\rho = \frac{V}{I} k$,

where k is known as the geometric factor which is particular to the electrode arrangement employed

The unit of resistivity is the ohm metre.

In the exceptional case where the ground in homogenous, this is the true ground resistivity, but in general, one measures a weighted average of the resistivities of the formations through which the current passes. An analysis of the variation of the apparent resistivity with a change in electrode spacing and position yields information about the variation of the subsurface as a function of depth.

5.2.1 Instrumentation

The necessary components for conducting resistivity measurements comprise a power source, meters for measuring current and voltage, electrodes, insulated cable and reels. The Geotron Model G41 earth resistivity meter was used in this study. An artificial current is injected into the ground by means of two point electrodes known as the current electrodes (C_1 and C_2 in Figure 5.4). The power source is a 12V rechargeable battery which may deliver either direct current (dc) or low frequency alternating current (ac), preferably less than 60Hz. Two probes, termed potential electrodes (P_1 and P_2 in Figure 5.4), are then used to map the resultant potential distribution due to the primary current along the emission line. Potential is measured with a voltmeter of high input impedance (1Mohm or greater).

In the system used, both the transmitter and the receiver were contained in a single aluminium housing. The current and potential electrodes consisted of stainless steel stakes each $\frac{1}{2}$*m* long. The electrodes were driven into the earth until they came into contact with moist soil. In some areas, this was only a few centimetres, while in other areas, the electrodes were placed 20cm below the earth's surface.

of a rock. However, processes such as metamorphosis tend to reduce fluid permeability and hence increase resistivity.

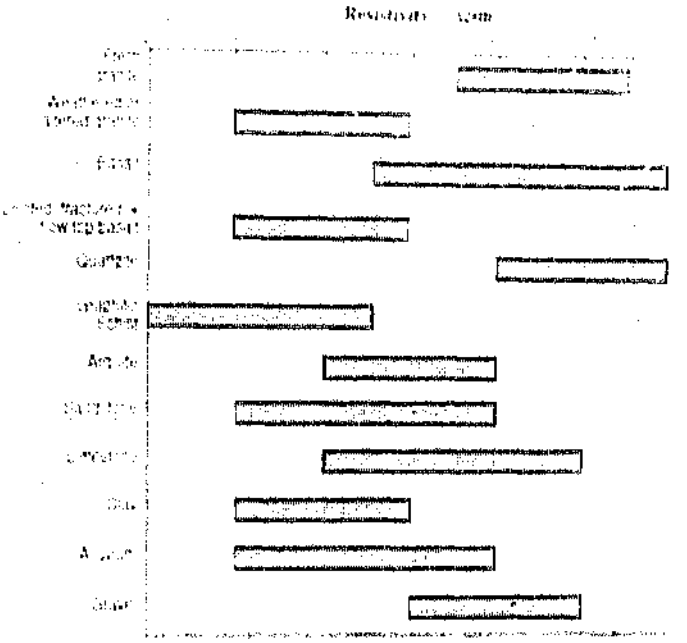

Figure 5.3: The resistivity of a rock formation as a function of porosity (after Meyer, 1994)

5.2 The Resistivity Method

The electrical resistivity method employs an artificial source of direct current, which is introduced into the ground by means of point electrodes. The resulting voltage drop produced by this current is measured across potential electrodes in the vicinity of the current flow. Knowledge of the magnitude of the potential drop, ΔV, the applied current, I and the electrode separation enable a quantity known as the apparent resistivity to be calculated as follows:

S_w is the fraction of the pores containing water

a (coefficient of saturation), m (cementation factor) are constants relating to the lithology and the texture of the rock
($0.5 < a < 2.5$), ($1.3 < m < 2.5$)

$n \approx 2$.

Archie's Law, however, applies only to a clay-free, non-conducting matrix formation. The resistivity of a water-saturated unconsolidated alluvium in the absence of any matrix conduction effects is given by the equation

$$\rho_r = \frac{\rho_w}{\phi^m}$$

where ϕ is the porosity and

ρ_r is the resistivity of the rock formation.

The influence of porosity on the resistivity of a rock formation is clearly illustrated in Figure 5.2. An order of magnitude change in porosity, all other variables being equal, results in a two order magnitude change in formation resistivity. It is important to establish the resistivity of the formation in question under "normal" or uncontaminated conditions.

5.1.2 Effects Of Rock Texture And Geological Processes

A simple generalised view of the large range of resistivities found in rocks of variable porosities, as they occur in the treatment of hydrogeological problems is given in Figure 5.3. These ranges reflect in part a variation in texture ranging from sandstones to the low-permeability, highly porous and well-sorted basalts, but also reflect the effects of geological processes. In general, these processes, which include weathering, hydrothermal alteration, jointing, shearing and fracturing, tend to reduce the resistivity

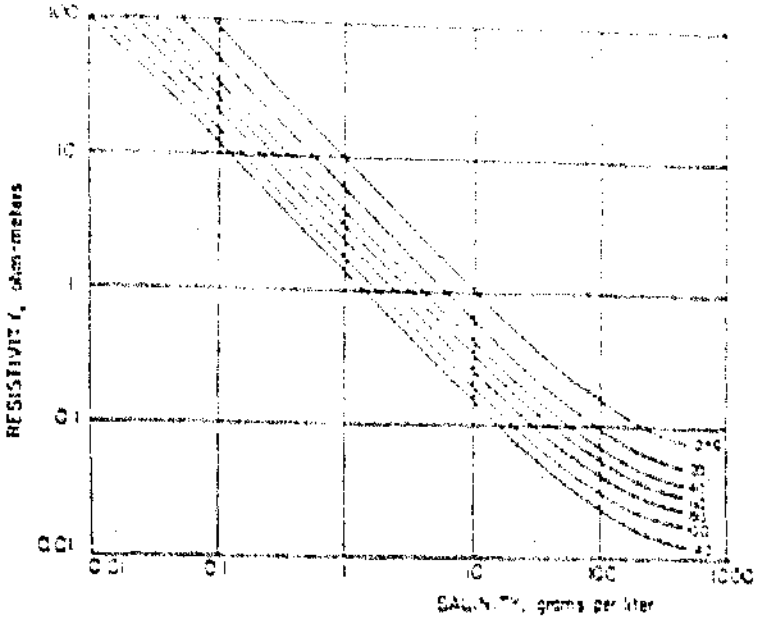

Figure 5.2: Resistivity Of Solutions Of Sodium Chloride As A Function Of Concentration And Temperature (After Dakhnow, 1962)

5.1.1 Resistivity And Porosity

In 1942, Archie first recognised the fact that the ratio of bulk rock resistivity to the resistivity of the saturating fluid and the porosity are directly related over a wide range of values. This empirical relationship, (Keller & Frischknecht, 1966) known as Archie's Law takes the following form:

$$F = \frac{\rho_r}{\rho_w} = a\phi^{-m}s^{-n}$$

where F is the formation factor,

ρ_r is the bulk rock resistivity,

ϕ is the functional pore volume (porosity),

ρ_w is the resistivity of the water,

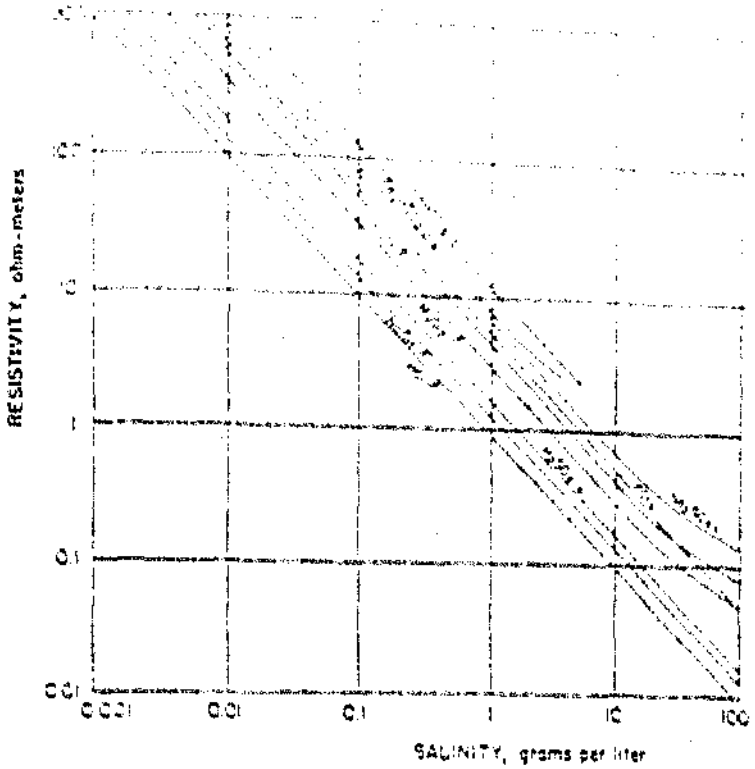

Figure 5.1: Relationship between resistivity and concentration for various salt solutions at a temperature of 18°C
(After Daknow, 1962)

However, sodium chloride is the primary and often the only salt present, so corrections can be made for the presence of other ions. Therefore, one may usually assume an equivalent salinity in terms of a salt such as sodium chloride in calculating the resistivity of water. A graph for the rapid conversion from resistivity to conductivity and to approximate sodium chloride (NaCl) concentration in milligrams per litre, at different water temperatures is shown in Figure 5.2. In the case of ground water where temperatures are relatively constant and usually approximately 20° the effect will be negligible (Meyer *et. al*, 1994).

iii) in a rock which is buried at a depth where all pore spaces are closed by overburden pressure

This study is not concerned with any of these cases and will therefore be restricted to geological formations which have at least some degree of primary or secondary porosity. By far the majority of rock formations transmit electrical current due to the mineralised water that they contain in pores, fractures, faults and in shear zones. This is known as *electrolytic conduction*

Since pure water is ionised only to a very small degree, conduction in pore waters depends largely on the *concentration* of *dissolved salts*. In general, for a given porosity, a rock which contains saline water within its pores will have a greater conductivity when the salinity of the water is high than when it is low. The *degree of saturation* (amount of water present) and the *effective porosity* or distribution of that water are additional factors which influence the resistivity of a medium (Keller & Frischknecht, 1966)

The resistivity of an electrolyte is given by the formula

$$\rho_e = \frac{1}{\sum_{i=1}^{n} c_i \, l_i \, c_i \, l_i}$$

where c_i and c_i are the concentrations of the various cations and anions in solution, respectively and l_i and l_i are the anionic and cationic equivalent conductances. The equivalent conductances are functions of concentration and temperature (Dakhnow, 1962)

In practise, since the equivalent conductances of ion species commonly found in ground water differ only slightly, the chemical composition of the ground water is not of great importance in determining the resistivity of the electrolyte. This is illustrated in Figure 5.1, where the resistivity of an electrolyte is shown as a function of the concentration of various salts

A further advantage of the Schlumberger array over other arrays is that the technique is the least prone to measurement distortions generated by electromagnetic coupling between the transmitter and receiver wires as a result of interruptions or changes in the transmitter current

Regardless of the particular electrode spread employed, there are really only two basic procedures in resistivity work. The first is known as the *vertical-electric* (VES) sounding method where the potential-electrode spacing (P P) remains fixed while the current-electrode spacing (C C) is expanded symmetrically about the centre of the spread in logarithmic steps thereby enabling the current and resultant fields to probe progressively increasing deeper sections of the subsurface. The depth of penetration of a given current depends directly upon the separation of the current electrodes as well as the nature of the subsurface layering.

The second technique is known as *lateral profiling* or mapping and involves investigation of the subsurface in a lateral direction with arrays having a more or less constant depth of penetration. This is achieved by maintaining a constant electrode spacing during successive readings while the entire spread is moved laterally as a unit.

The direction of the current was reversed to minimise the effects of both natural currents and polarisation.

5.2.3 Interpretation

Curve matching Preliminary interpretation of the resistivity soundings involves the comparison of field profiles with characteristic curves - a technique known as curve matching. The master curves are prepared with dimensionless co-ordinates and are normally drawn on a transparency. To match a field result it is only necessary to slide the master sheet around on the field profile until the latter coincides more or less with one of the master curves (or can be interpolated between adjacent master curves). Values for the apparent resistivities (ρ_a) and the depth of penetration (C_1) are

determined from the curve. Using these realistic estimates, the field curves are then 'forward-modelled' using a Schlumberger computer modelling program called VES 3.1.

For a three-layered earth, the apparent resistivity follows one of four basic types as shown in Figure 5.5.

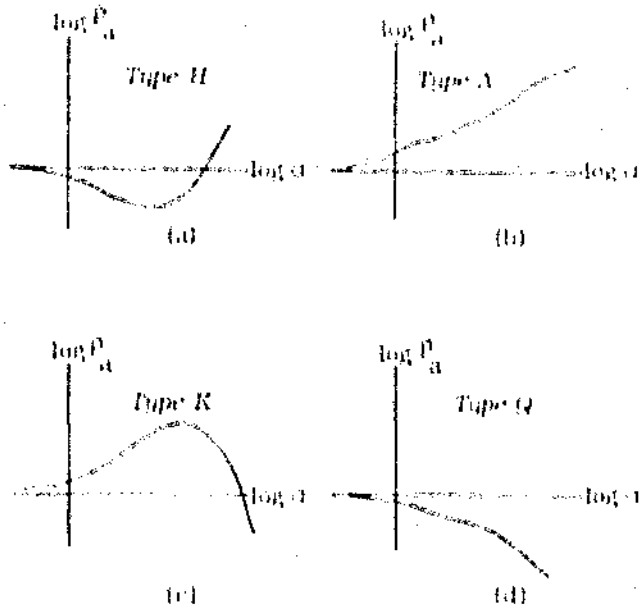

Note: 'log a' refers to log (C_1C_2), where (C_1C_2) is the current electrode spacing.

Figure 5.5. Four basic types of three-layered resistivity curves: (a) $\rho_1 < \rho_2 > \rho_3$ Type H; (b) $\rho_1 < \rho_2 < \rho_3$, Type A; (c) $\rho_1 > \rho_2 < \rho_3$, Type K; (d) $\rho_1 > \rho_2 > \rho_3$, Type Q.

5.2.2 *Electrode Layout And Field Procedure*

A variety of electrode configurations are possible, all of which are suited to specific applications. Since the presence of horizontal or gently dipping beds of differing resistivities is best detected by the expanding spread, the *Schlumberger (gradient)* technique was employed for determining the depth, structure and resistivity of the flat-lying sediments of tailings dam (4L4). For the Schlumberger arrangement illustrated in Figure 5.4, the apparent resistivity is given by:

$$\rho_a \approx \frac{\pi l^2}{2l}\left(\frac{\Delta V}{I}\right)$$

where: $L = \frac{1}{2}(C_1C_2)$; C_1C_2 is the current electrode spacing,

$l = \frac{1}{2}(P_1P_2)$; P_1P_2 is the potential electrode spacing

I is the current (Amperes) and

ΔV is the potential drop (volts) (Telford, 1990).

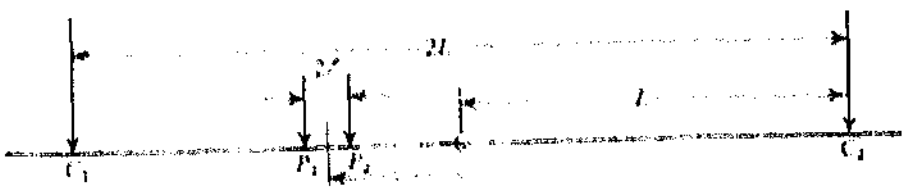

Figure 5.4: Schematic diagram illustrating the Schlumberger electrode configuration (after Telford, 1990)

5.3.3 Interpretation

A typical profile of the electromagnetic response due to a vertical conductor is shown schematically in Figure 5.7

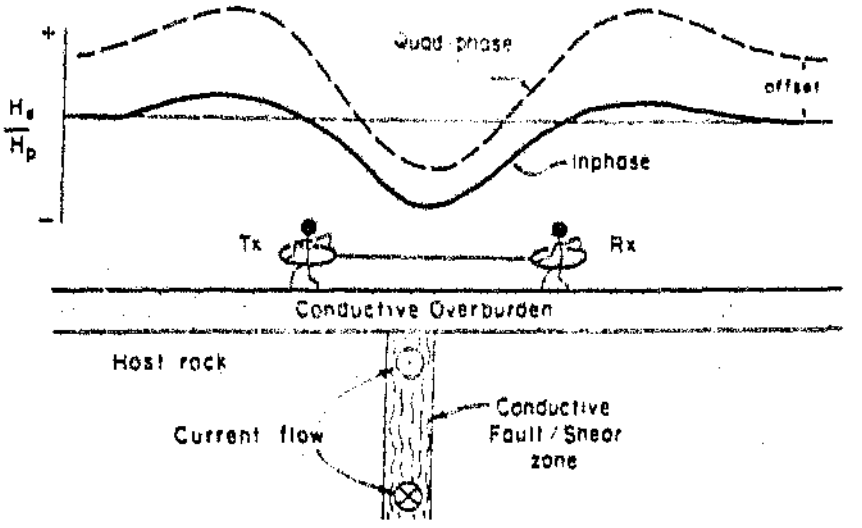

Figure 5.7: Horizontal loop electromagnetic (HLEM) response for a vertical thin sheet conductor of poor and good conductivity. Horizontal scale: x/L. (Modified after Botha et. al, 1992)

The response profile is symmetric about the y-axis and has a negative anomaly over the conductor, flanked by two positive "shoulder". The response is explained by Botha et. al., (1992) as follows.

- When both the transmitter and receiver coils are to one side of the conductor, the response is positive as the primary and secondary magnetic fields measured at the receiver location superimpose (i.e. add).
- When either the reciever/transmitter coil is located directly over the conductor, the response is zero due to the zero coupling configuration of the coils with the secondary magnetic field or the conductor, respectively.

$$\frac{H_s}{H_p} = \frac{(\omega\mu_0\sigma s^2)}{4}$$

where H_s is the secondary magnetic field at the receiver coil,

H_p is the primary magnetic field at the receiver coil,

$\omega = 2\pi f$

f is the frequency (Hz),

μ_0 is the permeability of free space,

σ is the ground conductivity (mho/m),

s is the intercoil spacing (m) and

$i = \sqrt{-1}$

The ratio of the secondary to the primary magnetic field is linearly proportional to the terrain conductivity. Given this ratio, the apparent conductivity indicated by the instrument is defined from the preceding as

$$\sigma_a = \frac{4}{(\omega\mu_0 s^2)}\left(\frac{H_s}{H_p}\right)$$

The M K S units of conductivity, are the Siemen per meter or the mS per meter

5.3.1 Instrumentation

A frequency domain system known as the EM34-3 was used in the survey. The system is a two-man portable, consisting of a transmitter and a receiver coil which are flexibly connected by a cable which acts as a reference from the transmitter coil. The transmitter and receiver coils may be held in a horizontal or vertical coplanar configuration in order to detect the vertical and horizontal magnetic components, respectively. Alignment of the coils is critical as a relative tilt of 10° between the coils

This poses a problem because a seemingly straightforward two layer curve could, in fact, be a three or four layer curve in which the electrical effect of the various thin layers has been suppressed. Therefore, since resistivity distributions that are quite different from each other can lead to similar sounding curves, every interpretation must be based on the integration of all geological and geophysical information available in the survey area.

5.3 The Electromagnetic Method

Electromagnetic methods differ principally from electrical methods in that no contact with the medium is necessary. Furthermore, the electromagnetic technique is very rapid to conduct and therefore ideal for reconnaissance studies. A transmitter coil is energised with an alternating current at an audio frequency and a receiver coil is located a certain distance away. The time-varying magnetic field, H_p, arising from the alternating current in the transmitter coil induces very small currents in the earth. These currents generate a secondary magnetic field, H_s, which is sensed together with the primary field by the receiver coil. The phase and amplitude of the currents induced in the receiver coil are a function of the electrical conductivity of the earth material. The total magnetic field is measured in terms of the voltage induced in the receiver coil.

The secondary magnetic field is a function of the intercoil spacing, s, the operating frequency, f and the ground conductivity, σ. To function as a direct reading instrument, the EM34-3 requires that the dimensionless induction number, B, satisfy the condition

$$B = \frac{\omega \mu \sigma s^2}{4} \ll 1$$

(The reader is referred to Appendix A for a detailed discussion of the induction number.) The secondary magnetic field is then a simple function of these variables (McNeill, 1980).

A typical four-layer curve is shown in Figure 5.6

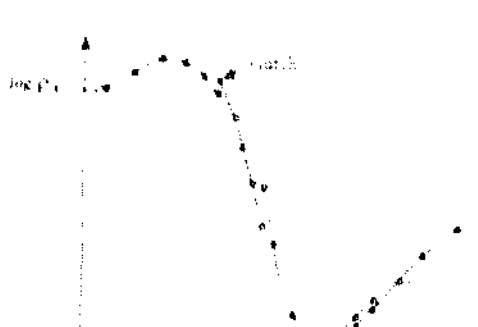

Figure 5.6 : A typical four layer Schlumberger sounding curve.

Sounding interpretation errors: Due to the interdependence of the resistivity and the thickness of a layer, ambiguity in sounding interpretation may arise owing to two factors. The first is known as the *principle of equivalence* which is defined as follows (Sheriff, 1991)

> *Two conductive layers will carry nearly the same electrical current if their ratios of thickness to resistivity (known as longitudinal conductance, S) are the same. Two resistive layers will carry nearly the same electrical current if their resistivity-thickness products (known as transverse resistance, T) are the same.*

It is therefore impossible to obtain a unique model unless one of the interdependent parameters has a known value. If boreholes exist which have been drilled to a suitable depth, it is possible to calibrate the electrical soundings and obtain the true resistivities from the known thicknesses. It is important to bear in mind that geological contacts may not necessarily coincide with geoelectric contacts.

The *principle of suppression* may also be a source of ambiguity in modelling. Sheriff (1991) defines the principle as follows

> *Resistant layers sandwiched between conducting beds are electrically equivalent if the product of their thickness and resistivity are the same.*

- When both coils straddle the conductor, the secondary magnetic field measured at the receiver coil opposes the primary field and the response is negative.

Conductor coupling refers to the orientation between the target and the primary electromagnetic field. For a conductor to be energised by the magnetic field, optimum coupling is necessary. This occurs when the magnetic field is perpendicular to the largest surface of the conductor.

The general aspects of the response of electromagnetic profiling methods are studied with the aid of response diagrams of the type shown in Figure 5.8. The effect of a dipping conductor produces an asymmetric anomaly with a higher positive shoulder on the down-dip side. Over the edge of a horizontal sheet conductor, the highest positive peak is located outside the edge and the negative peak is located over and inside the edge. Interpretation of such anomalies involves the measurement of the amplitude of the anomaly (in mS/m) from the peak to the average or background level as shown in Figure 5.7. This amplitude, measured at two or three intercoil spacings, is plotted vertically on tracing paper to the same scale as Figure 5.9. The data is then shifted horizontally and vertically on the graph until a satisfactory match is obtained, whereupon the depth is read off the x-axis.

inhomogeneities both the 10 and the 20 metre intercoil separations were used for Traverse 4. An attempt was made to use, as well, an intercoil spacing of 40 metres, but this approach was abandoned due to the electrical interference caused by overhead power lines. The station spacing along the lines traversed was 10m, however, in the vicinity of the main fracture zones, this spacing was reduced to 5m in order to improve upon anomaly resolution.

A number of limiting factors needed to be taken into account in order to optimise the design of the electromagnetic survey, viz. cultural noise in the form of:

- Traffic noise - the Southern boundary of the study area is bordered by a busy highway and consequently, field measurements were recorded over the relatively "quieter" weekend period.

- Electromagnetic coupling - this effect is extremely troublesome as it results from the mutual inductance between overhead power line (50Hz) and the electromagnetic coils and cable. The electromagnetic coupling effect can be quite large when co-axial wire layouts are used.

  Electromagnetic interference was encountered on the Eastern extremes of both Lines 1 and 2 due to the power lines in the nearby vicinity. The noise manifested itself as a slow variation in the output meter reading and consequently, these variations were averaged out by the receiver operator.

- Traverses were designed perpendicular to the strike of the assumed hydraulic gradient in order to best define conductivity peaks resulting from fractured aquifers.

results in an error of 1.5% or greater, depending on the strength of the subsurface conductor. The intercoil spacing is measured electronically so that the receiver simply reads a meter to accurately set the coils to the correct spacing which can be 10m, 20m or 40 metres so as to directly vary the effective depth of exploration (Table 5.1). The measurement recorded at the receiver coil is plotted midway between the transmitter and receiver coils. The terrain conductivity is displayed on a second meter which is calibrated in terms of milli-Siemens per metre.

Intercoil Spacing (m)	*Operating Frequency (Hz)*	*Maximum Exploration Depth (m)* *Horizontal Dipoles*	*Maximum Exploration Depth (m)* *Vertical Dipoles*
10	6,400	7.5	15
20	1,600	15	30
40	400	30	60

Table 5.1: Exploration depths for EM34-3 at various frequencies and intercoil spacings (Modified after McNeill, 1980)

5.3.2 Field Procedure

In order to locate fractured aquifers which act as narrow conductive zones or sheet-like conductors, electromagnetic profiling was carried out at the base of residue 4L3 and on the Northern and Southern banks of the Natalspruit River (Figure 1.1). Traverses 1-3 were surveyed with an intercoil spacing of 20m in both the horizontal and vertical coplanar modes. The former mode was preferred in view of the improved depth of penetration and the reduced sensitivity to near surface changes in conductivity (McNeill, 1980). In order to differentiate between surface conductivity

5.5 Geophysical Survey Layout

The layout of the conductivity and seismic traverses is presented in Figure 5.13. Four electromagnetic traverses (EM 1-4) were positioned perpendicularly to the direction of shallow subsurface water flow which was determined by the Water Research Commission in 1988 so as to optimally locate fractured aquifers (or faults) which act as narrow conductive zones.

Jones et al (1988) recognised tailings dam 4L4 as a significant source of pollution of the Rosherville Stream. In order to gain a better understanding of the subsurface structure, layering of the tailings dam and how waste material is passed through this residue, three resistivity profiles (VES 1-3) were sited on the top of the dam.

Finally, a seismic traverse was sited at the base of tailings dam, 4L3, (in the same position as EM traverse 4) so as to "map" the subsurface basement profile. Any wastewater stream emanating from tailings dam 4L3 and residues further north of this dam would flow along the basement rock in a direction perpendicular to the traverse. The largest volume of fluid would be concentrated in basement "depressions" and fractures / faults. Seismic profiling enables one to locate these focused areas of flow, thereby allowing siting of potential monitoring and "dewatering" boreholes.

Time-depth conversion

The raw data consists of sets of arrival times recorded at geophones spaced at regular intervals from the shotpoint. This information is plotted in the form of a reversed travel time graph where traveltimes are plotted as a function of distance from the source. The interpretation proceeds in a stepwise fashion to solve for each successively deeper layer. Three types of approach may be adopted to refraction interpretation, namely

i) Analytical methods (application of equations),

ii) Delay-Time methods and

iii) Wavefront reconstruction methods (Telford, 1990)

In this particular study the interfaces between subsurface layers are non-parallel and subsequently, the velocities obtained from the curves are apparent and not true velocities. Both analytical and delay time methods were applied in the interpretation of Line 1. The latter method is the least susceptible of the three interpretation techniques to the difficulties typically encountered when dealing with refractors that are curved or irregular.

The meaning of the term "delay time" is illustrated by reference to Figure 8.10, in which the delay time is defined at the shotpoint and at the detector.

> *"The delay time is the difference between the time actually spent by the pulse travelling in its upward or downward path through the upper layer and the time it would have spent travelling at the refractor velocity along the normal projection of this path on the interface."* (Redpath, 1973)

propagation. Until a certain angle of incidence, known as the *critical angle of incidence*, is reached, almost all of the compressional energy is transmitted into the higher velocity medium. When a ray is critically refracted, it travels along the boundary between the two media at the higher of the two velocities. Furthermore, as the critically refracted ray travels along this boundary, it continually generates seismic waves in the lower-velocity layer that depart from the boundary at the angle of critical incidence. These waves are referred to as *headwaves*. It is the arrival times of these headwaves that are recorded and converted to produce a velocity-depth section, which is ultimately used to map the subsurface structure of the survey area.

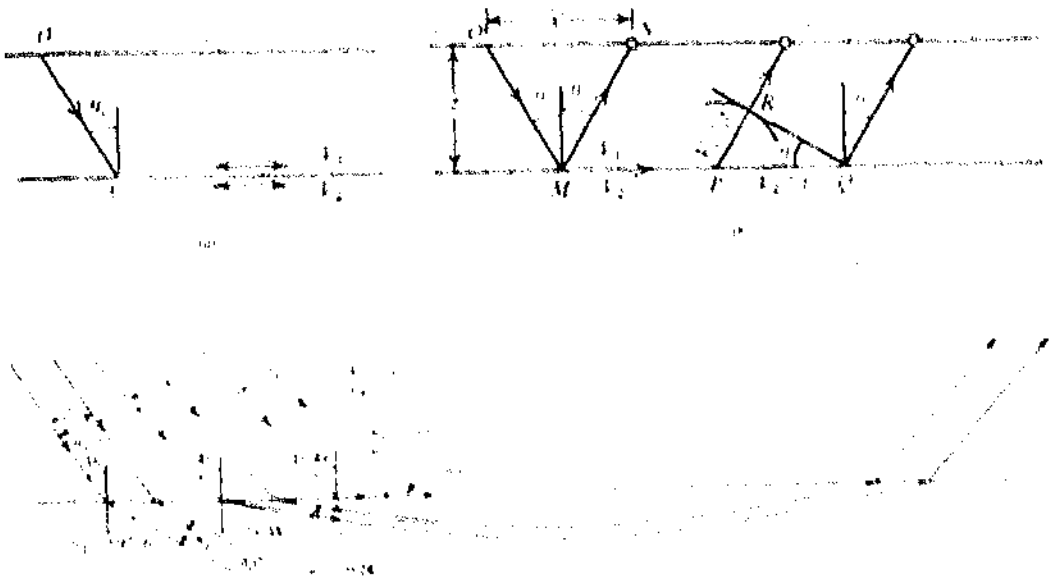

Figure 2-3. Snell's Law relations for incident P wave. (a) Motion at the interface; (b) Wavefront energy transmission at critical angle; (c) Changes in beam width upon refraction and bending or refracted wavepath because of the velocity gradient in the high velocity medium. (Modified after Sheriff, 1991)

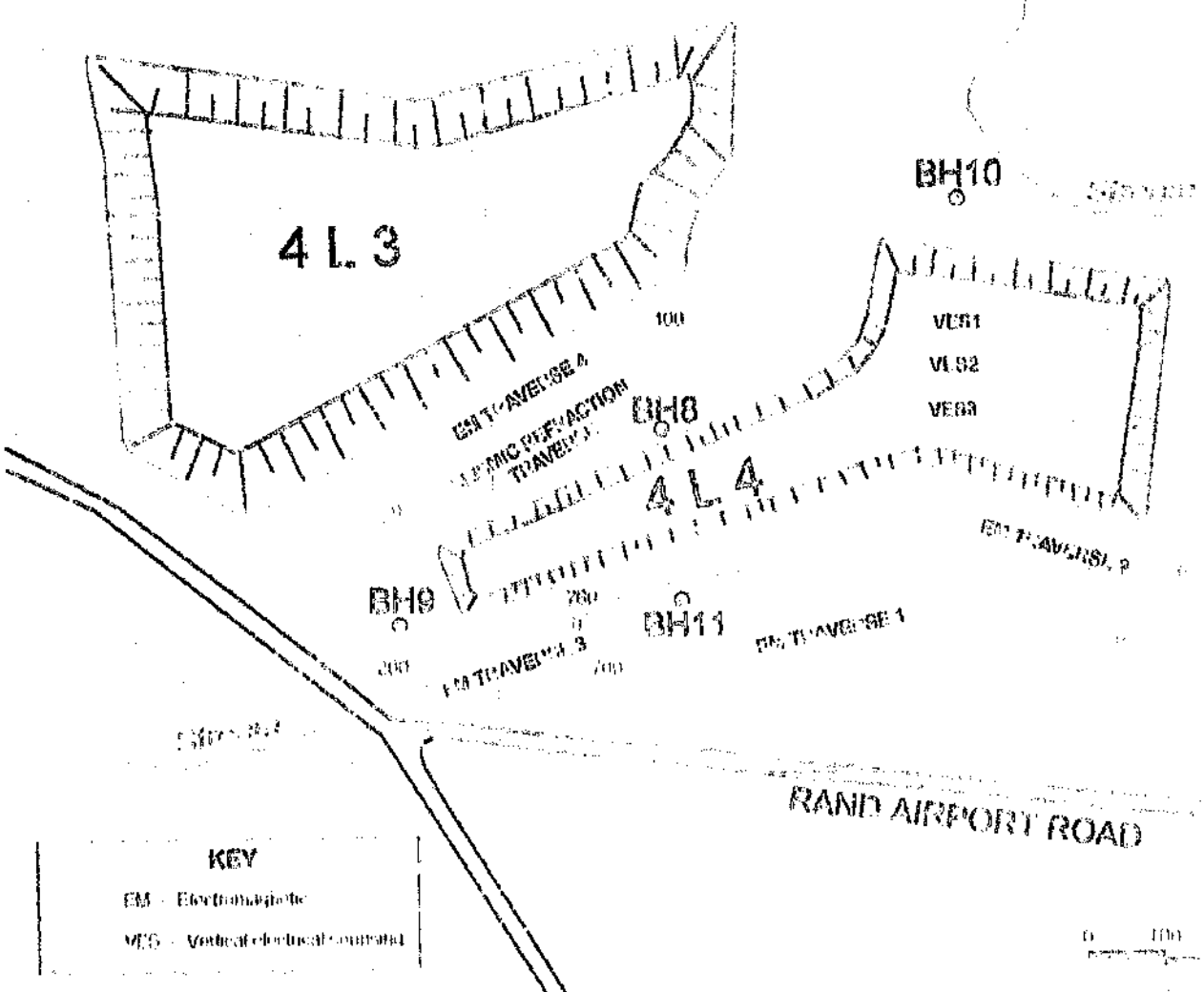

4 L 3
BH10
100
VES1
VES2
VES3
EM TRAVERSE 4
BH8
4 L 4
BH9
BH11
EM TRAVERSE 1
EM TRAVERSE 3
RAND AIRPORT ROAD
KEY
EM - Electromagnetic
VES - Vertical electrical sounding

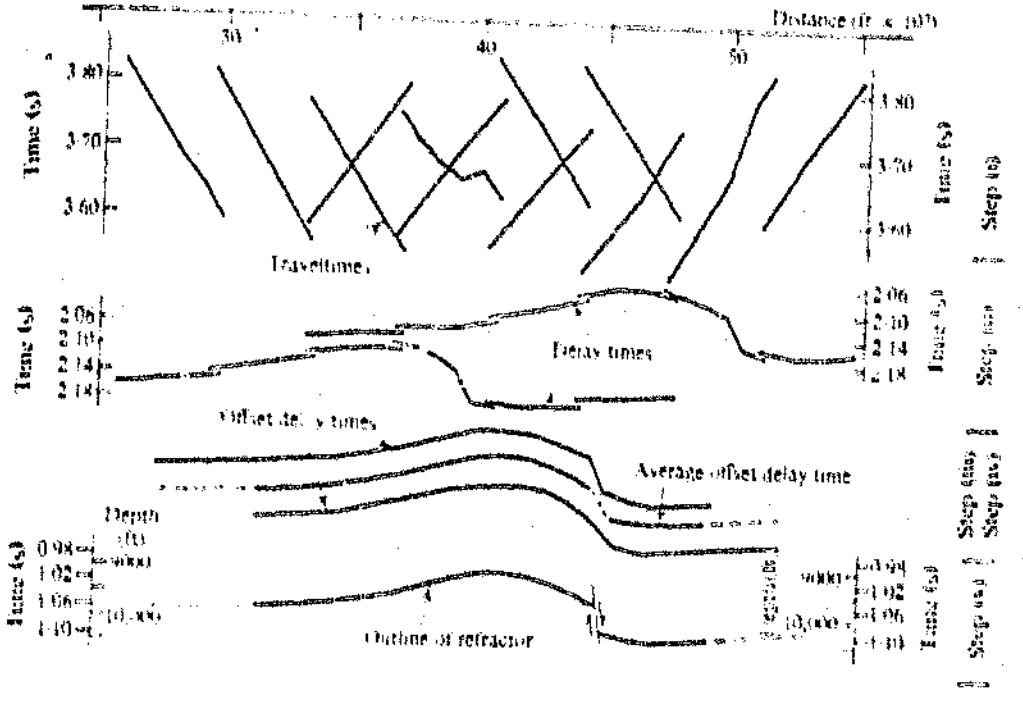

Figure 8.11: Delay Time methods used in the interpretation of seismic depths (After Redpath, 1973)

5.4.1 Instrumentation

The basic refraction method involves the use of an instrument known as a seismograph which measures the interval of time between the impact at a particular location and the arrival of elastic seismic waves at one or more sensing devices (geophones) some distance away. A geophone is a type of microphone (transducer) that converts seismic vibrations to electric impulses. These electric impulses are transmitted by cable to the seismograph where they are amplified and displayed on a CRT screen, enabling the quality of data to be monitored in the field. In this study the multichannel ES-122S Seismograph was used and the energy source was supplied by a ten pound hammer which was struck against a steel plate. The instant of impact is determined by an inertial switch attached to the hammer. The system is operated from an external 12-volt source, typically a storage battery. The instrument draws approximately 0.5 amperes normally with peak current perhaps twice as high during the brief periods when the plotter is running (E.G&G Geometrics, 1990).

(The reader is referred to Appendix B for a detailed description of the field procedure applied in this study.)

5.4.3 Data Processing and Interpretation

Elevation corrections

Variations in the elevation of the surface affect traveltimes and it is therefore necessary to correct for such changes. A reference datum is selected and corrections are calculated so that, in effect, the shotpoints and geophones are located on the datum surface. For the purpose of this study a horizontal reference datum was used due to the fact that elevation variations are small in the study area.

5.4 *The Seismic Refraction Method*

The basic technique of seismic refraction consists of generating compressional waves and measuring the time required for the waves to travel from the impulsive energy source to a series of geophones, disposed along a straight line, directed towards the source. Propagation of the waves depends on the elastic properties and the density of the rocks through which they travel. From a knowledge of the travel times and the distances travelled, one attempts to reconstruct the paths of the seismic waves. Structural information is inferred from interpretation methods based on the laws of energy propagation.

The propagation of seismic energy through subsurface layers is described by the same law that governs the propagation of light rays through transparent media, namely, Snell's Law which states the following:

> *When a wave crosses a boundary between two isotropic media, the wave changes direction such that* $\frac{\sin i}{V_1} = \frac{\sin r}{V_2} = p$
>
> *where* i *is the angle of the incident wave with a velocity of* V_1,
> r_1 *is the angle of refraction and*
> p *is the raypath parameter (Sheriff, 1991).*
>
> *The refraction or angular deviation that the seismic pulse undergoes when passing from one material to another depends upon the ratio of the transmission velocities of the two materials.*

Snell's Law, together with the phenomenon of "critical incidence" is the physical foundation of seismic refraction surveys. These phenomena are illustrated in Figure 5.9, which shows a medium with a velocity, V_1, underlain by a medium with a higher velocity, V_2. When a wave encounters the interface separating the two media, part of its energy is reflected and remains in medium 1. The balance of the energy is refracted into medium 2 and the wave undergoes an abrupt change in the direction of

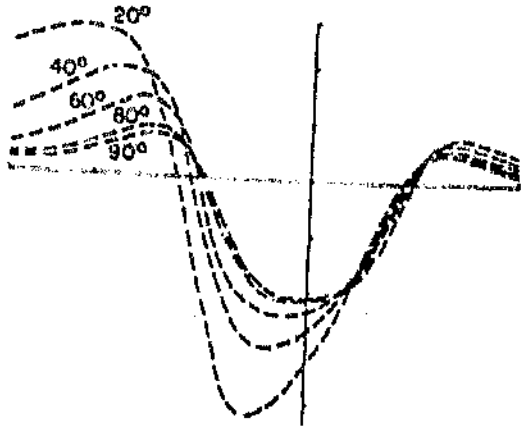

Figure 5.8: Response diagram used in the interpretation of EM/34-3 anomalies shows effect of varying dip on profile shape.

(After McNeill, 1980)

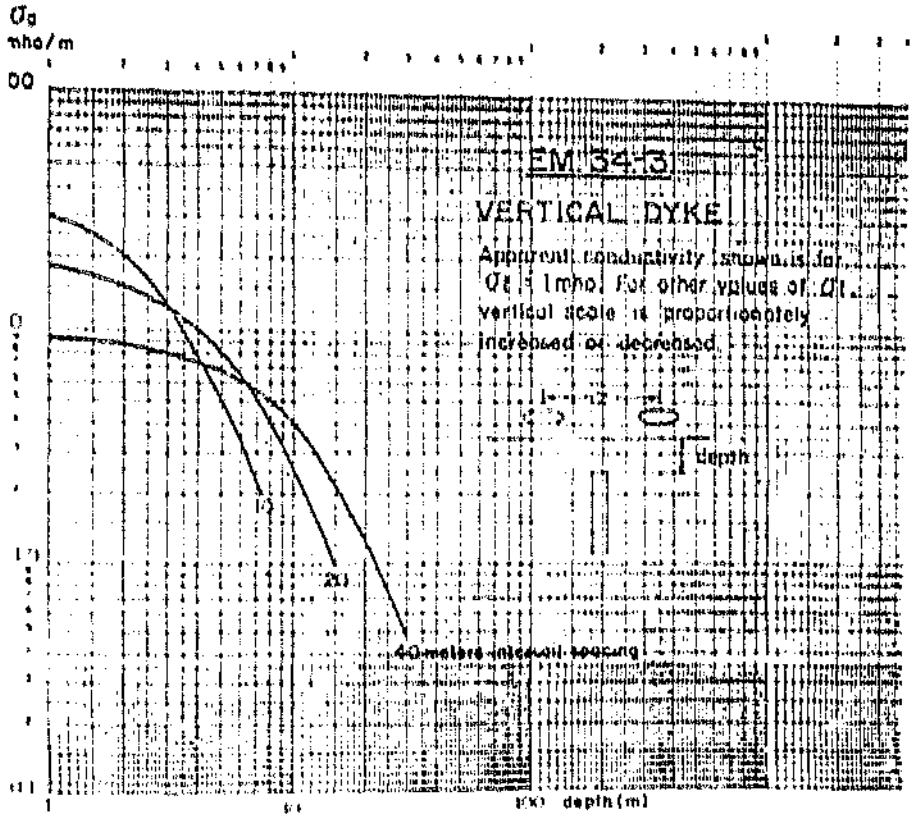

Figure 5.9. Depth Determination of Electromagnetic Conductors

(After McNeill, 1980)

Figure 6.7 :ELECTROMAGNETIC PROFILE 4
10m intercoil spacing

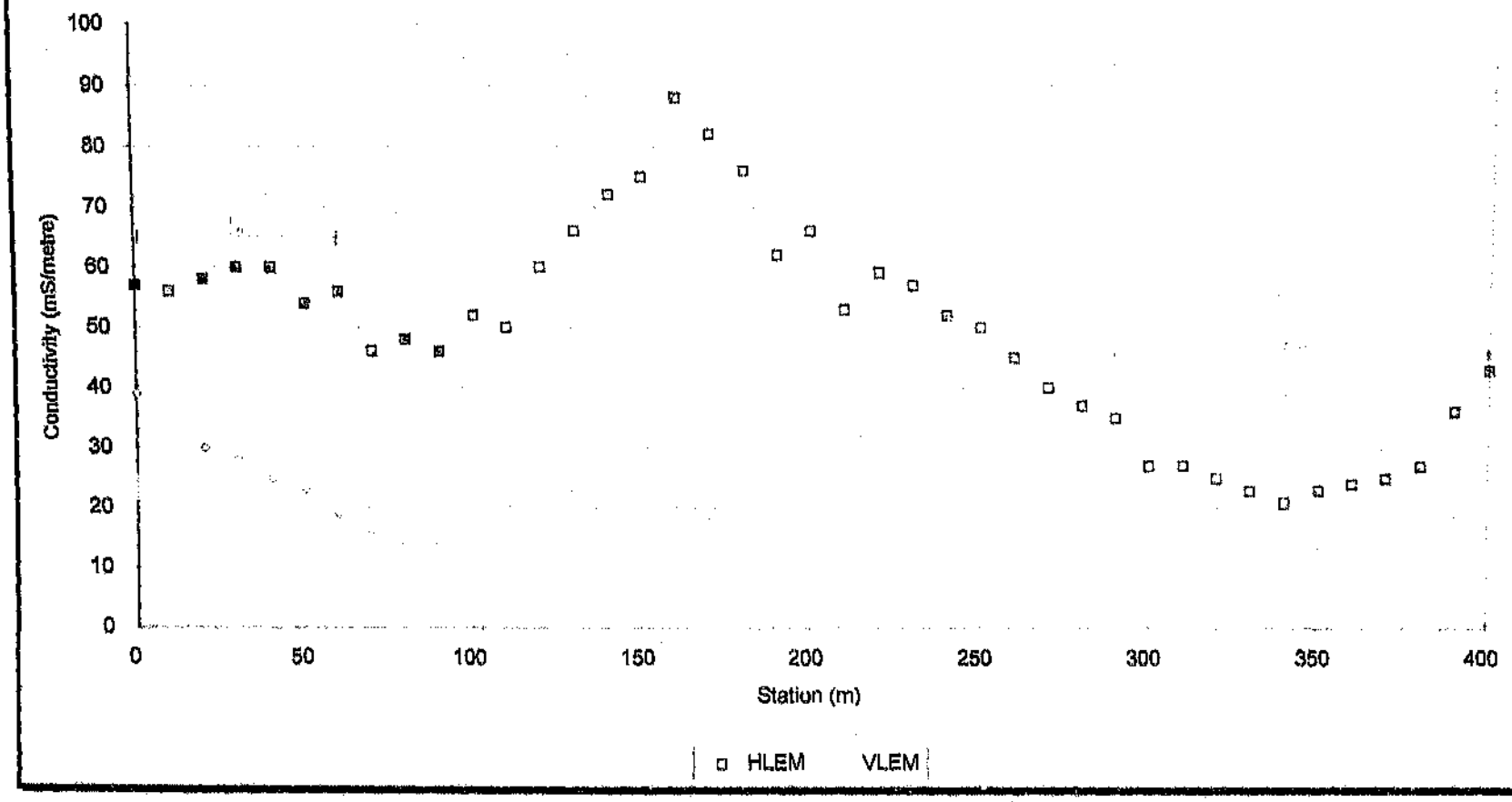

(iii) The relatively resistive zone B is broader and extends from Station 250 through Station 100.

The concomitant increase in amplitude of the well-defined anomaly in Figure 6.7 with the increase in coil separation suggests that the response is caused by seepage water migration (extending to a depth of approximately 30 metres) as opposed to near-surface salinity variations.

Examination of a borehole log produced by SRK (cited in Jones et al. 1988) in the vicinity of the traverse reveals that the interface between weathered quartzite and the underlying fresh quartzite bedrock occurs at a depth of 3.2 metres, coincident with the level of seepage concentration. Thus, one may conclude that the contaminated water flows along the boundary between the relatively permeable upper formation and the practically impermeable underlying quartzitic bedrock.

Figure 6.7 is characterised by three distinctive features, namely:

i) A broad conductive zone, A_{II}, spanning Stations 0 to 60. Such a zone is most likely representative of fractured and weathered coarse-grained quartzitic rock through which seepage of contaminated groundwater occurs.

ii) A well-defined positive peak occurs at Station 160. This anomaly is flanked by a relatively smaller peak centred at Station 200. (The latter response is not reflected in the vertical loop profile shown in Figure 6.7).

iii) A relatively resistive zone, B_{II}, extending from Stations 290 to 400.

Figure 6.8, which illustrates the results of the 20 metre intercoil separation shows all of the above-mentioned features with a few notable variations:

i) The maximum apparent conductivity is far higher than that recorded for the 10 metre dipole spacing - conductive zone, A_{II}, has an apparent conductivity of 114 mS/m, almost double that recorded in Figure 6.7. The zone is relatively narrower and better defined, extending from Stations 20 to 80.

ii) The well-defined positive peak has migrated 20 metres towards the centre of the profile in a northerly direction. The weaker conductor evident in the horizontal loop profile (Figure 6.7) at Station 200 has increased with respect to amplitude with an increase in coil separation (Figure 6.8). Furthermore, although the vertical loop mode failed to reflect this conductor with a 10 metre intercoil spacing, it was observed in the results of the larger spacing corresponding to a greater exploration depth, viz. 15 metres.

Figure 6.5: ELECTROMAGNETIC TRAVERSE 3
HLEM - 20m intercoil spacing

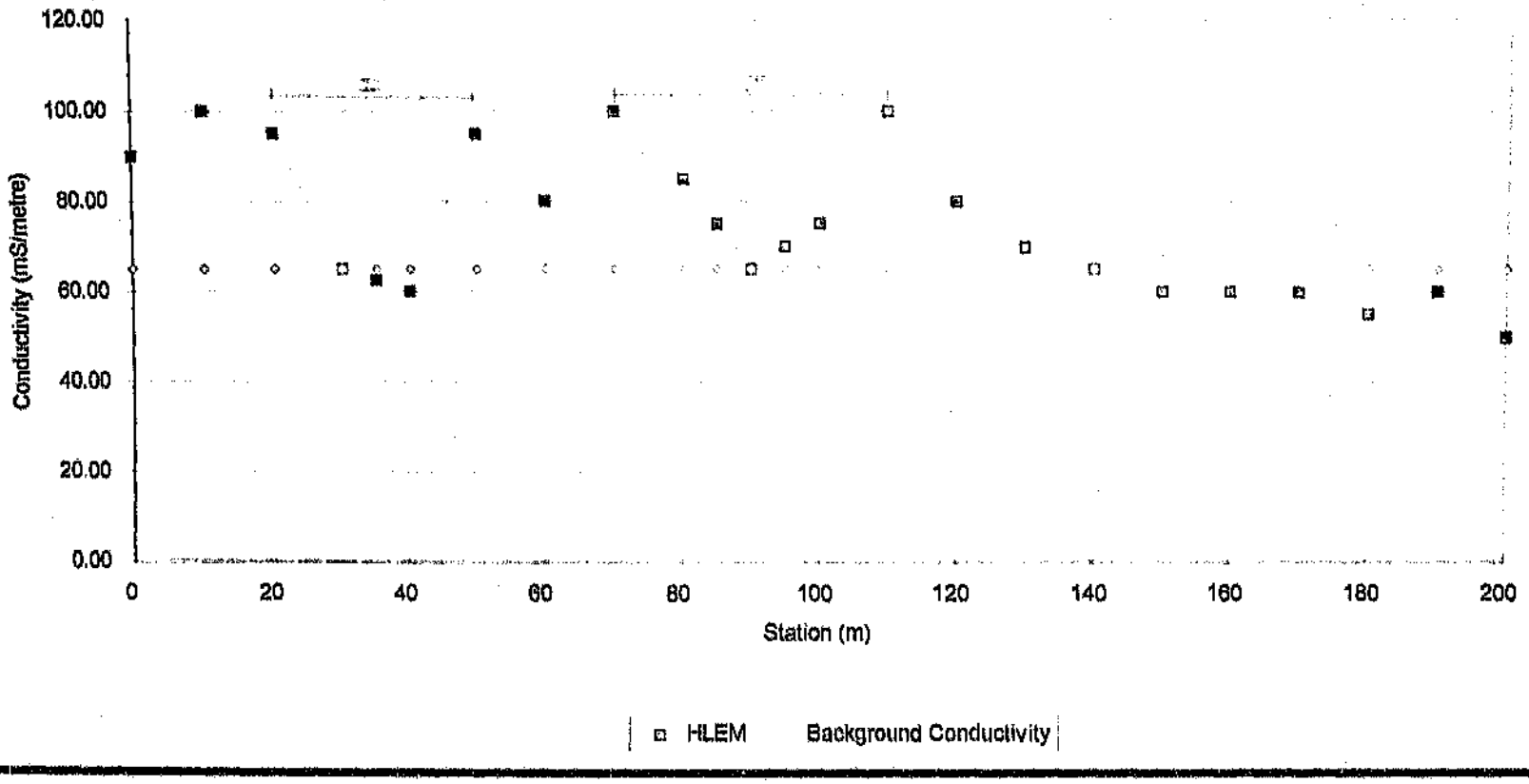

Anomaly II is flanked by a broad region (70 metres) which spans a distance between Stations 600 and 670. This conductive zone has a maximum apparent conductivity ranging between 110 and 130 mS/m and is believed to be due to a faulted, sheared or weathered region in which contaminated groundwater has accumulated.

6.3 Electromagnetic Traverse 3

Two distinctive anomalies, I and II (Figure 6.5), with maximum apparent conductivities of 100 mS/m, were identified at Stations 35 and 90. The former response is indicative of a conductor which dips steeply (~70°) towards the West, while the latter anomaly is symmetrical and as such, represents a vertical conductor.

These anomalies are manifested in the vertical loop profile (Figure 6.6) as positive peaks centred at Stations 40 and 90, with maximum apparent conductivities of 100 mS/m. The effective exploration depth corresponding to this mode of profiling is 15 metres.

6.4 Electromagnetic Traverse 4

Figures 6.7 and 6.8 depict the profiles for Traverse 4 corresponding to the horizontal and vertical dipole spacings. The maximum positive amplitude responses were obtained using the vertical dipole mode. This mode is characteristically more sensitive to near-surface variations in topography and as such, results are relatively more complex than those obtained using the horizontal dipole mode.

In order to differentiate between surface conductivity inhomogeneities and the saline plume, the author used two different transmitter/receiver coil separations, viz. 10 and 20 metres, to obtain different depths of investigation.

Figure 6.4 :ELECTROMAGNETIC PROFILE 2
V/LEM - 20m intercoil spacing

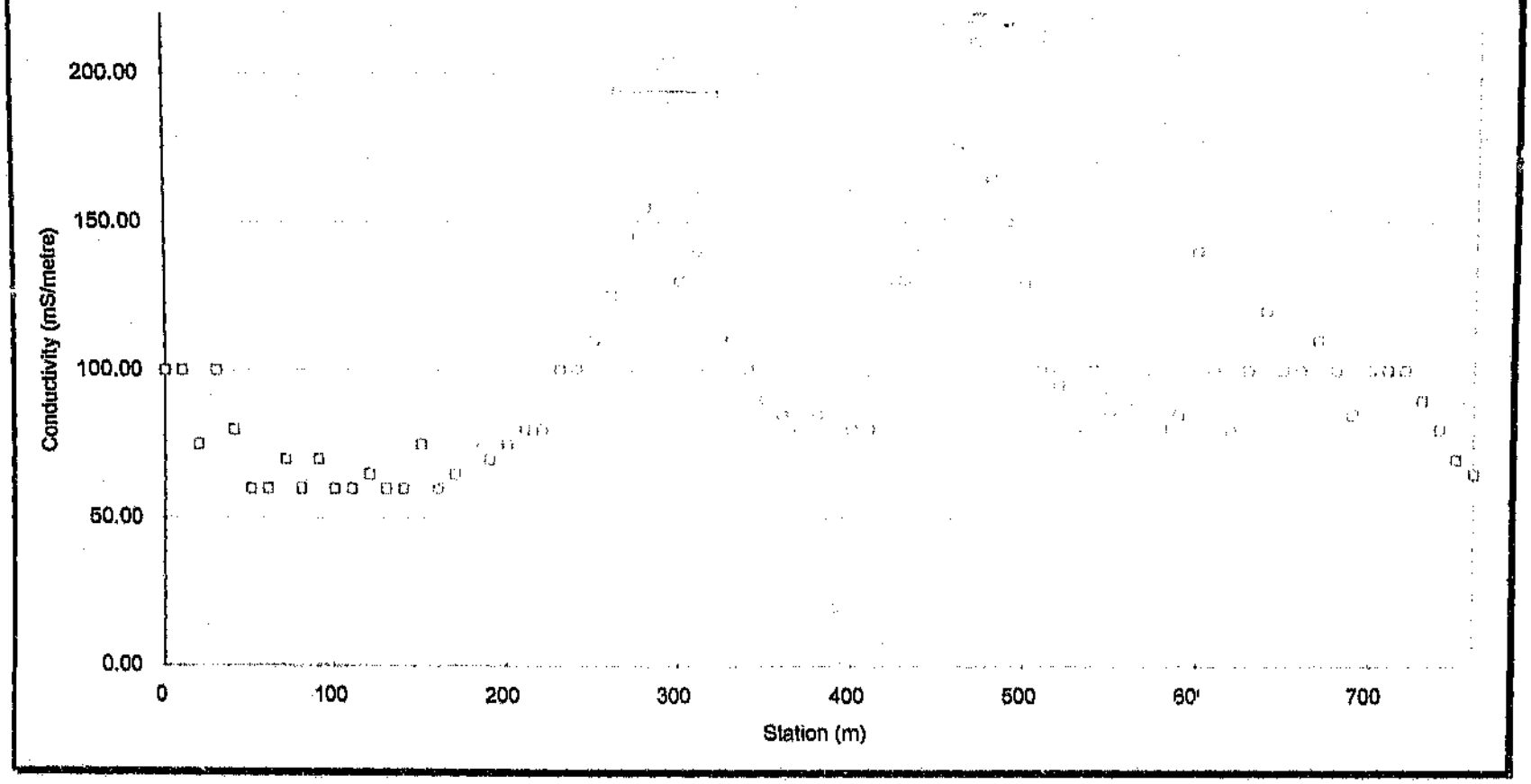

Figure 6.3 :ELECTROMAGNETIC PROFILE 2
HLEM - 20m intercoil spacing

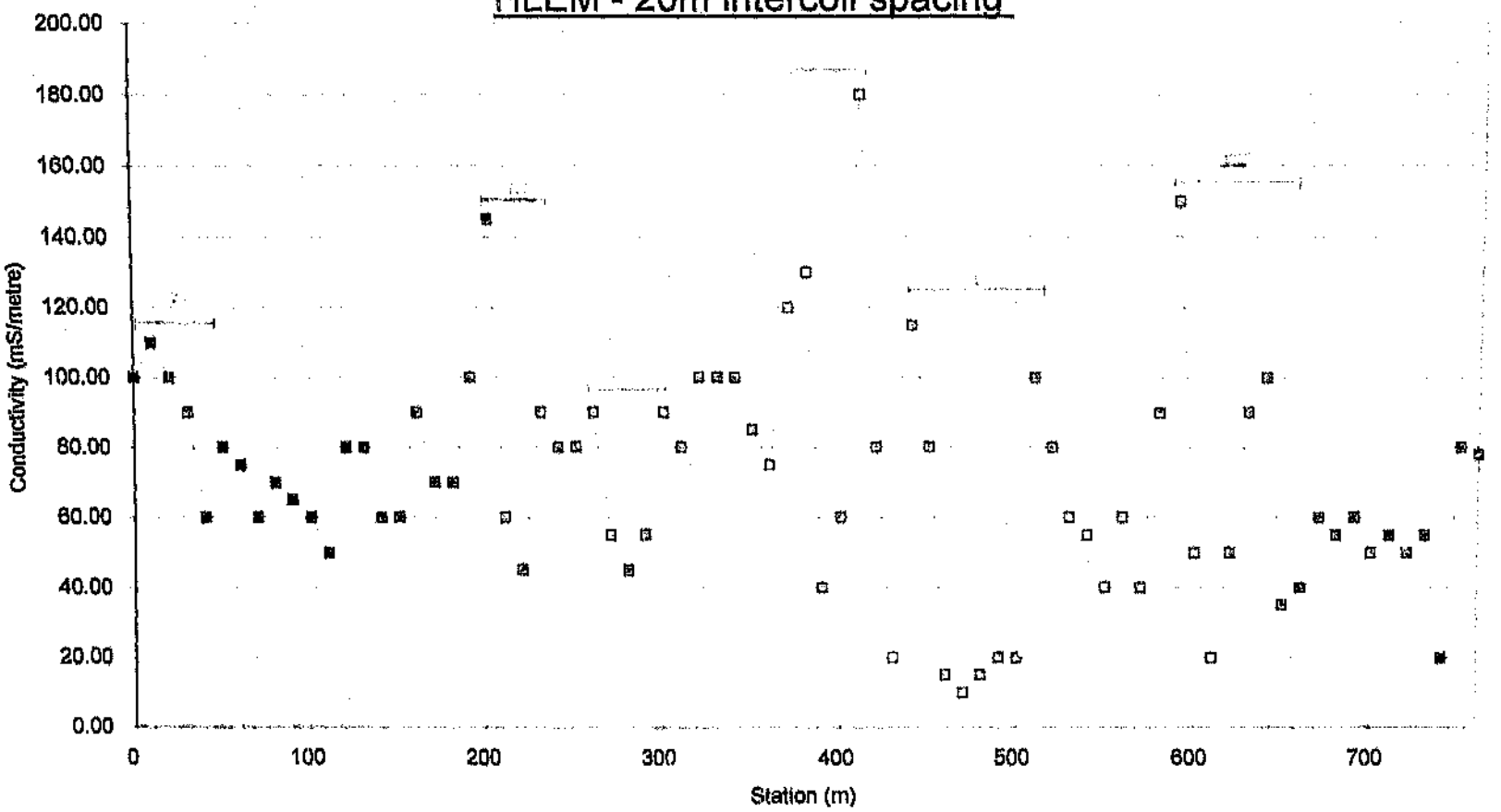

(Figure 6.2), which are all in excess of 40 metres wide, represent minor seepage plumes occurring in localised regions of relatively permeable quartzite.

Figure 6.1 shows a single-point anomaly at Station 60 which may be attributed to the presence of a nearby metal borehole casing situated at a depth of 1.5m.

6.2 Electromagnetic Traverse 2

The survey results for the horizontal coil configuration (Figure 6.3) show a series (I-VI) of anomalies representative of vertical or sub-vertical fractures or fissures occurring at a maximum depth of 30 metres. The most prominent of these features, viz. Anomaly IV, occurs at Station 390. The relatively steeper right-hand "shoulder" of the response indicates that the conductor dips in an Easterly direction at an angle of approximately 55°. The maximum apparent conductivity of this anomaly is 180 mS/m, which is significantly higher than the most pronounced anomaly evident in Profile 1 (100 mS/metre).

Anomalies I, II and VI are centred at Stations 25, 205 and 595 metres, respectively and are indicative of fractures or fissures along which seepage of contaminated groundwater occurs. These conductors dip at angles of 55-60° in a westerly direction. The negative anomaly V, dips gently to the West, while Anomaly III represents a vertical conductor with a maximum apparent conductivity of 90 mS/m.

Figure 6.4 depicts the profile for the horizontal dipole mode (vertical coil configuration) and is characterised by a far lower noise level than the vertical dipole mode. Two positive peaks (I and II) with maximum apparent resistivities of 180 and 210 mS/m, are centred over Stations 290 and 470, respectively. These distinctive features correlate with the negative-trending anomalies encountered at Stations 285 and 470 in Figure 6.3.

Figure 6.2: ELECTROMAGNETIC PROFILE 1
VLEM - 20 m intercoil spacing

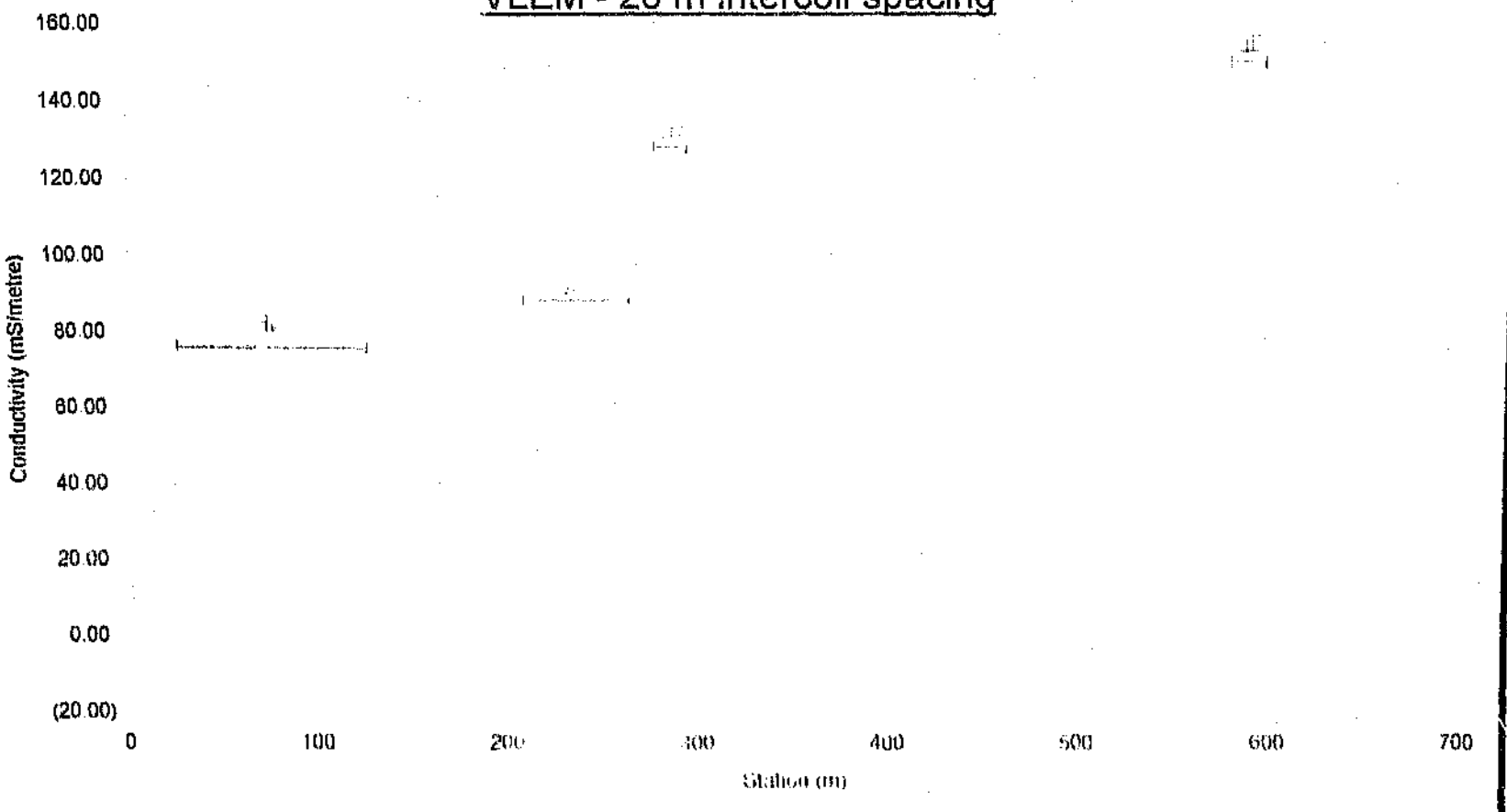

Figure 6.1 :ELECTROMAGNETIC PROFILE 1
HLEM - 20 m intercoil spacing

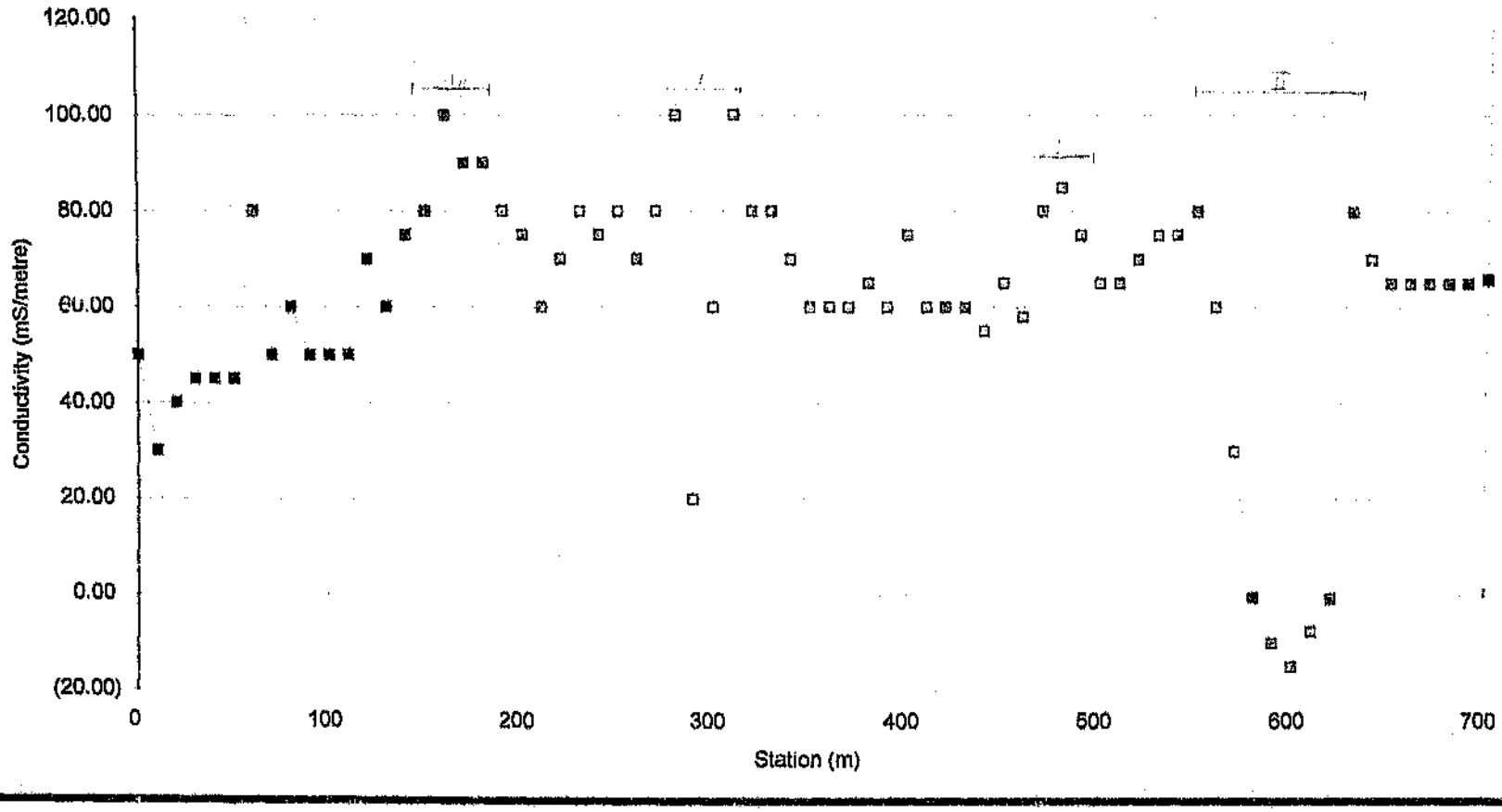

6. RESULTS AND ANALYSIS

6.1 Electromagnetic Traverse 1

Figures 6.1 and 6.2, which depict the profiles for EM traverse 1, show the results for the 20 metre vertical dipole (plane of the coils horizontal) and the horizontal dipole modes (plane of the coils vertical), respectively. Background or uncontaminated water values were found to lie between 60 and 65 mS/metre (Figure 6.1). Both profiles are characterised by the presence of two symmetrical anomalies corresponding to Stations 290 and 590. Anomalies I and II (Figure 6.1) illustrate the typical response of near vertical conductors to an induced electromagnetic field, i.e. the profile passes through the background value of conductivity, namely, 60 mS/m, at two locations, symmetrically spaced apart by a distance approximately equivalent to twice the intercoil spacing (40 metres in this case). McNeill (1980) explains the response as follows. When the EM34-3 is some distance away from the vertical conductor (in excess of two intercoil spacings), the conductivity measurement corresponds to the correct response for the homogenous subsurface or "half-space". As the instrument approaches and passes over the vertical conductor, the current flow in the conductor becomes essentially the same as if it were in free space, thus giving rise to a negative-trending anomaly as indicated by Anomaly II.

The maximum apparent conductivities at the effective depth of exploration (30 metres) for the vertical dipole mode are 100 and 80 mS/m for anomalies I and II, respectively. Figure 6.2 shows that the corresponding apparent conductivities for the horizontal dipole mode, with an exploration depth of 15 metres, are somewhat higher, viz. 12 and 14 mS/metre, respectively.

These anomalies are indicative of near-vertical fissures or fractures within the otherwise impermeable quartzite, which provide conduits for the movement of groundwater. The broad conductive zones, A_1 and B_1 (Figure 6.1); and A_2 and B_2,

oxidation process. Willier and Loos (1984) have shown that bacterial activity is found in regions of high moisture content and low pH. However, at greater depths within the deposit, where conditions may be saturated, oxygen diffusion would seem to be depressed to a level unable to support the bacteria.

6.6.3 Electrical Layer 3: Perched Aquifer

All sounding curves reveal the presence of a layer of contaminated ground water starting at depths ranging between 5.5 metres in VES 1 and 8.0 metres in VES 3. This layer gives rise to the very low apparent resistivities (of the order of 10 ohm.metres). This conductive zone is indicative of an unconfined aquifer (i.e. the aquifer is not overlain by material of lower permeability and consequently, the water-table is "open" to the atmosphere). The transition between the zone of aeration and the zone of saturation (or phreatic zone) marks the position of the water-table. This transition is clearly illustrated in Figure 6.13.

6.6.4 Electrical Layer 4: Resistive Basement

Layer 3 is bounded below by a region of highly resistive material corresponding to the unweathered crystalline quartzite comprising the bedrock. A permeability contrast exists between this layer and the soils of the overlying Layer 3, resulting in an increased flow of contaminated water along the soil-rock boundary. A slight increase in resistivity with depth in this region (as shown in Figures 6.10, 6.11 and 6.12) may be a function of decreasing pore, fracture, fault and shear-zone porosity due to increased lithostatic load. This postulation would need to be confirmed by the results of borehole data. It is well to keep in mind, however, that fractures and faults are known to remain open to depths in excess of 15km due to departures from lithostatic loading whenever the major component of the stress tensor is other than vertical.

6.6.2 Electrical Layer 2: Resistive Tailings Material

The second electrical layer in VES 1 and 3 is significantly less conductive, averaging a resistivity of 93 ohm metres and extending to depths of 8.5 to 8.0 metres. This layer corresponds to the first electrical layer in VES 2 and represents a zone of relatively porous tailing material constituting the intermediate belt of Meinzer's classification. Such a belt occurs when the water-table is far enough below the surface for the soil-water belt not to extend to the capillary fringe. In the capillary fringe, which occurs immediately above the water-table, water is held in the pores by capillary action. The degree of saturation decreases from the water-table upwards, saturation occurring only in the immediate neighbourhood of the table.

Note that for Ves 1, the above-mentioned zone corresponds to the first electrical layer in the profile presented in Figure 6.13.

The Depth Of Oxidation

The *depth* of oxidation in Electrical Layer 2 is limited to the depth of oxygen penetration. In 1985, this depth was situated between 2m and 3m below the surface of the tailings dam and between 5m and 10m in the coarser grained sand deposit (Marsden, 1985). It has been shown (Mrost, 1973, cited by Jones et al, 1988) that complete oxidation of pyrite within the upper 0.1m of the Witwatersrand mine residues is achieved rapidly, usually within approximately one month, after which the rate of oxidation decreases to the extent that complete oxidation to a depth of about 1.0m is not usually achieved even within two to three years. Results of the resistivity survey reveal that the current depth of oxidation for the tailings dam ranges between 8.5 and 8 metres (a depth migration of approximately 2.5 metres from that recorded in 1985).

The Rate Of Oxidation

The *rate* of oxidation of pyrite is related to the availability of oxygen and the presence of the bacterium, Thiobacillus ferrooxidans, which functions as a catalyst in the

Figure 6.13: RESISTIVITY PROFILE of Tailings Dam 4L4

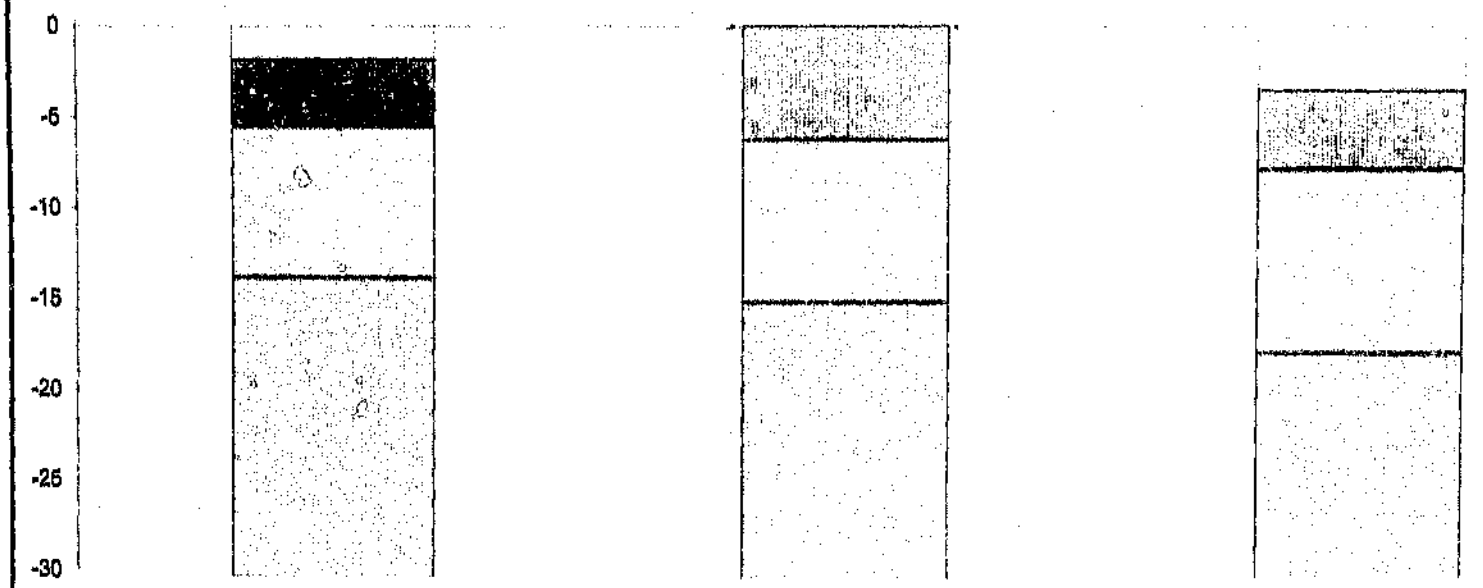

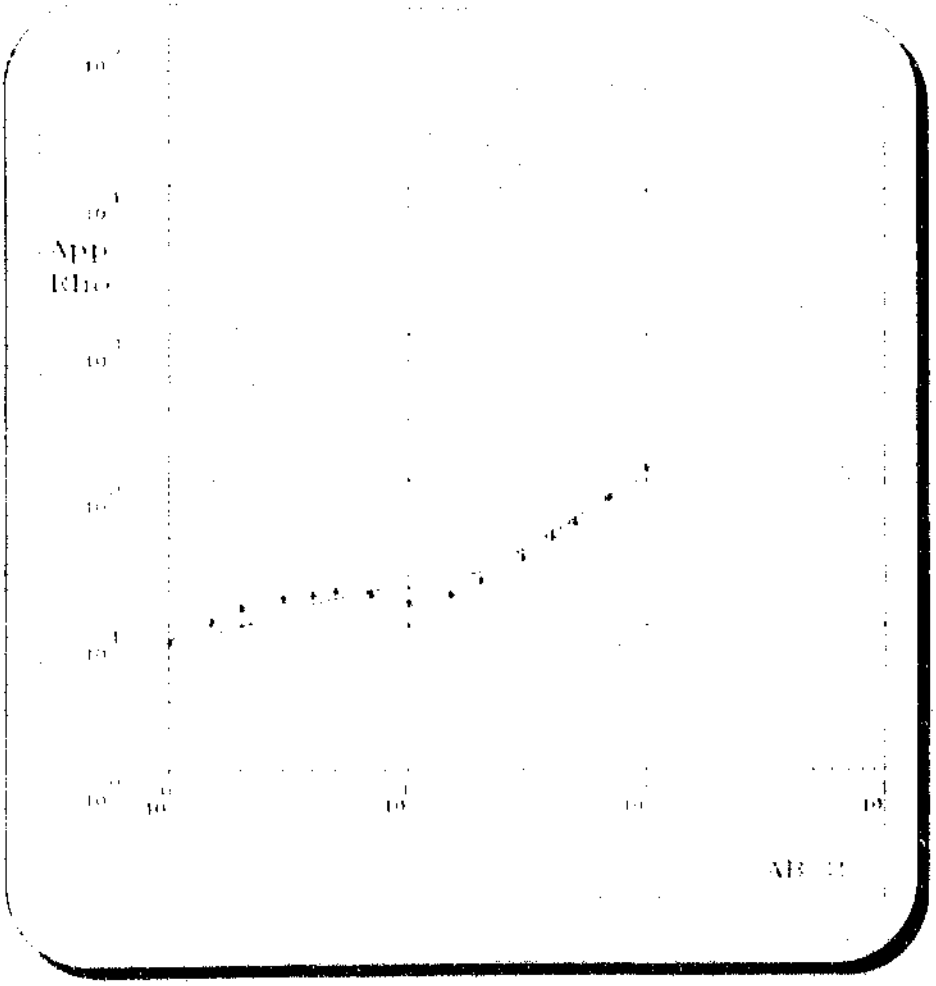

Figure 6.12: Vertical Electrical Sounding 3 (VES 3)

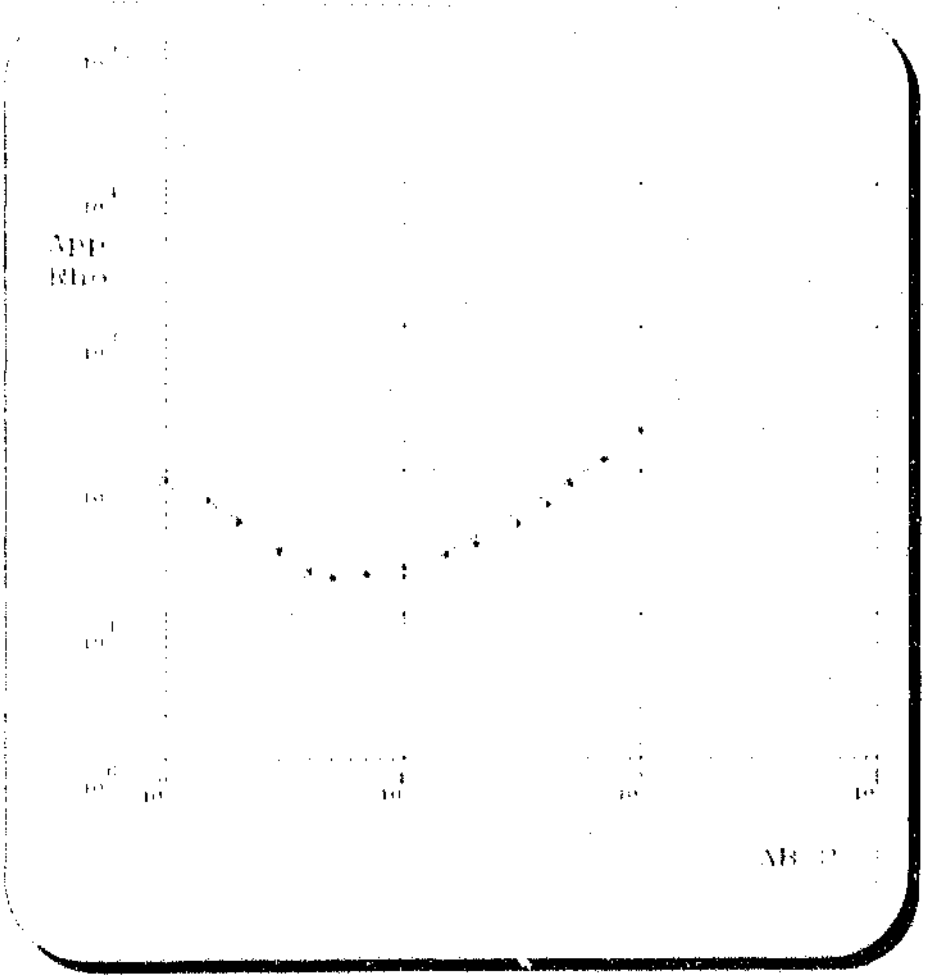

Figure 6.11: Vertical Electrical Sounding 2 (VES 2)

degree of moisture was observed in this soil water belt, the apparent resistivities are anomalously low. Furthermore, a thin layer of crusty material was observed in the upper 10cm of the dam with the implication that the elevated conductivity levels may be attributed to a high salt concentration within this layer.

Note that this is not the case as shown by Sounding 2. The apparent resistivity of the first layer is an order higher (~100 ohm meters). The absence of "Electrical Layer 1" in Sounding 2 is due to the substantial erosion which has occurred in this localised area.

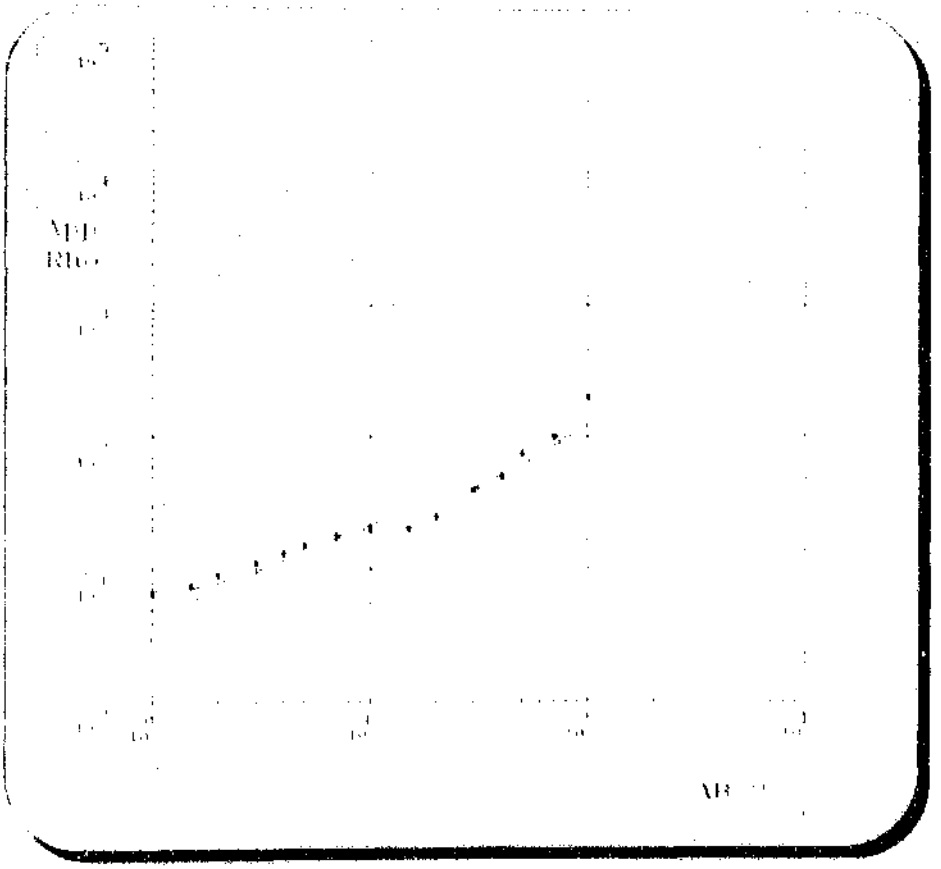

Figure 6.10: Vertical Electrical Sounding 1 (VES 1)

(Note AB is the Current electrode spacing and App Rho is the apparent resistivity)

6.6 *Resistivity Profiles*

Table 6.2 summarises the results of three vertical electrical soundings which were carried out along Traverse Lines ves1, ves2 and ves3 (Figure 5.12) on Tailings Dam 4E4. These results are presented graphically in the form of a depth-section in Figure 6.13. The reader is referred to Figures 6.10, 6.11 and 6.12 for the theoretical curves obtained from the Vertical Electrical Sounding Modelling Procedure. The field data and numerical results of the modelling are presented in Appendix E.

	Layer 1 (metres)	Layer 2 (metres)	Layer 3 (metres)
North - VES 1	1.8	3.7	8.3
VES 2	0	6.2	8.9
South VES 3	3.3	4.3	10.1

Table 6.2: Results of Vertical Electrical Soundings, ves 1-3 showing individual layer thicknesses.

6.6.1 *Electrical Layer 1: Colluvial Material*

Soundings 1 and 3 indicate the presence of a highly conductive uppermost layer which represents the thin, partially saturated crust occurring on the surface of the tailings dam. This layer forms part of the zone of aeration, commonly referred to as the vadose zone, in which both air and water occupy the pores. Meinzer (1942) (cited by Bell, 1993) divided this zone into three subzones:

i) Soil water,
ii) intermediate belt and
iii) the capillary fringe.

The uppermost or soil water belt, corresponding to electrical layer 1 in VES 1 and 3, discharges water into the atmosphere by evapotranspiration. Although a certain

Therefore considering the results of both the seismic and electromagnetic surveys for this area, the zone of anomalous conductivity may be explained by two possible scenarios.

i) Conductive zone, B_1, may be representative of a region of planar discontinuities (or faults) along which displacement of the bedrock has occurred. Such a zone would provide a conduit for the flow of groundwater. Borehole results would be necessary to ascertain the extent of such a fault and the degree of water accumulation in this area.

ii) Intrusive dolerite sills and dykes are commonly encountered in the City Deep Study Area (Jones et al, 1988). Where these igneous features are present, fractured conditions are enhanced along contacts, leading to an accumulation of groundwater and hence anomalously high conductivity values. Once again, borehole information would be necessary to confirm the presence of such igneous intrusions below Station 198 on the seismic profile.

The study area has a relatively uniform geology – transported and residual soils are approximately 1-2 metres thick and slightly weathered quartzite is first encountered at depths ranging between 3.7 and 8.5 metres.

The depth section confirms the basic geology shown on the composite geological map (Figure 4.1). Further corroborating evidence of the subsurface geology is shown in both the drill cuttings logged from the percussion drilling of the boreholes drilled for water sampling, as well as the borehole logs supplied by SRK (Jones et al., 1988).

The average velocities calculated for the upper, intermediate and lower layers are 422, 1644 and 3015 metres/second, respectively. Qualitatively, such velocities are indicative of a colluvial topsoil underlain by a relatively weathered, hard rock, which in turn, is underlain by an extremely hard, unweathered basement rock. (The reader is referred to the classification of rock hardness, weathering and seismic velocity characteristics in Appendix F).

As previously mentioned in Section 6.4, there is a localised zone of enhanced conductivity, A_{II} (Figures 6.7 and 6.8). This feature coincides with a basement "low" situated at a depth of 7.1 metres and centred at Station 39 (Figure 6.9) on the seismic profile. One may infer from this correlation between electromagnetic and seismic results, that the concentration of contaminated water may well be due to the localised depression in the basement rock, providing gravitational control on the movement of the water.

Similarly, the electromagnetic profile for traverse 4 and the seismic profile may be correlated where a second and relatively more pronounced zone of enhanced conductivity, B_{II} (Figure 6.8), is associated in part with a basement "low" which spans Stations 96 to 138 on the seismic profile (Figure 6.9). The Northern edge of the electric zone appears to coincide with a localised basement plateau. In the region of Station 198 (Figure 6.9), however, there is a fairly sudden change in basement profile, possibly due to a localised fault where displacement has occurred in a sub-vertical direction.

Figure 6.9 SEISMIC REFRACTION PROFILE

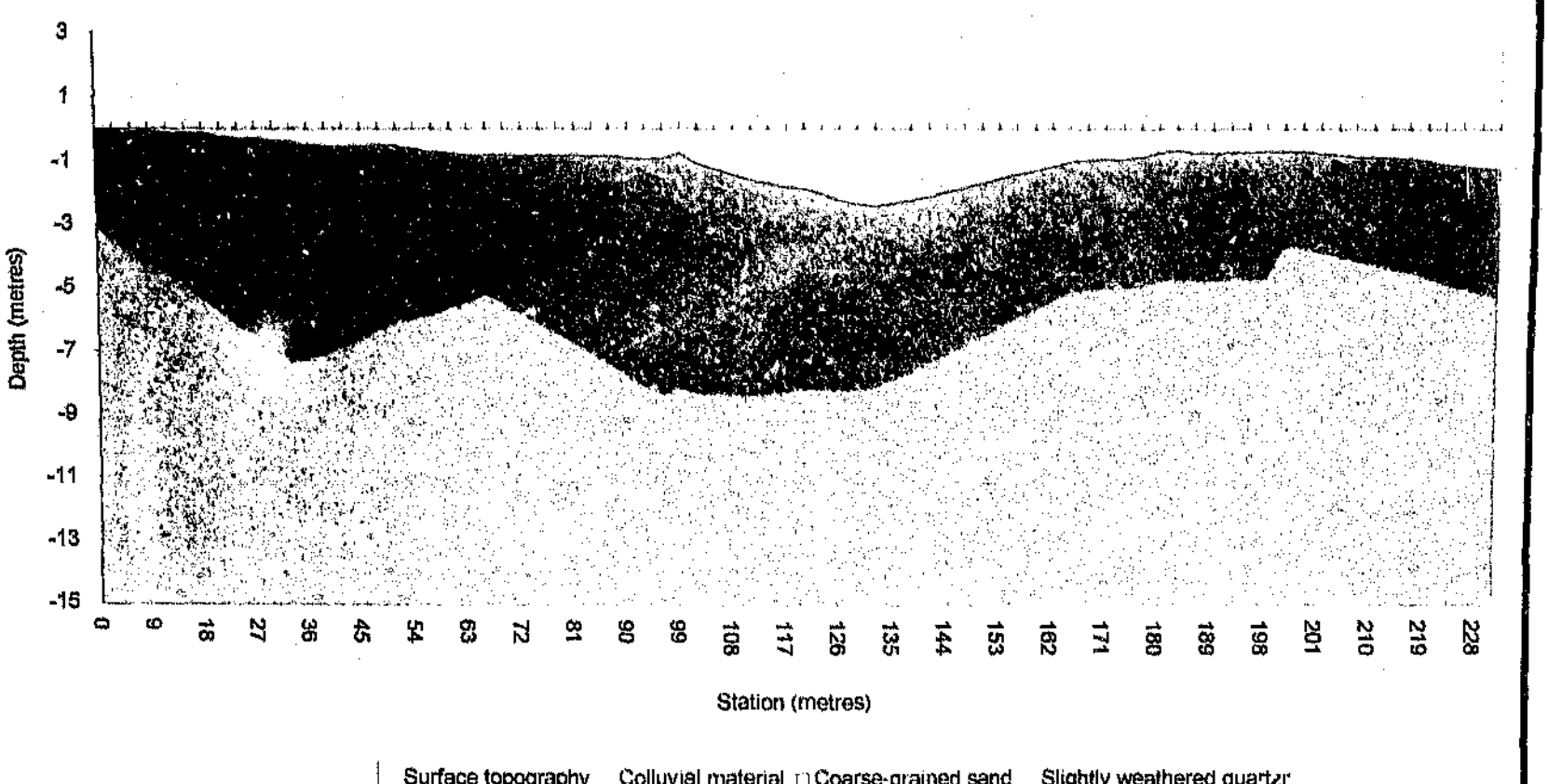

6.5 Seismic Refraction Profile 1

Figure 6.9 shows the seismic depth section derived from the results of a refraction seismic survey which was conducted along a north-south trending profile at the base of the sand dump. The profile runs parallel to the strike of the dump and spans a length of 400 metres. (This profile is located along the same survey line as that for Electromagnetic Traverse 4). The raw data which are presented as travel-time curves, are presented in Appendix D.

Distinct velocity layers were readily resolved by application of both delay-time and analytical methods as shown in Table 6.1. (The reader is referred to Table D1, Appendix D for a more detailed presentation of the calculated velocities and thicknesses corresponding to each of the seven profiles).

Lithology	*Depth Range derived from seismic results (metres)*	*Depth Range derived from borehole logs (metres)*	*Velocity Range (metres/second)*
Reddish-brown colluvium	2-4	1 - 2	297 - 847
Pinkish-grey weathered and slightly weathered quartzite	3 - 10	2 - 15	1324 - 2063
Yellowish-grey and greenish-grey unweathered quartzite	9	15	2268 - 3763

Table 6.1. Velocity and Depth ranges for refraction seismic Profile 1.

Figure 6.8 :ELECTROMAGNETIC PROFILE 4
20m inte ": spacing

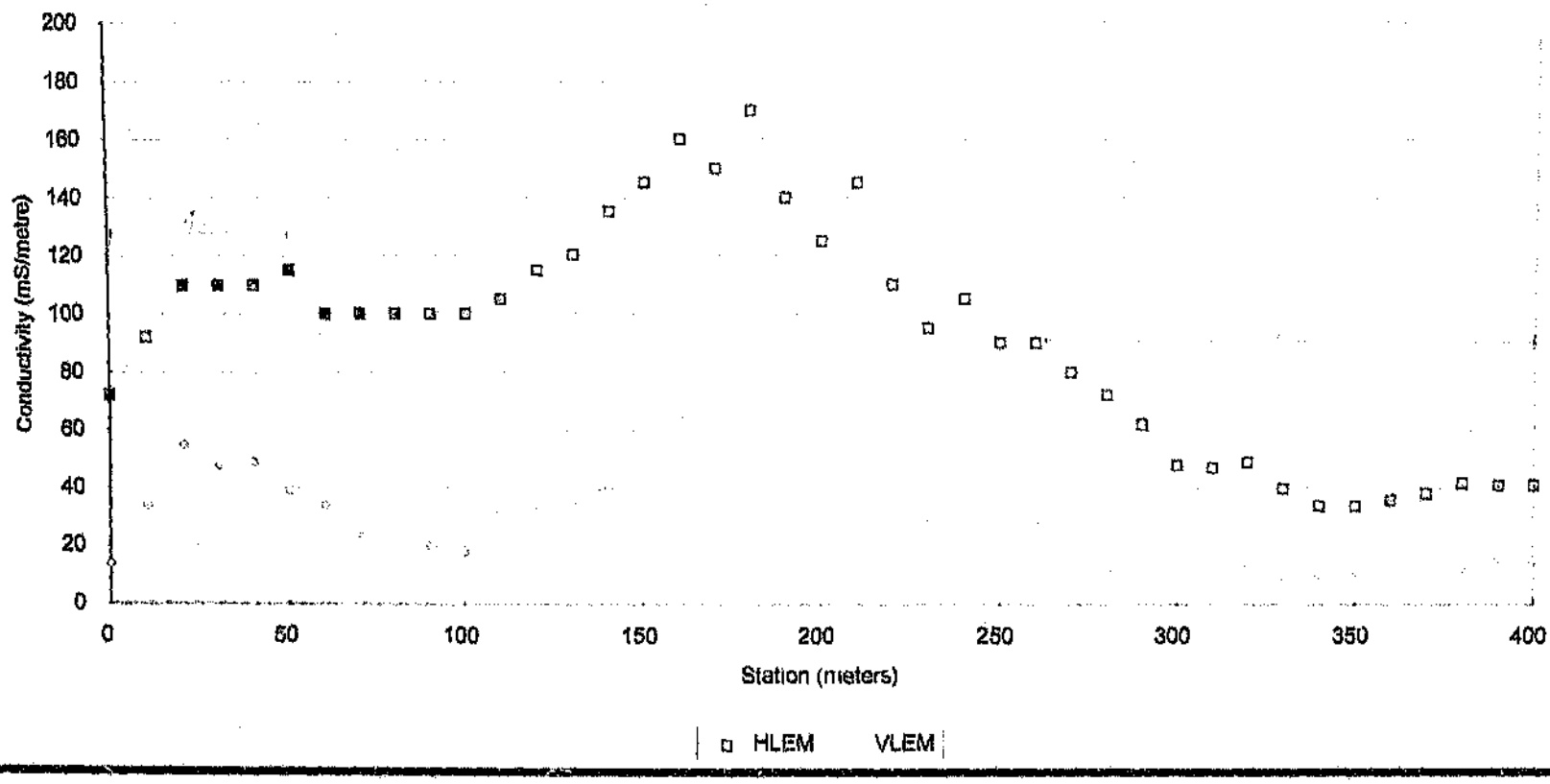

Extent and Degree of Ground Water Pollution. **WRC Report No. 267/1/94.** August 1994

Mineral and Energy Affairs, Dept. of (1989). The Geology of the Republics of South Africa, Transkei, Bophuthatswana, Venda and Ciskei and the Kingdoms of Lesotho and Swaziland. Compiled by D.J.J. Visser.

Mooney, H.M. (1973). Analysis for the multiple dipping layer structure - a hand computation method of solution.

Mrost, M. and Lloyd, P.J.D. (1970). Bacterial Oxidation of Witwatersrand Slimes. **Proc. of Simp. on Recovery of Uranium from its ores and other sources.** Int. Atomic Energy Agency, Sao Paulo.

Mrost, M. (1973). The Rehabilitation of Gold Mine Tailings Deposits. **S.A.I.C.E. 5th Quinquennial Convention.** Div. of Soil Mechanics and Foundation Engineering Speciality Session - Engineering aspects of erosion.

Redpath, B.B. (1973). Technical Report E-73-4. Seismic Refraction Exploration for Engineering Site Investigations.

Sitarz, D. (1993). Agenda 21 - The Earth Summit Strategy to save our planet.

Sole, J. (1994-09-25). Sunday Tribune.

Sheriff, R.E. (1991). Encyclopaedic Dictionary of Exploration Geophysics. Third Ed. Soc. of Expl. Geophys. 376pp.

Steffen, Robertson and Kirsten (1989). **Acid rock drainage. Draft Technical guide. Volume 1.** Prepared for the British Columbia AMD Task Force. August 1989.

Kempster & Smith (1984) Review of Water Pollution Problems and Control Strategies in the South African Mine Industry **Wat.Sci.Tech. Vol 15**, pp 37-58

Klemmann, R I P , Crerar, D A and Pacelli R R (19..) Biogeochemistry of Acid Mine Drainage and a Method to Control Acid Formation **Mining Engineering, March 1981;** pp300-305

Lundgren, D G and Silver, D (1980) Ore leaching by bacteria **Ann. Dev. Microbiol. Volume 34;** pp 263-283

Marsden, D D (1985) The Current Limited Impact of Witwatersrand Gold Mine Residues on Water Pollution in the Vaal River System Paper submitted to the South African Institute of Mining and Metallurgy (Published **J. SAIMM, Vol 86, 1986, p481**)

Mazac, O , Cisletova, M , Kelly, W E Landa, I and Venhodovoa, D (1990) Determination of hydraulic conductivities by surface geoelectrical methods **Geotechnical and Environmental Geophysics (1990), Volume II.** Published by the Society of Exploration Geophysicists (S E G), pp 125-132

McNeill J D (1980) EM34-3 Survey interpretation Techniques Geonics Limited Technical Note TN-6 (rev 1983) Mississaugon, Ontario

Meinzer, O (1942) Occurrence, Origin and discharge of groundwater In **Hydrology** (ed O Meinzer) Dover, New York, pp 385-443

Meyer R and Coetsee, V d A (1991) Determination of Hydraulic Aquifer Characteristics from resistivity sounding parameters

Meyer R , Davenhare A W A , Coetsee, V d A and Weaver, J M C (1994) The Evaluation and Development of Geophysical Techniques for Characterising the

Department of Environment Affairs (1983) **Hazardous Waste in South Africa**. Volume 1 Situation Analysis. Edited by R G Noble CSIR Pretoria

Department of Water Affairs (DWA) and Steffan, Robertson and Kirsten (SRK) (1990) Acid Mine Drainage - A short course Draft Technical Guide, Vol 1

EG&G Geometrics (1990) Model ES-1225 operation manual

Flathe, H (1967) Interpretation of geoelectrical resistivity measurements for solving hydrogeological problems. **Mining and Groundwater Geophysics, 1967. Economic Geology Report No. 26:** pp 880-897

GEONEX Aerodat Inc (1993) Environmental and engineering investigations using helicopterborne geophysical surveys 47pp

Goldstein, N E., Benson, S M and Alumbaugh, D (1990) Saline groundwater plume mapping with electromagnetics **Geotechnical and Environmental Geophysics, Vol. II** Ward, S H., Ed. Society of Exploration Geophysicists pp 17-26

Greenhouse, J P and Monier-Williams, M (1988), Geophysical monitoring of ground water around waste disposal sites **Groundwater Monitoring Review, 5, pp 63-69.**

Jones, G A., Brierley, S E., Geldenhuis, S J J and Howard, J R (1988) Research on the contribution of mine dumps to the mineral pollution load in the Vaal barrage **Water Research Commission Report No. 136/1/89,** Water Research Commission, Pretoria

Kelly, M (1987) Mining and the Freshwater Environment Elsevier Publishers

Keller, G V and Frischknecht, F C (1966) Electrical Methods in Geophysical Prospecting. Pergammon Press Inc Oxford, 519pp

9. *References*

Archie, G E (1942) The electrical resistivity log as an aid in determining some reservoir characteristics. **Trans. American Institute of Mineral Metallurgy and Petroleum Engineering: Volume 146**. pgs 54-62

Bell, F G (1993) Engineering Geology (ed) Blackwell Scientific Publications, London). pp 389

Botha, W J., Wiegmans, F E., Van der Walt, J J and Fourie, C J S (1992) Evaluation of electromagnetic exploration techniques in groundwater exploration **Water Research Commission, TR 212/1/92**

Brink, A B A (1979) Engineering Geology of Southern Africa Volume I 1st Ed Building Publications, Pretoria

Carruccio, F (1968) An Evaluation of Factors Affecting Acid Mine Drainage Production and the Groundwater Interactions in Selected Areas of Western Pennsylvania **2nd Symposium on Coal Mine Drainage Research, Monroeville, PA**, pp 107-182

Coetzee, H (1996) Pollution of soil and water in the Witwatersrand Goldfields Geophysical evidence and a methodological approach to understanding pollution risks. Council for Geoscience Report No 1996-0204, pp 21

C S I R (Pretoria) Department of Environment Affairs (1992) **Hazardous Waste in South Africa.** Volume I Situation Analysis Edited by R G Noble

Dakhnow, V N (1962) Geophysical well-logging The application of geophysical methods electrical well-logging Colorado School of Mines Quart, 57(2), pp 445

much of the documented research is fragmented, spanning individual mines which are relatively small in scale. A more holistic approach needs to be adopted in tackling the problem, i.e. initial or reconnaissance investigations should span an areal extent, starting at the drainage basin scale. Follow-up studies would then focus on specific problem areas.

- Coetzee (1996) documented the success of the airborne magnetic and radiometric surveys which have recently been undertaken by the Council of Geoscience in identifying contaminated soils and water courses over large parts of the Witwatersrand. In the City Deep Study Area, however, these airborne surveys were prevented due to the presence of numerous power lines and the general density of industries. It is therefore recommended that a ground radiometric study be undertaken in this area to ascertain the levels of radioactive contamination both on and around the tailings dams and in the surrounding streams.

- A recommended approach to the environmental problem is to initially develop a master database (relating to the entire Witwatersrand drainage basin) which would contain all relevant datasets ranging from geophysical through to biochemical information. Application of GIS (Geographical Information Systems) methods of interpretation based on this fully integrated master database, would facilitate the assessment of the severity of the problem, the prioritisation of remedial actions and future predictions of potential contamination. Such a system, would form an integral part of provincial or regional policy development and strategic planning.

- The depths to the perched water-table within the tailings dam, derived from Soundings 1-3, are shown in Table 8.2.

Vertical Electrical Sounding	*Depth to perched water-table (metres)*
VES 1	5.5
VES 2	6
VES 3	8

Table 8.2 Depths to the water-table of the tailings dam.

Refer to profiles in Section for extent of trenches

** First Priority Borehole*

- It is evident that the terrain conductivity and seismic techniques have the potential to give a good indication of the position and extent of the sources and flow of the groundwater contamination when combined with some knowledge of the subsurface hydrogeology. In this study, however, there is insufficient geochemical and hydrogeological information to provide the full picture of the precise depths and migration of the contaminated water. It is therefore recommended that prior to undertaking a remediation programme, it would be necessary to drill a number of boreholes in the positions mentioned in Table 8.2 for geochemical analyses and for verification of the depths and extent of contamination. It is recommended that the changes in both water level and geochemistry be monitored over an extended period of say, two to three years.

- To date, no integrated study has been undertaken to determine the full nature, extent and effects of mine-related pollution on the Witwatersrand. Most of the currently available information is based on observations by residents of areas surrounding mines. Furthermore,

the resistivity profile

- Results of Electromagnetic Profile 1 indicate that background conductivity values for the groundwater in the region of the stream are of the order of 60-65 mS/m. This value is consistent with a reasonably well-drained, porous, granular material containing water with natural levels of mineralisation

- Comparison of Electromagnetic Traverses 2 and 4 indicate that within this particular study area, the substantially eroded Tailings Dam 4L4 provides a more serious pollution threat than Tailings Dam 4L3 (The average conductivity for Traverse 2 lies between 90-100 mS/m, while for Traverse 4, the average value is 55-60 mS/m). Residue 4L3 is well vegetated and produces significantly lower levels of contaminated water due to the relative shortage of oxygen required for bacterial activity in the oxidation of pyrite.

- Optimal sites for the drilling and excavation of dewatering/monitoring boreholes and dewatering trenches, respectively, are presented in Table 8.1.

Profile Number	*Borehole Site (Station Number)*	*Trench*
EM 1	290°, 590°	A_1, A_2, B
EM 2	30, 90°, 280, 390°, 470°, 610°	"
EM 3	55, 90°	"
EM 4	180°, 310	A_2

Table 8.1. Optimal sites for dewatering monitoring boreholes and dewatering trenches, derived from results of electromagnetic profiling.

8. CONCLUSIONS AND RECOMMENDATIONS

The objective of the study was essentially three-fold, namely, to present a detailed overview of Acid Rock Drainage and previous studies relating to the City Deep Study Area, to obtain a better estimate for the probable extent of the groundwater contamination and to provide information needed to design an effective ground water sampling and ground water quality monitoring programme. Conclusions reached from the foregoing literature research, field results and analysis thereof are as follows

- A detailed description of the principles underlying Acid Rock Drainage was presented. Results of previous studies undertaken over the past decade were reviewed and compared to results obtained during the course of this study. results of the geophysical ground methods show broad agreement with the hydrogeological model of the transport of waste leachates in the groundwater, initially proposed by Jones et. al (1988). Relatively low levels of contamination were observed at the Northern extremity of Traverse 4, while a steady increase in conductivity (hence contamination) was observed in a south-westerly direction

- Surface geoelectrical and electromagnetic profiling techniques afford a relatively fast and cheap means of determining the most feasible *surface* locations for test well drilling, provided the contrast in the conductivity of contaminated to natural groundwater is sufficiently high
  It was found that the *horizontal* positioning of shallow water contamination could be determined accurately using the electromagnetic technique, however, without verification from borehole data, only a broad vertical range could be given for the *depth* of the contaminated water
  The vertical electrical sounding (resistivity) technique proved useful in delineating areas of deeper groundwater contamination as evident in

Figure 7.2a
Average TDS composition for Site S11
pH = 2.5 TDS = 973

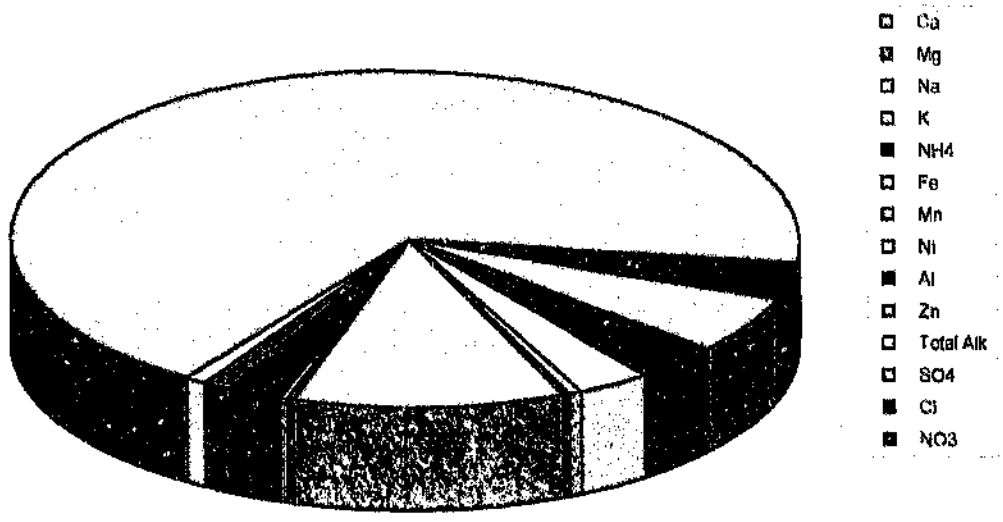

Figure 7.2b
Average TDS composition for Site S12
pH = 3.8 TDS = 767

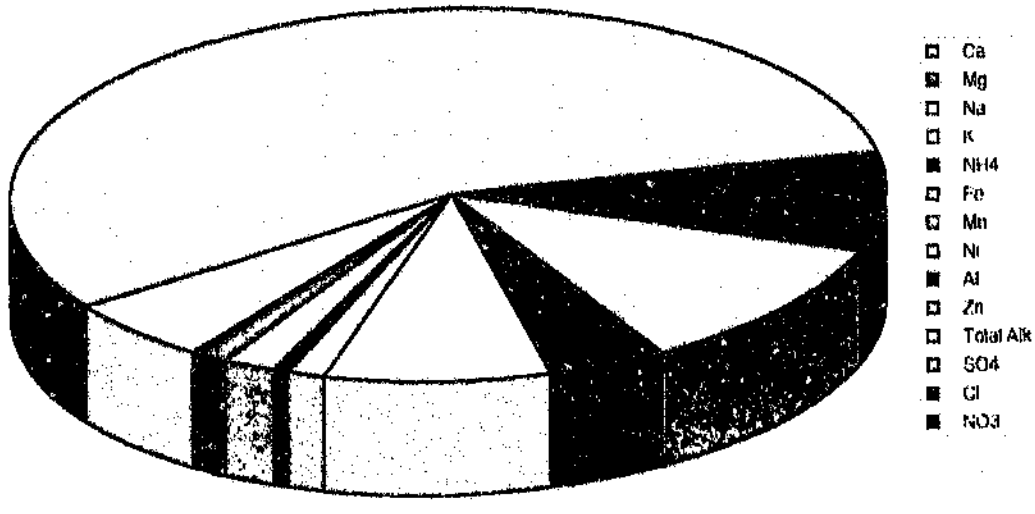

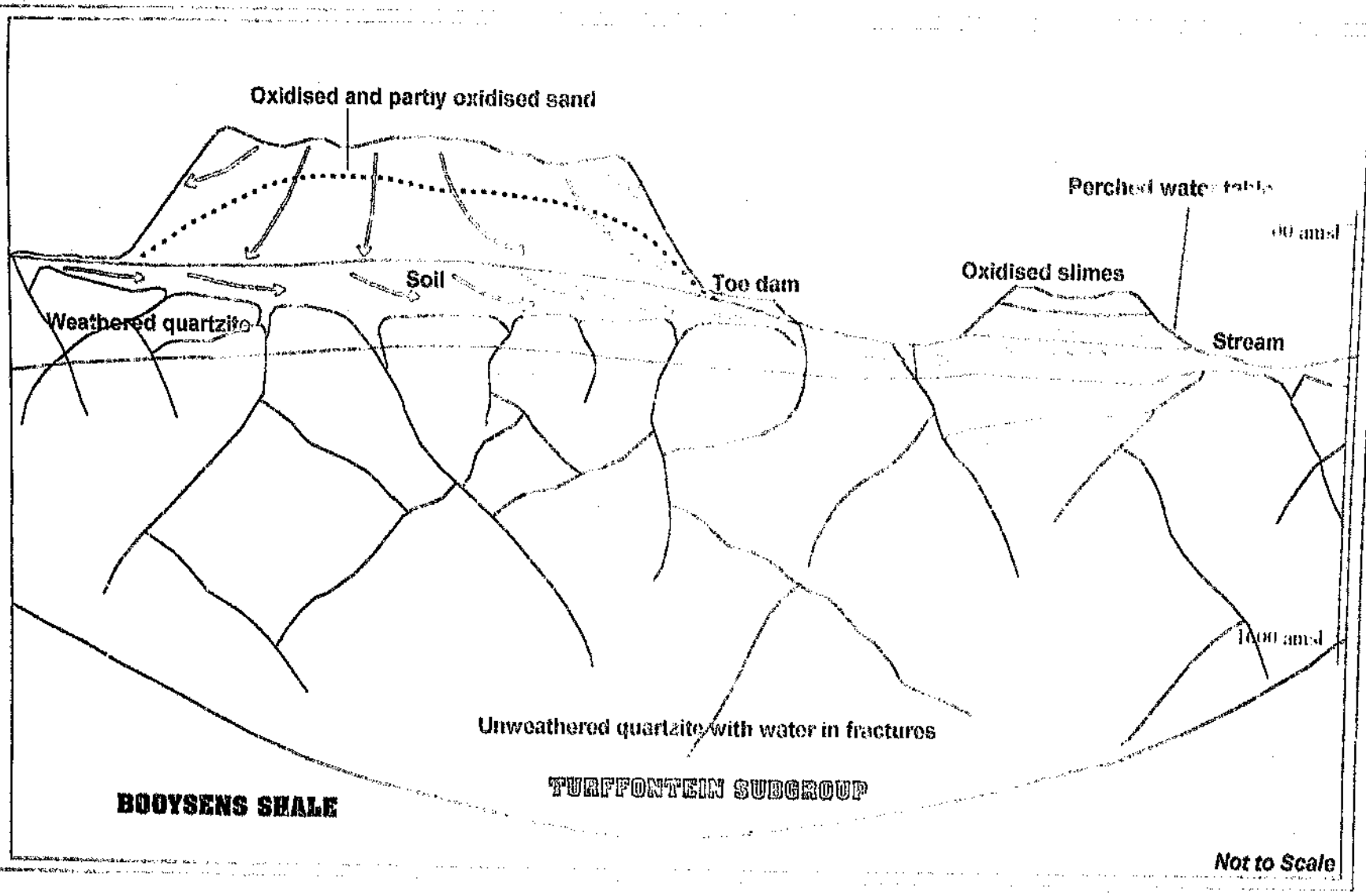

Figure 7.1 : Conceptual Hydrological Model of the City Deep Study Area.

The overlying weathered zone, which is usually in direct hydraulic continuity with these fractures, acts as a reservoir. Once in the fracture zone, pollution spreads rapidly in those fractures where groundwater movement occurs.

Borehole studies would be needed to ascertain the presence of fractured and subsequently weathered igneous intrusions which would enhance the rate of pollution movement where there is ground water flow. Conversely, where wide, solid and unweathered dykes and sills occur, ground water flow across the intrusion would be impeded and often prevented.

The conceptual model proposed by Jones et al (1988) used the findings of conductivity measurements taken at the bases of tailings dams 4L3 and 4L4. These geochemical results obtained by the Water Research Commission (Jones et al., 1988) indicate that although subsurface zones of concentrated wastewater are evident at the base of residue 4L3, tailings dam, 4L4 is a more serious pollution threat. Surface sampling site S11 is situated downstream of tailings dam 4L4, while S12 is located upstream of the residue. A comparison of Sites 11 and 12 (Figures 7.2) illustrates that the primary environmental contaminant, namely, sulphate salts, occurs in substantially higher concentrations at Site S11.

These geochemical findings are corroborated by the results obtained from electromagnetic surveys along traverses 2 and 4, where traverse 4 is situated upstream of residue 4L4 and traverse 2 is situated downstream of the residue. Results from the horizontal dipole surveys (20 metre intercoil spacing) indicate maximum conductivity values of 68 mS/m for Traverse 4, while the two most conductive features along Traverse 2 recorded far higher values of 210 mS/m and 180 mS/m.

These electromagnetic results indicate that Tailings Dam 4L4 does indeed pose a more serious pollution threat than residue 4L3.

7. CONCEPTUAL GEOHYDROLOGICAL MODEL

The mechanism[1] postulated for the contamination of the surfa[illegible]d shallow ground water at the base of the residues 4L3 and 4L4 is illustrated in Figure 7.1 and described as follows:

Rainwater accumulates on the surface of mine residue during periods of precipitation and a large proportion consequently infiltrates into the residue material collecting the products of pyrite oxidation and gradually increasing the thickness of the aerated or oxidised zone. Results of the resistivity survey indicate that the current limit of oxidation occurs at a depth of 4.3 metres for tailings dam 4L4. As this zone is relatively thin, there is minimal vertical retardation and the contaminated water reaches the underlying fractured bedrock unimpeded. A combination of the horizontal layering and the permeability contrast between the coarse-grained, weathered material and the practically impermeable bedrock encourage a perched water-table to develop. Seepage consequently occurs towards the sides of the tailings dam.

In the region of residue 4L3, the weathering of sediments comprising the Turffontein Subgroup produces a variably thin weathered zone which has the characteristics of an unconfined aquifer. Contaminated w[illegible] flows at the shallow depth of 3 to 8.5 metres along the soil-rock boundary, parallel to the surface in a south-easterly direction and ultimately into the stream where it mixes with the surface water. Borehole piezometer results obtained by SRK (cited by Jones et al. 1988) indicate that a small proportion of this seepage is not intercepted by the stream, i.e. a degree of contaminated water has penetrated the non-porous bedrock by means of fractures or faults which provide conduits for the seepage of groundwater at depths in excess of 8.5 metres.

[1] *The conceptual model is based on the initial geohydrological model proposed by Jones et al. (1988) and the results of the geophysical survey.*

Schlumberger Resistivity
Modelling
VES 1

The current model is :-

layer	Thickness	Resistivity
1	2.60	6.60
2	3.50	96.20
3	5.00	9.80
4	infinite	2500.00

AB/2	Observed Resistivity	Calculated Resistivity
1.00	6.5	6.8
1.50	7.5	7.2
2.00	8.0	7.8
3.00	11.0	9.5
4.00	13.0	11.6
5.00	15.0	13.6
7.00	18.0	17.7
10.00	20.0	21.4
15.00	20.0	26.4
20.00	25.0	30.2
30.00	40.0	40.1
40.00	50.0	51.0
50.00	75.0	63.8
70.00	100.0	87.0
100.00	200.0	138.7

Figure D7: SEISMIC REFRACTION LINE 7
Shotpoints: 198m and 234m

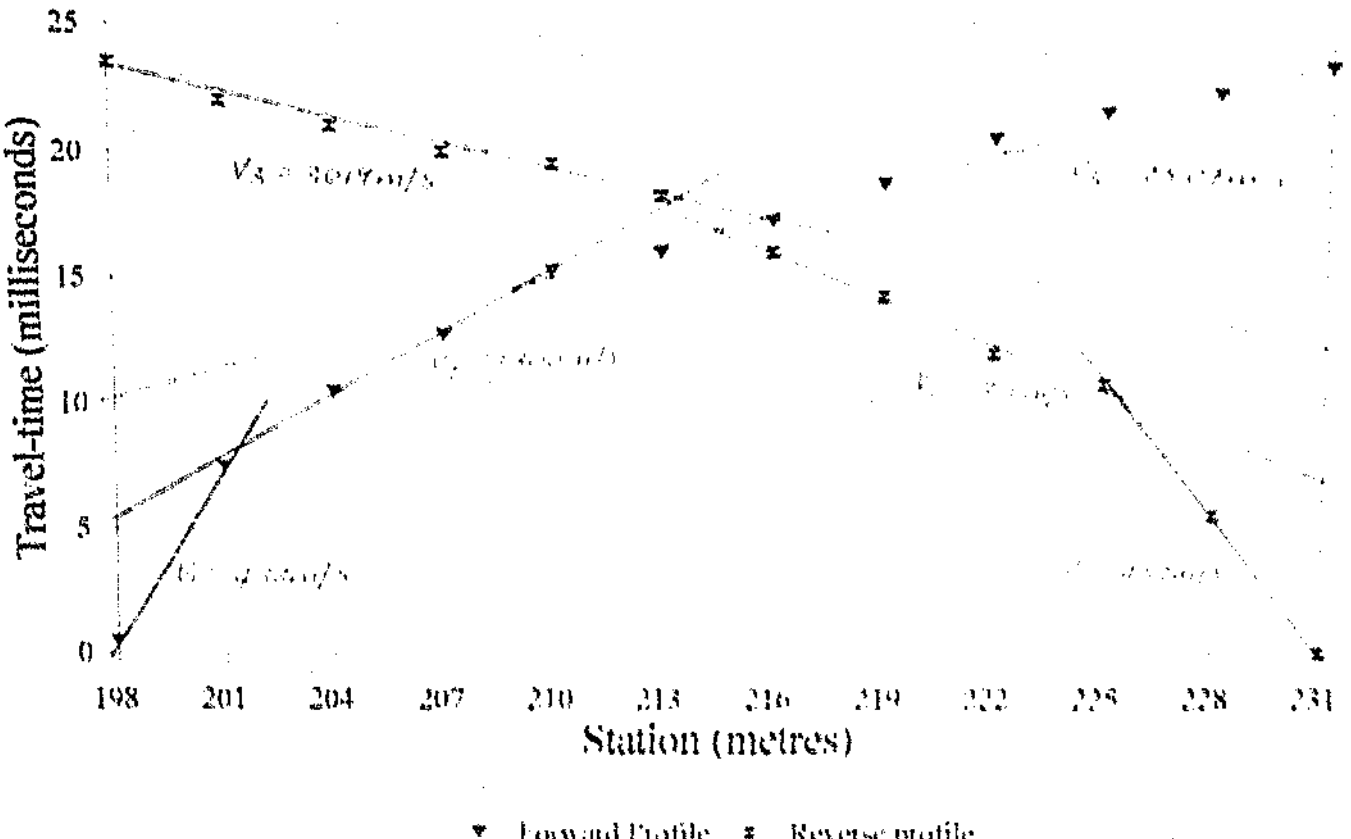

Schlumberger Resistivity
Modelling

The current model is :-

Layer	Thickness	Resistivity
1	6.20	95.00
2	8.90	6.60
3	infinite	2054.00

AB/2	Observed Resistivity	Calculated Resistivity
1.00	85.0	76.7
1.50	62.0	61.6
2.00	48.0	48.3
3.00	28.0	25.7
4.00	20.0	16.9
5.00	13.2	14.2
7.00	14.0	14.4
10.00	21.2	17.3
15.00	20.0	20.6
20.00	31.0	25.3
30.00	43.0	42.5
40.00	56.0	69.5
50.00	80.0	86.2
70.00	120.0	119.2
100.00	190.0	167.0

Compute angle of incidence

$$a_1 = b_1 = (\alpha_1 + \beta_1)/2$$

Compute dip angle

$$B_1 = (\alpha_1 - \beta_1)/2$$

Compute true velocity in second layer

$$V_2 = \frac{V_1}{\sin a_1}$$

Compute a temporary quantity which we call P

$$P = \frac{1}{(\sin a_1)(\cos \beta_1)}$$

Compute layer thicknesses

$$HA_1 = (P)(HA_2)$$

$$HB_1 = (P)(HB_2)$$

(c) Third layer

Compute *new* angles α_1 and β_1 from

$$\sin \alpha_1 = \frac{V_1}{V_2} \qquad \sin \beta_1 = \frac{V_1}{V_2}$$

Physically, α_1 and β_1 are as shown in Figure C2

X is any point on the VA, segment

Compute *new* a_1 and b_1 from

$$a_1 = \alpha_1 - B_1$$

$$b_1 = \beta_1 + B_1$$

Appendix C: Calculations Of Seismic Depths.

For a multiple-layer problem, the Delay-Time Method is presented by Mooney (1973) as follows:

(a) First layer

VA_1 (first layer velocity corresponding to forward profile) and VB_1 (first layer velocity corresponding to reverse profile) are computed from the first slopes of the traveltime curve. The two velocities must be approximately equal; if not, the surface layer is not uniform from one end of the line to the other.

$V_1 = VA_1 \quad VB_1$ is the true velocity

(b) Second layer

Compute angles α_1 and β_1 from:

$$\sin\alpha_1 = \frac{V_1}{V_2} \qquad \sin\beta_1 = \frac{V_1}{V_2}$$

Physically, α_1 and β_1 are shown in Figure C1



Figure C1: Angles for the second layer.

Line No.	TV_c metres South	TV_c metres North	V_c metres/second	TV_c metres South	TV_c metres North	V_c metres/second	V_c metres/second
1	0.88	1.97	297	3.57	5.67	1,363	2,268
2	1.02	1.06	400	6.6	4.2	1,224	3,224
3	1.7	1.37	438	2.33	6.51	2,063	3,762
4	0.91	1.5	513	6.27	3.84	1,520	3,333
5	2.41	1.7	424	2.48	2.25	1,282	2,515
6	1.65	0.84	547	3.23	2.18	1,352	2,351
7	1.44	1.78	489	3.9	4.3	1,538	2,761

Table D1: Results of Refraction Seismic Time-Depth Conversion

Key

VT_c - thickness of seismic layer 1

V_c - velocity of seismic layer 1

VT_c - thickness of seismic layer 1

V_c - velocity of seismic layer 1

VT_c - thickness of seismic layer 1

V_c - velocity of seismic layer 1

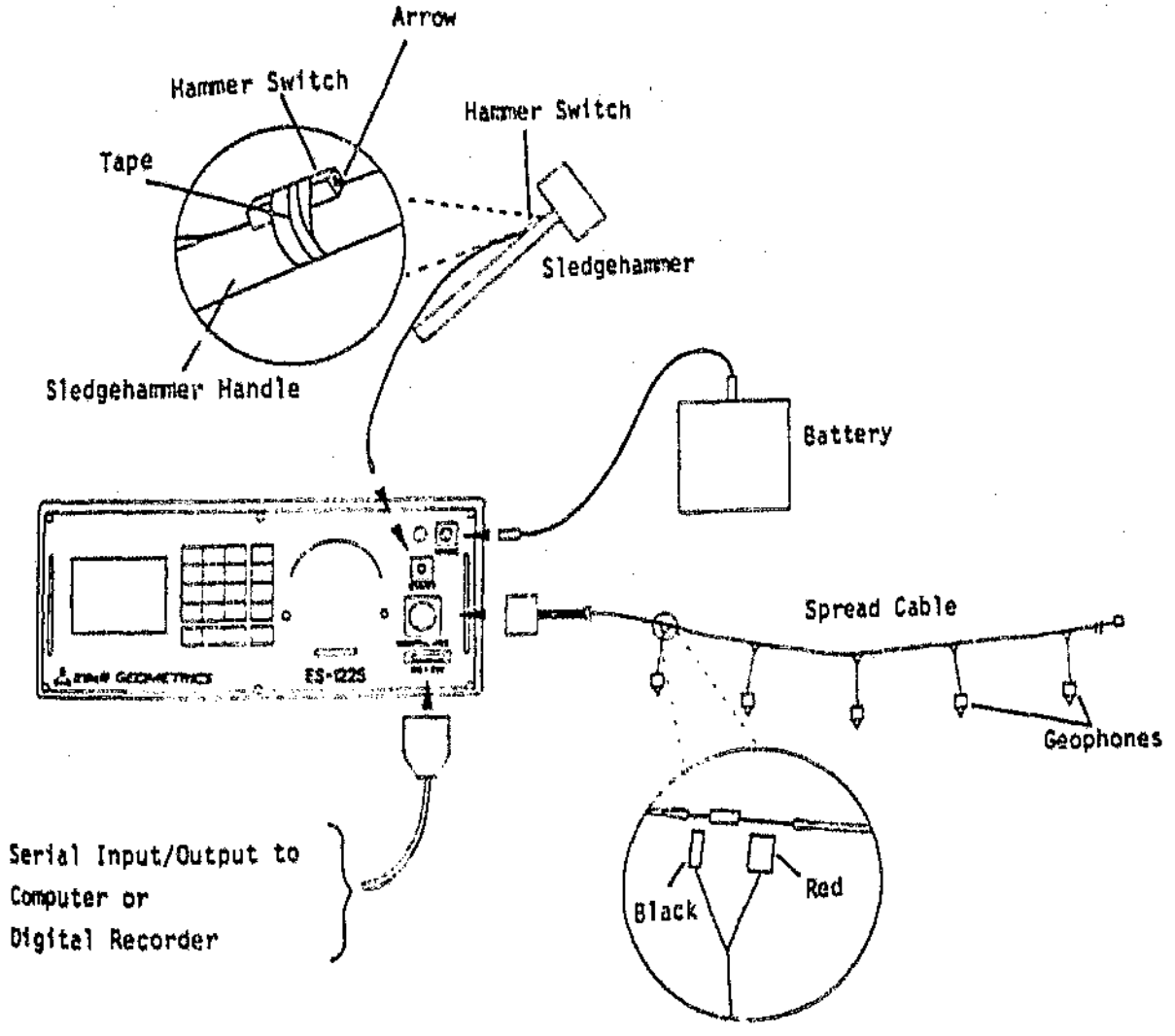

Figure B.1: Assembly of the ES-1225 System. (After EG&G Geometric, 1990).

MAXIMUM INPUT SIGNAL	0.35 volts (+ or -) before clipping
PREAMPLIFIER GAIN	33db
AMPLIFIER GAIN	0 6 12 18 24 30 36 42 48 54 60 66 db (user-selectable)
QUANTIZATION LEVEL	.95 millivolts
FREQUENCY RESPONSE	3hz to 1000hz
FILTER	Lowcut, 40hz corner frequency, butterworth filter. Damping factor is 0.5, rolloff is 12db per octave
TRIGGERING	By contact closure, positive or negative voltage pulse, geophone signal, or saturation of NPN transistor. Recording may also be initiated by a manual START key
POWER SUPPLY	11 to 14 volts DC at approximately .3 .8 amps. standby

Seismograph Settings

NUMBER OF CHANNELS	12
RECORD TIME	250 milliseconds (user-defined)
RECORD SIZE	8 bits by 1000 sampled points for each channel
SAMPLE INTERVAL	250 microseconds (user-defined)
DELAY TIME	0 (user-defined)
SIGNAL ENHANCEMENT	Successive shots may be summed in digital memory, to aid detection of weak signals. The maximum stack count (number of summed shots) that can be displayed is 255.
STORE / RECALL	Up to 12 sets of channel settings (each set consists of gain and trace size settings for all 12 channels) may be stored in and retrieved from non-volatile memory
TIMING	crystal-controlled, 0.01% accurate
DISPLAY	Built-in daylight-visible CRT, 8in. (12cm) diagonal, wiggle-trace or variable-area display capability: 512 pixels horizontal by 256 pixels vertical. Set to variable area display
HARD COPY	Built-in printer / plotter
INPUT IMPEDANCE	50,000 ohms resistive

vi) Since it was impractical to simultaneously record many geophone groups spread over the entire distance the refraction profiles were shot in seven segments

vii) The arrival times of the first seismic pulse (or headwave) corresponding to each geophone was recorded from a visual display
Close examination of a typical seismic record usually reveals the following sequence of arrivals

i) P-wave (or headwave),
ii) Sound wave (or direct wave) and
iii) Surface waves

The direct wave and surface waves are easily distinguished from the headwave due to the lower velocities of the former The sound wave may be identified as a small, high-frequency pulse, with arrival times consistent with the speed of sound in air (335m/s). The surface waves are usually the largest in amplitude, lowest in frequency and may travel as slowly as 150m/s (ECG&G Geometrics, 1990)

viii) Successive sets of waves from successive shots were added together or "stacked" to strengthen weak signals and to increase the signal to noise ratio through cancelling of random background seismic noise This process is termed *signal enhancement*.

ix) The procedure was repeated with the source at the other extremity of the profile for each segment This process is known as *reverse profiling* and is used to establish the dips of the respective subsurface interfaces

Appendix B: Seismic refraction survey: field procedure and Es-1225 Seismograph settings

Field Procedure

i) The geophone cable was laid out along a straight line directed toward the source or "shotpoint". Care was taken to minimise the adverse effects of wind "noise" by firmly planting the geophones in the ground and in some instances, by shallow burial. The rustling of grass or small bushes was avoided by locating the geophones in an open, non-vegetated area.

ii) The 12 geophones were connected to the cable, which in turn, was connected to the signal input connection on the instrument's front panel (Figure 5.11). The geophone-interval was set to 3m.

iii) The FILTER option was set to OUT, the TRACE SIZE to a midrange value of 15 and the DELAY to 0.

iv) The INITIAL RECORD TIME was set to 250 milliseconds by estimating the total travel time from the hammer to the farthest geophone. A good rule of thumb states that the record time in milliseconds should be approximately equal to the spread length in feet. Since almost any geologic material has a P-wave velocity in excess of 1000ft/s (305m/s), this ensures that all arrivals will be detected (EG&G Geometrics (1990)).

v) The AMPLIFIER GAINS were set just high enough so that the background noise was barely visible for each channel.

That is, having decided on a value for s (which fixes the effective depth of penetration under the condition B = 1), the maximum probable ground conductivity is estimated and the operating frequency is chosen so that equation (above) is always satisfied. The apparent conductivity which the instrument reads is then defined by

$$\sigma_a = \frac{4}{\omega\mu s^2}\left(\frac{H_z}{H_p}\right)_{\text{quadrature component}}$$

These expressions are complicated functions of the variable, γs, which in turn, is a complex function of frequency and conductivity. However, as will be shown below, under certain conditions, they can be greatly simplified.

A well known characteristic of a homogeneous half-space is the electrical skin depth, δ which is defined as the distance in the half-space that a propagating plane wave has travelled when its amplitude has been attenuated to (1/e) of the amplitude at the surface. The skin depth is given by:

$$\delta = \sqrt{\frac{2}{\omega\mu\sigma}} = \frac{503}{\sqrt{f\sigma}}$$

and therefore

$$\gamma s = \sqrt{2i}\frac{s}{\delta}$$

The ratio, $\frac{s}{\delta}$, the intercoil spacing, divided by the skin depth, is defined as the induction number, B, whereupon

$$\gamma s = \sqrt{2i}\,B$$

Now, if B is much less than unity (i.e. $\gamma s << 1$) it is a simple matter to show that the field ratios of equations (1) and (2) reduce to the simple expression

$$\left(\frac{H_s}{H_p}\right)_{\perp} = \left(\frac{H_s}{H_p}\right)_{//} = \frac{i\omega\mu\sigma s^2}{4}$$

The magnitude of the secondary magnetic field is now directly proportional to the ground conductivity and the phase of the secondary magnetic field leads the primary field by 90°.

To make B much less than unity, we see that we must make s very much less than δ and thus

$$\omega << \frac{2}{\mu\sigma s^2}$$

Appendix A: Theory Of Operation At Low Induction Numbers.

Consider the two coil configurations shown in Figure A1. In each case, the transmitter coil is energised with alternating current at a frequency, f Hertz. The measured quantity is the ratio of the secondary magnetic field, H_s, at the receiver when both coils are lying on the surface of the homogenous half-space of conductivity, σ, to the primary magnetic field, H_p in the absence of the half-space (i.e as if the coils were in free space). The spacing between the coils is s metres.

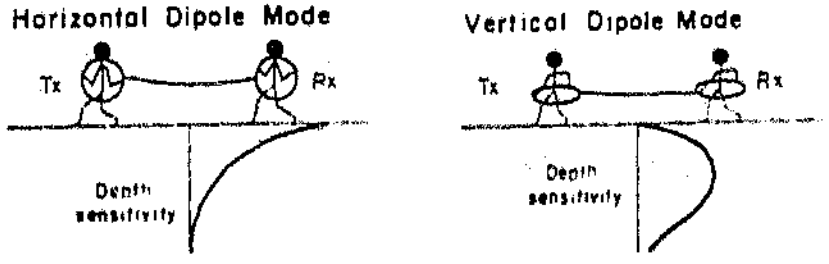

Figure A1: Vertical and horizontal dipole coil configurations.

The field ratios for vertical and horizontal dipole configurations are given by equations (1) and (2), respectively:

$$\left(\frac{H_s}{H_p}\right)_v = \frac{\gamma^2}{(\gamma s)^3}\{9 - [9 + 9\gamma s + 4(\gamma s)^2 + (\gamma s)^3]e^{-\gamma s}\}$$

$$\left(\frac{H_s}{H_p}\right)_H = 2\left|1 - \frac{3}{(\gamma s)^3} + (3 + 3\gamma s + (\gamma s)^2)\frac{e^{-\gamma s}}{(\gamma s)^3}\right|$$

where $\gamma = \sqrt{i\omega\mu_0\sigma}$

$\omega = 2\pi f$

f = frequency (Hertz)

μ_0 = permeability of free space

$i = \sqrt{-1}$

APPENDICES

Telford, W M, Geldart, L P and Sheriff, R G (1990) Applied Geophysics Cambridge University Press, Cambridge, 770pp

Thompson, J G (1980) Acid Mine Waters in South Africa and their Amelioration **Water S.A. Volume 6, No. 3,**

Visser, D J L (1989) comp. Geological Survey of South Africa. The geology of the Republics of South Africa, Transkei, Bophuthatswana, Venda and Ciskei and the Kingdoms of Lesotho and Swaziland. Pretoria Government Printer, 491pp.

Walsh, F (1978). Biological control of acid mine drainage. **Water Pollution Microbiology. Volume 2.** Edited by R Mitchell pp 377-389

Ward, S H (1990) Resistivity and Induced Polarisation Methods **In: Geotechnical and Environmental Geophysics** (Ed. S H Ward) Society of Exploration Geophysicists (S E G), 389pp.

White Paper WPE-87 (1987). Report on the Proposed Water Pollution Control Works at Abandoned Coal Mines in Northern Natal

Willier, A and Loos, M A (1984) Further Studies on the Inhibition of Thiobacillus ferrooxidans and Occurrence of the Bacteria in Gold Mine Sand Dumps in Relation to Pyrite Oxidation Unpublished reports to the Water Research Commission

Zmatowicz, K P S (1992) Radioactive and heavy metal pollution associated with a gold tailings dam on the East Rand submitted in partial fulfilment for the degree of Bachelor of Science with Honours - University of the Witwatersrand

Figure D4: SEISMIC REFRACTION LINE 4
Shotpoints: 99.0 and 132.0 metres

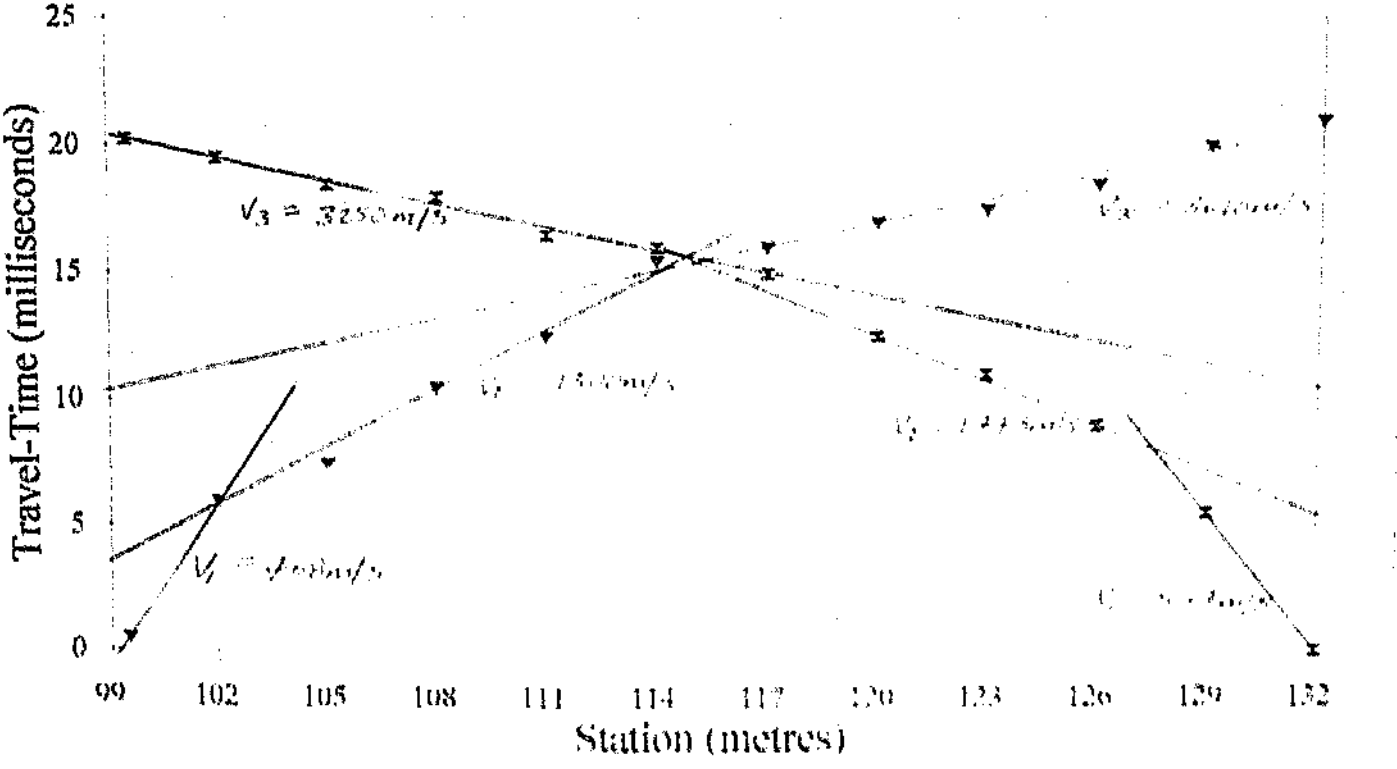

Figure D5: SEISMIC REFRACTION LINE 5
Shotpoints: 132.0 and 165.0 metres

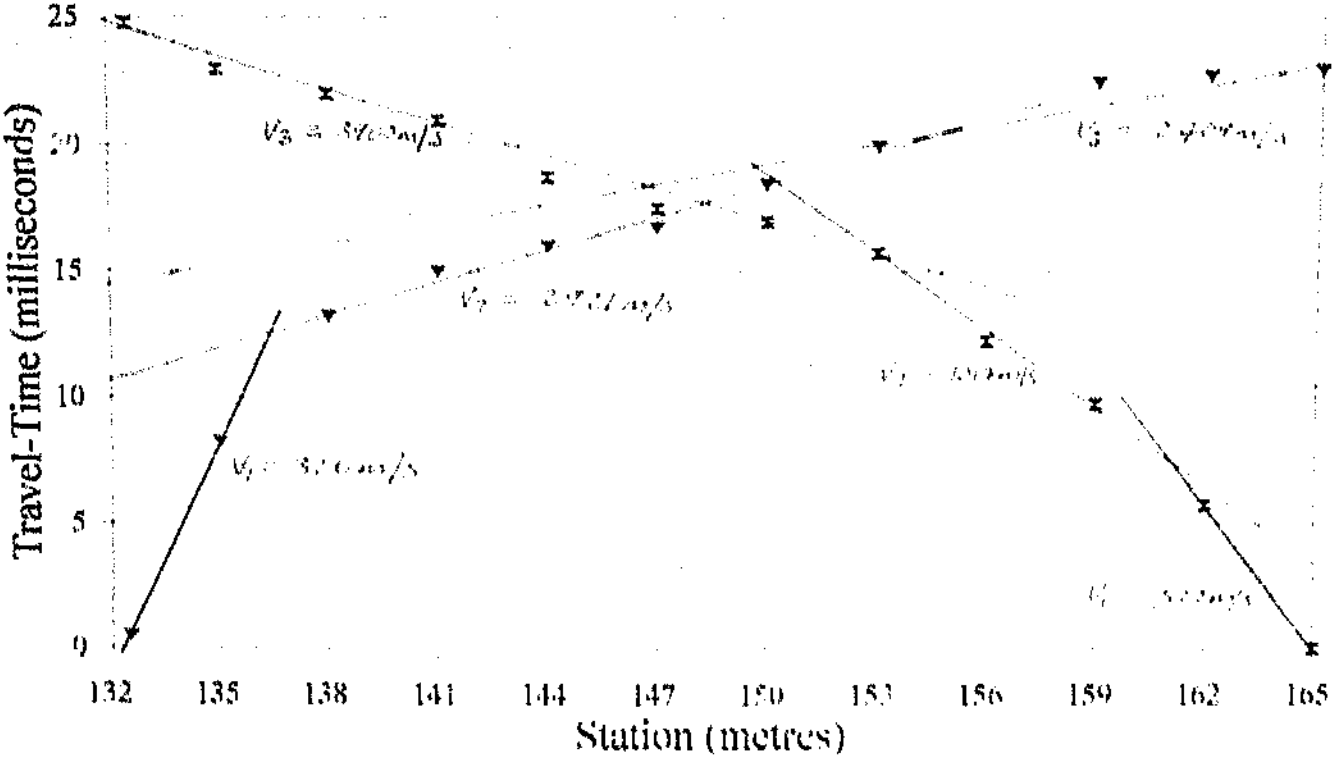

Figure D3: SEISMIC REFRACTION LINE 3

Shotpoints: 66.0 and 99.0 metres

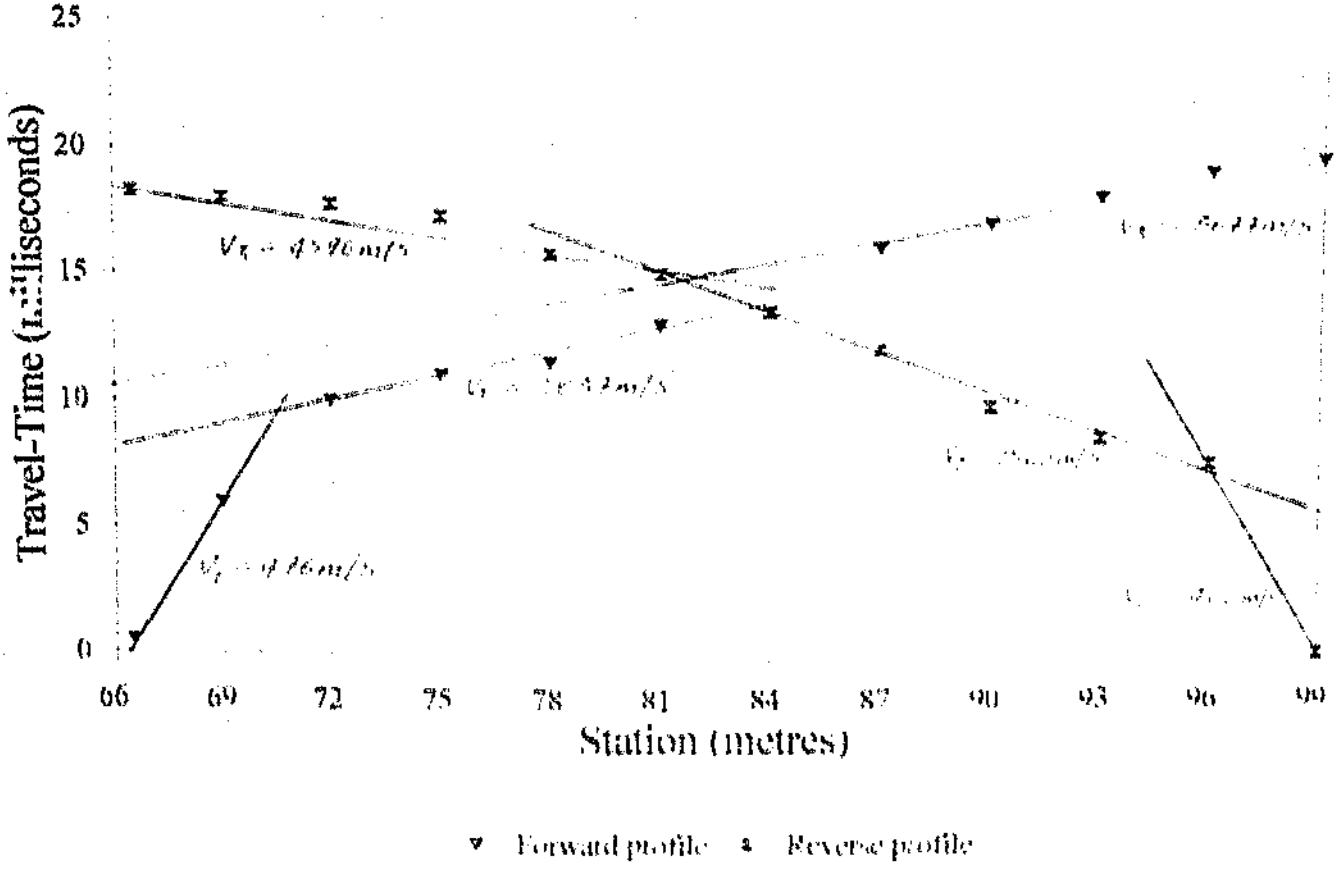

Figure D1: SEISMIC REFRACTION LINE 1
Shotpoints: 0m and 33m

Figure D6: SEISMIC REFRACTION LINE 6
Shotpoints: 165.0 and 198.0 metres

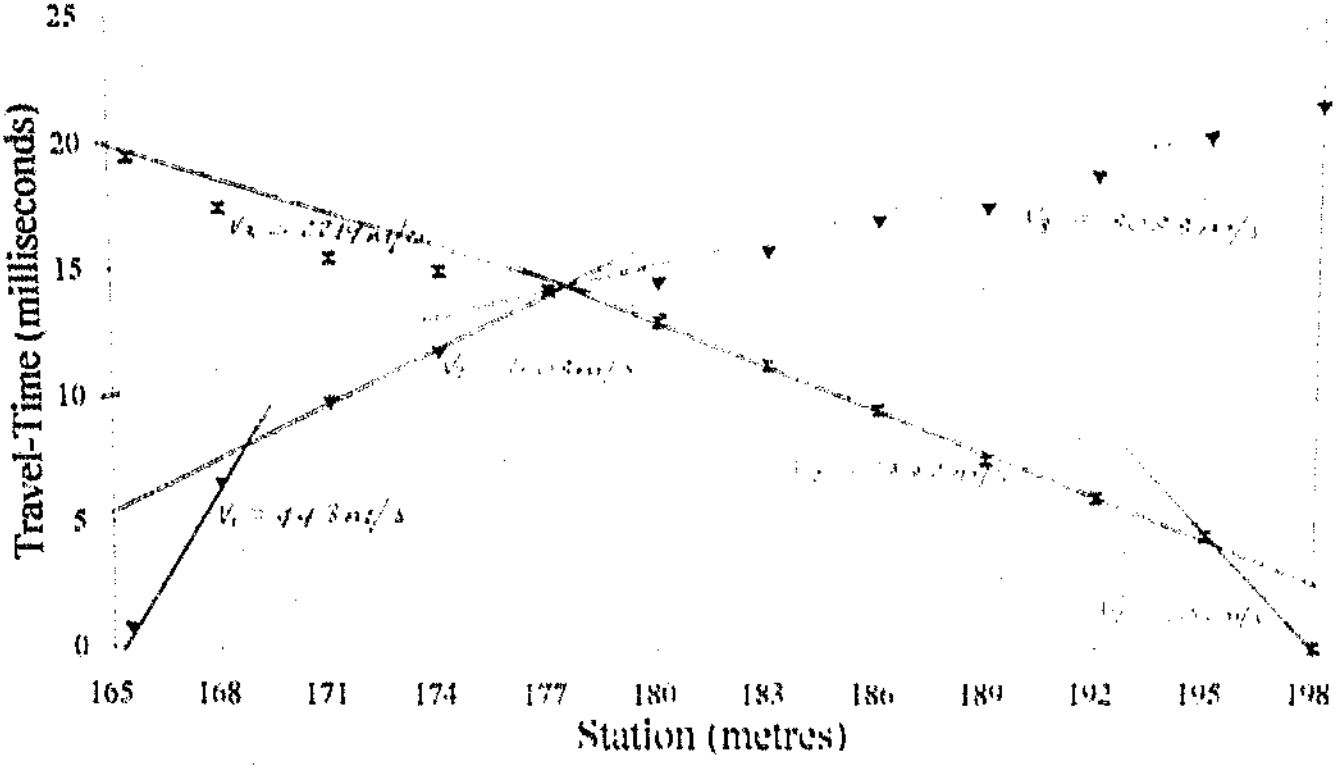

Figure D2: SEISMIC REFRACTION LINE 2

Shotpoints: 33.0 and 66.0 metres

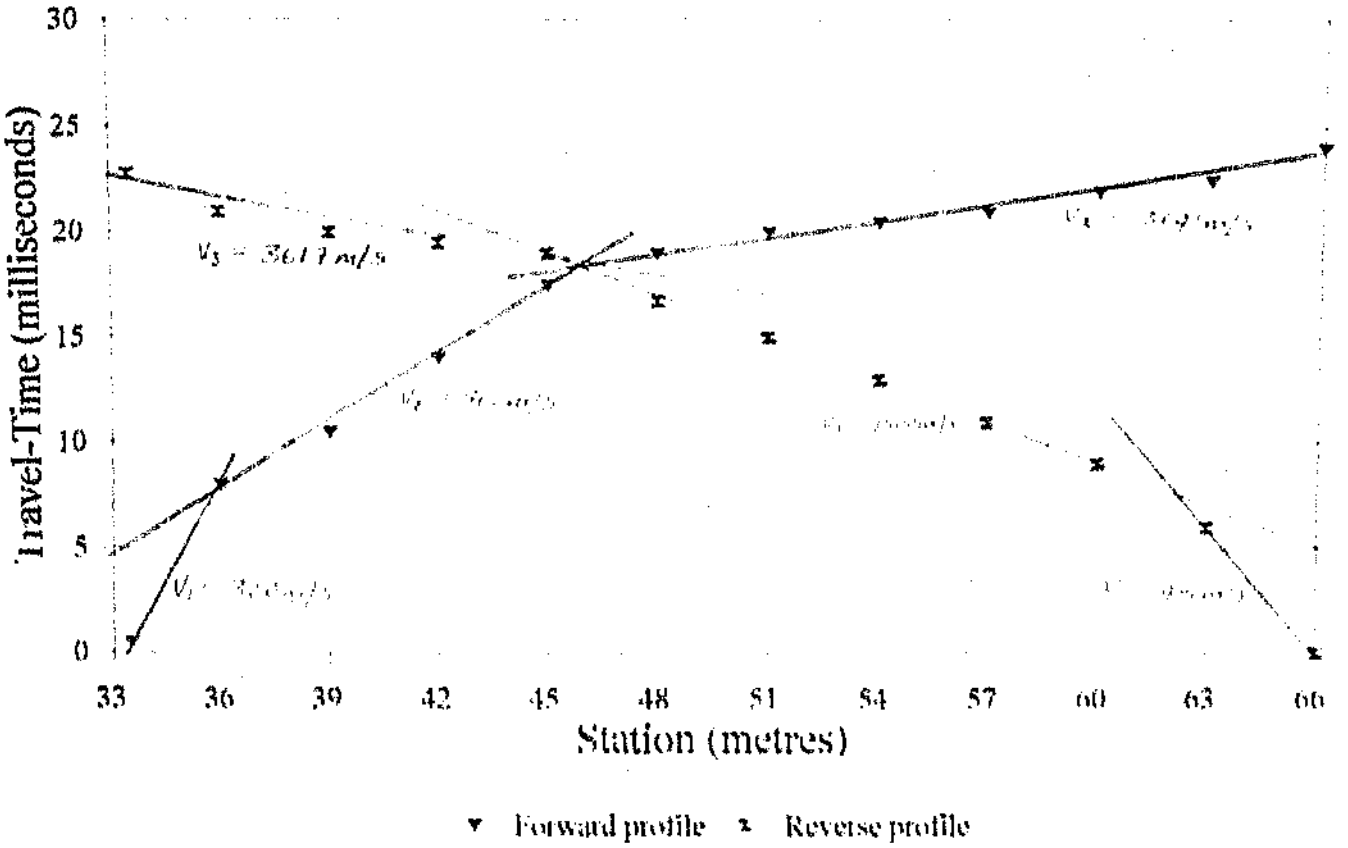

Compute true velocity in the third layer

$$V_3 = \frac{V_2}{\cos(\alpha_2 - \beta_2)}$$

Compute layer thicknesses

$$IIA_2 = \frac{V_1}{\cos\alpha_1 + \cos\beta_1} \quad IIA_3 = \frac{H_2}{V_2}(\cos\alpha_2 + \cos\beta_2)$$

$$IIB_2 = \frac{V_1}{\cos\alpha_1 + \cos\beta_1} \quad IIB_3 = \frac{H_2}{V_2}(\cos\alpha_2 + \cos\beta_2)$$

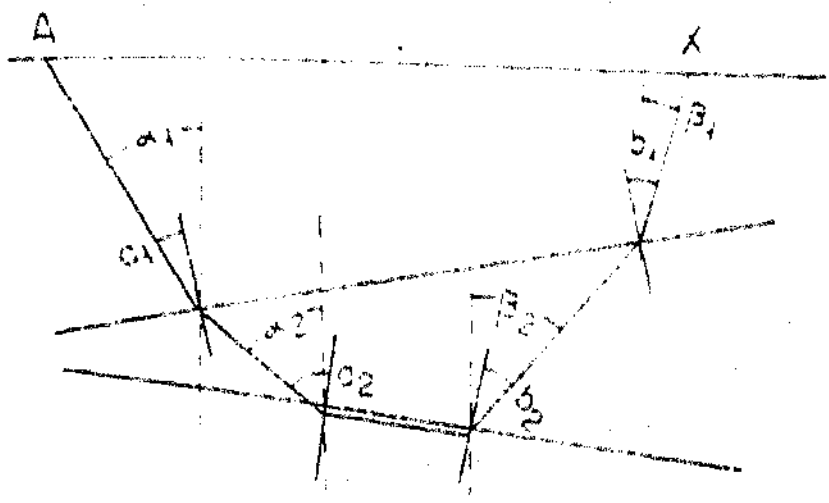

Figure C2: Angles for third layer.

Compute temporary quantities which will be called P_2 and Q_2.

$$\sin P_2 = \frac{V_2}{V_1} \sin a_1$$

$$\sin Q_2 = \frac{V_2}{V_1} \sin b_1$$

Compute angles of incidence at top of third layer.

$$a_2 = b_2 = (P_2 + Q_2)/2$$

Compute dip at top of third layer.

$$B_2 = B_1 + (P_2 - Q_2)/2$$

Compute angles of incidence measured from the vertical.

$$\alpha_2 = a_2 + B_2 \qquad \beta_2 = b_2 - B_2$$

Appendix F: Classification Of Rock Hardness, Texture And Seismic Velocity.

after Weaver, J. M., Geological factors significant in the assessment of rippability. Civil Engineering Equipment Digest. July 1976, 2-8.

Rock hardness description	Weathering description	Identification criteria	Seismic velocity (m/s)	Excavation character
		Topsoil	< 450	
Very soft rock	Completely weathered	Totally discoloured and decomposed, in a friable condition with only frag ments of the rock texture and structure preserved. External appearance is that of soil. Material crumbles under firm blows with sharp end of geological pick. Pieces up to 3 cm thick can be broken by finger pressure.	450 - 1200	Easy ripping
Soft rock	Highly weathered	Weathering extends through-out rock mass and material is partly friable. Rock has no lustre. All material except quartz discoloured. Can just be scraped with a knife, indentations 1mm to 3mm show in the specimen with firm blows of the pick point, has dull sound under hammer.	1200 - 1500	Hard ripping
Hard rock	Weathered	Slight discolouration extends through the greater part of the rock mass. Material is not friable (except in the case of poorly cemented sedimentary rocks).Discontinuities are stained and/or contain a filling comprising altered material. Cannot be scraped with a knife. Hand specimen can be broken by a single firm blow with geological pick.	1500 - 1850	Very hard ripping
Very hard rock	Slightly weathered	Penetrative weathering developed on open discontinuity surfaces, but	1850 - 2150	Extremely hard ripping

Schlumberger Resistivity
Modelling
VES 3

The current model is :-

Layer	Thickness	Resistivity
1	3.50	7.50
2	4.30	88.00
3	10.10	8.20
4	infinite	2500.00

AB/2	Observed Resistivity	Calculated Resistivity
1.00	7.5	7.9
1.50	10.5	8.7
2.00	13.0	9.7
3.00	15.0	12.0
4.00	16.0	14.0
5.00	17.0	15.4
7.00	16.0	17.0
10.00	14.0	18.0
15.00	16.0	19.9
20.00	20.0	23.1
30.00	29.0	32.9
40.00	40.0	43.5
50.00	50.0	54.1
70.00	75.0	75.3
100.00	120.0	106.7

Author: Audouin, Jeanne-Claire.
Name of thesis: Geophysical study of acid rock drainage in the City Deep Area, Johannesburg, Gauteng.

PUBLISHER:
University of the Witwatersrand, Johannesburg
©2015

LEGALNOTICES:

Copyright Notice: All materials on the University of the Witwatersrand, Johannesburg Library website are protected by South African copyright law and may not be distributed, transmitted, displayed or otherwise published in any format, without the prior written permission of the copyright owner.

Disclaimer and Terms of Use: Provided that you maintain all copyright and other notices contained therein, you may download material (one machine readable copy and one print copy per page)for your personal and/or educational non-commercial use only.

The University of the Witwatersrand, Johannesburg, is not responsible for any errors or omissions and excludes any and all liability for any errors in or omissions from the information on the Library website.